Spring 1-1-2018

Impact of Breakthrough Battery Technology on Energy Use and Emissions from the U.S. Transportation Sector

Azadeh Keshavarzmohammadian
University of Colorado at Boulder, azadeh.k.moh@gmail.com

Impact of Breakthrough Battery Technology on Energy Use and Emissions from the U.S. Transportation Sector

by

Azadeh Keshavarzmohammadian

B.S., University of Tehran, 2001

M.S., Polytechnic University of Tehran, 2005

MBA, University of Tehran, 2009

M.S., University of Colorado Boulder, 2014

A thesis submitted to the

Faculty of the Graduate School of the

University of Colorado in partial fulfillment

of the requirements for the degree of

Doctor of Philosophy

Department of Mechanical Engineering

2018

This thesis entitled:
Impact of Breakthrough Battery Technology on Energy Use and Emissions from the U.S. Transportation Sector
written by Azadeh Keshavarzmohammadian
has been approved for the Department of Mechanical Engineering

Prof. Jana B. Milford

Assoc. Prof. Daven K. Henze

Prof. SeHee Lee

Assoc. Prof. Stephen R. Lawrence

Asst. Prof. Sherri M. Cook

Date _____

The final copy of this thesis has been examined by the signatories, and we find that both the content and the form meet acceptable presentation standards of scholarly work in the above mentioned discipline.

Keshavarzmohammadian, Azadeh (Ph.D., Mechanical Engineering)

Impact of Breakthrough Battery Technology on Energy Use and Emissions from the U.S. Transportation Sector

Thesis directed by Prof. Jana B. Milford and Assoc. Prof. Daven K. Henze

Electric vehicles (EVs) have known to have a potential for deep reduction in oil consumption and emissions, but their successful adoption requires technological advances (batteries) and overcoming customer barriers (high upfront cost). In this research, we analyze the impacts of introducing inexpensive and efficient EVs on energy use and emissions from the U.S. transportation sector using an integrated energy model, conduct life cycle assessment (LCA) for a pyrite battery suitable for EV applications, and design efficient regionally targeted subsidies using a modified cascading diffusion model which minimizes the social costs (MSC) of driving EVs in place of gasoline vehicles (GVs). Different policy scenarios targeting the well-to-wheel cycle are explored to examine the impacts of greater EV penetration in the U.S. light duty vehicle (LDV) fleet from now to 2055. Our results show that having 50% of the fleet demands fulfilled by BEVs as a result of technology advances can reduce the emissions from the LDV sector significantly, but the reductions in economy-wide emissions are smaller. LCA is conducted on a newly developed solid-state lithium pyrite battery to understand the impacts of vehicle cycle. The results show that the cumulative energy demand (CED) and global warming potential (GWP) impacts associated with battery production are significantly lower than well-to-wheel energy consumption and emissions. The comparison between impacts of pyrite and Li-ion batteries are limited to GWP and CED, and the impacts of pyrite battery are comparable to those of LIBs. To design more efficient subsidies for the purchase of EVs, we augment the cascading diffusion model, which designs the minimum subsidy based on customers direct willingness-to-pay, to minimize the social cost (subsidy minus external benefits) by incorporating regionally differentiated air quality and climate externalities from EVs. The results show that the environmental externalities from driving EVs in place of GVs

vary significantly across the regions. When the environmental externalities are incorporated into the U.S. regional market curves, the most favorable region to start the cascading diffusion changes. Subsidies designed based on the MSC model are slightly higher than those from the original model, but their social cost is significantly lower.

Dedication

This thesis is dedicated to the love of my life, Reza, for supporting me with his perpetual love.

Acknowledgements

This work was supported by a Sustainable Energy Pathways grant from the National Science Foundation, award number CHE-1231048. I am deeply indebted to my advisors, Jana Milford and Daven Henze, for guiding me throughout this long journey and being extremely supportive. I would like to thank my committee, Sherri Cook, SeHee Lee, and Stephen Lawrence for their insights and collaborations on this project. I would like to thank Kristen Brown, Jeffery McLeod, Dan Loughlin, and Carol Shay for contributions to and assistance with the MARKAL/US9R model. Thank to Nathalie Moyen for her business, market, and financial insight and Arash Mehraban for assistance with the subsidy analysis. I also would like to thank Justin Whitely, and Conrad Stoldt for their insight for battery chemistry and Alex Gold from Solid Power for the insight for the battery manufacturing process.

Also, I would like to express my gratitude to my amazing friends Farhad, Hamidreza, Romik, Jannet, and Joanna for their moral support who I could count on them just as I could count on my family. Thank you for making my life joyful, a beautiful memory that I will never forget. Arash you are one of the best. Thank you for being there all the time for me. Thanks to my parents and my amazing family for inspiring me to persist.

Reza, I could not do this without you.

Contents

Chapter

Tables

Table

Figures

Figure

Chapter 1

Overview

Transportation sector accounts for 27% of U.S. 2015 greenhouse gas (GHG) emissions (EPA, 2017a) and 72% of total U.S. 2012 oil consumption (EIA, 2012). Oil is the dominant primary energy source for the transportation sector (93%) (EIA, 2012). The U.S. light duty vehicle (LDV) sector is responsible for 60% and about 55% of the U.S. transportation GHG emissions and oil consumption, respectively (EIA, 2016d; EPA, 2017a). Transportation sector is also responsible for over 50% of NO_x, 30% of VOCs and 20% of PM emissions in the U.S. (EPA, 2017d). In recent years, electric vehicles (EVs), including both battery electric vehicles (BEVs) and plug-in hybrid vehicles (PHEVs), have been considered as one of the promising alternative technologies to cut oil consumption and emissions from the U.S. LDV sector (DOE, 2017b; NRC, 2013). Successful EV adoption requires technological advances, in particular for batteries, as well as overcoming customer, market, and infrastructure barriers; Among these barriers, the higher capital cost of EVs (mainly from the battery cost) compared to their gasoline vehicle (GV) counterparts is the most significant barrier to wider adoption (Deloitte Consulting LLC, 2010; Egbue and Long, 2012; Krupa et al., 2014; NRC, 2013; Sierzchula et al., 2014; Tran et al., 2012). Addressing these requirements has been the topic of a variety of ongoing studies such as developing new battery chemistries with higher energy densities at lower costs. However, concerns about the effectiveness of LDV technology advances on reducing GHG and air quality (AQ) constituents across the entire energy system in the U.S. need to be addressed, including life cycle emissions associated with newly developed batteries. We explore these concerns in the first and second parts of our research. Moreover, a variety of financial

incentives and policies have been implemented to reduce EV capital costs and increase their market penetration. U.S. federal income tax credits for EV purchases are offered uniformly throughout the whole country. Some researchers have questioned the efficiency of these incentives because they fail to reflect variations in potential social benefits or costs associated with EV operations in different locations (Holland et al., 2016; Skerlos and Winebrake, 2010). Therefore, in the third part of our research, we also explore how consideration of regionally differentiated willingness-to-pay (WTP) and pollution externalities affect the minimum level of subsidies required to achieve a target level of EV production in the U.S. We also analyze how incorporating pollution externalities in subsidy design might minimize the social costs associated with driving EVs in place of GVs in different U.S. regions.

In the first part of our research, we investigate how effectively advances in LDV technology could reduce emissions from the entire U.S. energy system. Although EVs have low or no tailpipe emissions, they may indirectly contribute to emissions, depending on the technology used to generate electricity for battery charging. They could also shift emissions to other sectors beyond the electric sector. In this part of the analysis (chapter 2), we assume mass scale production of EVs has been achieved and barriers to their adoption have been overcome. That is, they have become competitive with GVs. We develop scenarios using an integrated energy model, ANSWER-MARKAL, in connection with the U.S. Environmental Protection Agency's (EPA's) 9-region (US9R) database to evaluate emissions associated with introduction of inexpensive and efficient EVs into the U.S. LDV sector. We also seek to evaluate the U.S. energy system responses to such technology changes, and we consider coordinated policies (such as technology advances along with emission fees) that could increase EV penetration. The results of these scenarios show the possible emission reductions from the LDV and other economic sectors from 2005 to 2055. In addition to the sectoral emissions, our results provide insight into the well-to-wheel (WTW), or fuel cycle, emissions of vehicles, but do not yet consider emissions from vehicle manufacturing. Our ANSWER-MARKAL modeling assumes a future situation when EVs have reached the mass production, but do not investigate the transition phase. ANSWER-MARKAL model provides both national and regional results for

technology mixes, fuel mixes, and emissions that help us determine how different regions and the country as a whole may benefit environmentally from adoption of improved EVs. However, this analysis cannot provide insight about which would be the best region to introduce this emerging technology, EV. It also does not provide social cost-benefit estimates of switching to EVs, which can vary significantly depending on the location. That is, from economic performance and social costs standpoints, the model does not suggest a market mechanism or a region to introduce the new product.

To account for emissions from vehicle production cycle, we conduct life cycle assessment (LCA) for manufacturing of a solid-state lithium pyrite battery, developed in the CU-Boulder material group (Yersak et al., 2013), in a hypothetical BEV. For EV applications, Li-ion batteries are used based on the current practices; however, the need for lighter batteries with higher energy densities to provide longer vehicle range has encouraged development of new battery chemistries, like lithium batteries which offer higher gravimetric and volumetric energy densities than Li-ion batteries (Väyrynen and Salminen, 2012). On the other hand, solid-state batteries show potential advantages over those using liquid electrolytes, due to lower safety issues which escalates when the size of battery increases (Takada, 2013). We apply a process-based attributional LCA technique, utilizing characterization of different mid-point indicators from a LCA database. Since we conduct our analysis for a new solid-state pyrite battery which exists only in the lab scale, special treatment is required to adapt a new battery assembly process based on current production practices for liquid Li-ion batteries. Also, a battery mass inventory needs to be estimated for a battery with suitable size for EV applications. We conduct these analyses in this part of our study. If we assume the same size and vehicles, and account for drive train differences, the results from our LCA and WTW emissions can provide insight into the life cycle emissions of BEVs compared to their GV counterparts. The results of this chapter provide insight regarding the environmental impacts of solid-state lithium batteries, suitable for EV applications that may be of value prior to finalization of battery design and mass production.

In the last part of the research, we explore how EVs, as emerging technologies, should be in-

troduced in an economically and environmentally viable manner in different regions in the U.S. Due to differences in regional market conditions, some market mechanisms such as subsidies could be designed and implemented to initially introduce new EVs to regions with more favorable economic conditions. Targeting initial subsidies toward regions with the most favorable economic conditions helps advance production levels along the learning curve to reduce costs, making EVs more competitive in subsequent regions. To determine the subsidies that should be granted to which regions, we adapt the framework of Herron and Williams (2013) for modeling the cascading diffusion of EVs across regionally defined sub-markets in the U.S. The model accounts for consumer's WTP for the new technology along with the technology's projected learning curve. We augment the cascading diffusion model by considering whether the subsidies advance current social welfare by reducing external damages. That is, we consider EV learning curves and direct WTP along with environmental externalities from deploying EVs (or external cost of driving GVs) across nine U.S. regions. The new model proposes subsidies based on the minimum social costs and accounts for spatial differences in consumer and environmental benefits of EV applications in different U.S. regions by linking market and air-quality models.

In the rest of this thesis, we explain the details of our energy modeling system and assumptions, and the scenarios developed based on the LDV vehicle's optimistic cost and efficiencies (Chapter 2). We also provide the details of LCA analysis for the solid-state lithium pyrite battery (Chapter 3). Next, we illustrate the results of subsidy and social cost analyses for promotion of EVs (Chapter 4). Due to the diversity of topics covered in chapters 2–4, we provide subject-specific introduction, motivation, and literature, individually, for each chapter. Finally, we conclude by highlighting the main results and findings of this research (Chapter 5).

Chapter 2

Emission Impacts of Electric Vehicles in the U.S. Transportation Sector Following Optimistic Cost and Efficiency Projections[1]

2.1 INTRODUCTION

A variety of alternative fuels, vehicle technologies, and policy options have been considered to reduce dependence on oil and emissions from the transportation sector (DOT, 2010; Greene et al., 2011; Heywood et al., 2009; Pedersen et al., 2011). In particular, greenhouse gas (GHG) emissions from light duty vehicles (LDVs) can be reduced by improving efficiency of vehicles with conventional internal combustion engines (ICEVs) and hybrid electric vehicles (HEVs) via load reductions and powertrain improvements; however, deeper reductions may require electrification (NRC, 2013).

This study evaluates potential emissions implications of future use of electric vehicles (EVs) in the LDV sector, following optimistic assumptions about improvements in vehicle cost and efficiency. We use an integrated energy system model to evaluate how the U.S. energy system might respond to increased EV penetration. Although EVs, both plug-in hybrid (PHEV) and all-electric (BEV), have low or no tailpipe emissions, they may lead to indirect emissions, depending on the technology used to generate electricity for battery charging (Choi et al., 2013; Kromer et al., 2010; NRC, 2013; Peterson et al., 2011; Yeh et al., 2008). Moreover, increased penetration of EVs could shift emissions in sectors beyond electricity generation (Loughlin et al., 2015). For example, increased EV penetration could draw natural gas from the industrial sector to the electricity sector and push

[1] The content of this chapter is from Keshavarzmohammadian et al. (2017).

the industrial sector to use more carbon-intensive fuels.

Prior studies have examined potential reductions in fuel use and GHG emissions from the LDV sector, including through introducing EVs (Bandivadekar et al., 2008; Choi et al., 2013; Elgowainy et al., 2016, 2013; Kromer et al., 2010; Meier et al., 2015; Nealer et al., 2015; NRC, 2013; Peterson et al., 2011). Some of these studies examined how to reduce emissions to a set target level (Elgowainy et al., 2013; Kromer et al., 2010; Meier et al., 2015; NRC, 2013); others examined reductions achievable under specified policies (Bandivadekar et al., 2008; Choi et al., 2013; Elgowainy et al., 2016; Nealer et al., 2015; Peterson et al., 2011). The prior studies examined specific pathways such as demand reductions or use of alternative fuels and technologies; some investigate electrification in particular (Bandivadekar et al., 2008; Choi et al., 2013; Elgowainy et al., 2016; Loughlin et al., 2015; Meier et al., 2015; Nealer et al., 2015; NRC, 2013; Peterson et al., 2011). However, recent advances in EV technology have outpaced vehicle cost and performance assumptions used in earlier assessments, so consideration of more optimistic projections is needed. Furthermore, most prior studies of implications of EV introduction have focused on the transportation and electricity sectors alone without considering implications for energy use in other parts of the economy (Bandivadekar et al., 2008; Choi et al., 2013; Elgowainy et al., 2016, 2013; Kromer et al., 2010; Meier et al., 2015; Nealer et al., 2015; NRC, 2013; Peterson et al., 2011). Although some studies have accounted for "life cycle" emissions upstream of the electric sector (Bandivadekar et al., 2008; Elgowainy et al., 2016, 2013; Meier et al., 2015; Nealer et al., 2015; NRC, 2013), they still lack the intersectoral connections of an integrated model and a feasibility check for their exogenous assumptions such as the assumed penetration rates of EVs. Integrated assessments are needed to develop coordinated policies covering LDVs within the whole energy sector (NRC, 2013).

In one of the few previous cross-sectoral studies Yeh et al. (2008), applied the integrated energy modeling system ANSWER-MARKAL with the 2008 U.S. EPA 9-Region (US9R) database to evaluate CO_2 emission reductions and fuel use in the LDV sector considering PHEVs and ethanol flex-fuel vehicles, but not BEVs, as alternative technologies. Their study suggests that a tight economy-wide cap is required to be able to sharply reduce CO_2 emissions from the transportation

sector (Yeh et al., 2008). Loughlin et al. (2015) included deploying PHEVs and BEVs among the pathways they investigated for reducing NO_x emissions, using the 2014 EPA US9R database. They find the EV pathway to be complicated due to offsetting emissions from intersectoral shifts (Loughlin et al., 2015). Rudokas et al. (2015) used MARKAL with the 2012 US9R database and examined the influence of system-wide CO_2 emissions fees or a 70% CO_2 emissions cap on the transportation sector, looking out to the year 2050. They find that EV penetration increases with a transportation sector CO_2 emissions cap, but see little influence of economy-wide emissions fees on that sector. Babaee et al. (2014) developed a U.S. data set for the MARKAL-EFOM (TIMES) model and investigated combined HEV and EV penetration and associated emissions under numerous combinations of assumptions about natural gas and oil prices, CO_2 emissions cap, renewable portfolio standards and battery costs. They find low battery costs to be an important driver of EV and HEV adoption (Babaee et al., 2014). However, their national-level model ignores regional trades and fuel supply curves, transmission constraints and energy conversion and processing technologies other than power plants. Furthermore, while Babaee et al. (2014) investigated the effect of battery cost on EV penetration, their study ignores the effect of other technology improvements on efficiency and cost, not only for EVs but also for other LDV technologies. Unlike these prior studies, here we develop scenarios representing consistent optimistic technology advances across ICEVs and EVs to investigate the effect of these advances on emissions not only from the LDV sector, but also from the whole U.S. energy system.

In this study, we use ANSWER-MARKAL in connection with the EPA US9R database (version v1.1; 2014) to examine the impacts of greater EV penetration in the U.S. LDV fleet from now to 2055. Compared to prior studies, the model includes a relatively comprehensive suite of available and viable forthcoming technologies, focusing on improved ICEVs and EVs, for meeting demand for energy services in all economic sectors, including the LDV portion of the transportation sector. Rather than pre-specifying mixes of energy sources and shares of technologies in any of the sectors of the economy, we use an optimization model to determine the least costly choices for meeting demand, with key cost and performance assumptions detailed below. We modeled an optimistic

scenario by adapting cost and efficiency estimates for ICEV and EV technologies from the optimistic case developed by the National Research Council Committee on Transitions to Alternative Vehicles and Fuels (NRC, 2013). As shown below, this case projects greater improvements in vehicle efficiency and cost than assumed in previous analyses. We compare results from this optimistic scenario with those from EPA's original 2014 US9R database. We also examine how the energy system responds to GHG fees with and without the optimistic LDV assumptions, and examine the sensitivity of the results with respect to the future level of LDV travel demand, oil prices, and fees. In addition, we estimate well-to-wheel (WTW) GHG, SO_2 and NO_x emissions for BEV and gasoline ICEV technologies based on our OPT scenario results.

2.2 METHODS

2.2.1 ANSWER-MARKAL

MARKAL uses linear programming to estimate energy supply shifts over a multidecadal time frame, finding the least-cost means to supply specified demands for energy services subject to user-defined constraints, assuming a fully competitive market (Loulou et al., 2004). The model computes energy balances at all levels of an energy system from primary sources to energy services, supplies energy services at minimum total system cost, and balances commodities in each time period (Loulou et al., 2004). Outputs consist of the penetration of various energy supply technologies at both regional and national levels, technology-specific fuel use by type, and conventional air pollutant and GHG emissions.

2.2.2 EPA US9R Database

The 2014 EPA US9R database provides inputs to the MARKAL model for nine U.S. regions (shown in Figure 2.3) and an international import/export region. The database specifies technical and cost features of current and future technologies at five-year intervals, with a structure that connects energy carriers (e.g., output of mining or importing technologies) to conversion or process

technologies (e.g., power plants and refineries) and in turn to the transportation, residential, industrial, and commercial end use sectors. Demand for energy services of end-use sectors is given from 2005 through 2055. Primary energy supplies are specified via piece-wise linear supply curves. The database includes comprehensive treatment of air pollutant emissions from energy production, conversion, and use, accounting for existing control requirements and including a range of additional control options. Current regulations including Renewable Portfolio Standards and biofuel mandates are included as constraints. The database includes joint Corporate Average Fuel Economy (CAFE) and GHG emission standards for LDVs, requiring average fuel economy for passenger cars and light trucks of 34.1 mpg by 2016, rising to 54.5 mpg by 2025 (EPA, 2012a; Federal Registrar, 2010). The 2015 Clean Power Plan (CPP) requirements are not included, since they were not finalized at the time of the 2014 release (EPA, 2015). All costs are presented in 2005 U.S. dollars, with deflator factors from the Department of Commerce Bureau of Economic Analysis used to adjust prices to the base year. More details are provided in the US9R database documentation (Lenox et al., 2013).

Future LDV transportation demand in the US9R database is specified based on Annual Energy Outlook (AEO) 2014 projections (EIA, 2014a), allocated to the model's nine regions and to seven vehicle size classes ranging from mini-compacts to light trucks. Demand rises from 2687 billion vehicle miles traveled (bVMT) in 2005 to 3784 bVMT in 2055. This future demand can be met with gasoline (conventional), diesel, ethanol, CNG, and liquefied petroleum gas (LPG) or flex-fueled ICEVs; HEVs; PHEVs; fuel cell vehicles; and BEVs. PHEVs have 20 or 40-mile ranges; BEVs have 100 and 200-mile ranges. All technology and fuel combinations are available in all size classes, except that mini-compact cars have limited options. That is, mini-compact cars are only available for ICEVs, and BEVs. Technology-specific hurdle rates are used to reflect customer, market, and infrastructure barriers. Hurdle rates range from 18% for gasoline and diesel ICEVs to 28% for BEVs. Cost and efficiency of vehicles other than BEVs are taken from AEO2014 projections and data from EPA's Office of Transportation and Air Quality. Cost and efficiency estimates for BEVs are based on expert judgment (Baker, 2011). Emissions factors are calculated from the EPA MOVES model (Lenox et al., 2013). For EV charging, the year is partitioned into summer, winter,

and intermediate seasons and the day into am, pm, peak, and nighttime hours. The fraction of EV charging in each time period is fixed as an input in the model and is uniform across regions. Most charging happens at night in all seasons.

2.2.3 Changes to the EPA US9R Database and Scenarios Modeled

Table 2.1. Scenarios and sensitivity analyses included in this study.

Scenario name	Description
BAU	Reference scenario with unmodified 2014 EPA US9R database, including EPA's efficiency and cost estimates for future gasoline ICEV, HEV, PHEV, BEV, and ethanol vehicles.
OPT	Substitutes optimistic efficiency and cost improvement for gasoline ICEV, HEV, PHEV, BEV, and ethanol vehicles from NRC (2013); adds and refines upstream emissions and refines cost and performance estimates for other sectors.
BAUFEE/ OPTFEE	Moderate CO_2 and CH_4 fees are applied to BAU and OPT scenarios, starting in 2020, based on social cost of carbon and methane (Marten and Newbold, 2012)
BAUHIFEE/ OPTHIFEE	CO_2 fees are 52% higher in 2020 and 41% higher in 2050 compared to moderate fees; CH_4 fees are 36% higher in 2020 and 21% higher in 2050 (Marten and Newbold, 2012).
BAULOFEE/ OPTLOFEE	CO_2 fees are 69% lower in 2020 and 63% lower in 2050 compared to moderate fees; CH_4 fees are 50% lower in 2020 and 48% lower in 2050 (Marten and Newbold, 2012).
BAUHIDMD/ OPTHIDMD	LDV demand is increased by 0% in 2005 to 6% in 2040 relative to BAU and OPT scenarios, based on AEO2014 high LDV demand projections. See Figure 2.4 for complete high demand projections.
BAULODMD/ OPTLODMD	LDV demand is reduced by 0% in 2005 to 19% in 2040 relative to BAU and OPT scenarios, based on AEO2014 low LDV demand projections (see Figure 2.4).
BAUHIOIL/ OPTHIOIL	Oil prices are increased by 0% in 2005 to 78% in 2040 relative to BAU and OPT scenarios, based on AEO2015 high North Sea Brent crude oil price projections. For complete high oil price projections refer to Figure 2.5.
BAULOOIL/ OPTLOOIL	Oil prices are reduced by 0% in 2005 to 47% in 2040 relative to BAU and OPT scenarios, based on AEO2015 low North Sea Brent crude oil price projections (see Figure 2.5).

Table 2.1 lists the scenarios examined in this study. The reference case (BAU) uses the unmodified 2014 EPA US9R database, including EPA's efficiency and cost estimates for all LDV.

In contrast, the optimistic scenario (OPT) uses cost and efficiency estimates for gasoline and ethanol ICEV, HEV, PHEVs, and BEVs based on the optimistic projections given by NRC (2013). Costs and efficiencies for other fuels and technologies, including FCEV and CNG vehicles, were not modified for the OPT case as they were little used in the BAU case (as shown below) and were not the focus of this study.

The NRC Committee developed their projections considering both technology-specific powertrain technology improvements and common improvements via reductions in weight and rolling resistance and aerodynamic drag, and improved energy efficiencies for accessories across all technologies. Learning curves were considered for technology improvements and costs, which are calculated based on mass production assumptions. According to the NRC Committee, meeting the optimistic projections would entail significant research and development, but no fundamental technology innovations (NRC, 2013). The Committee also found that meeting these projections would require significant incentives or regulatory requirements to spur development and increase production levels. Compared to other available projections, the NRC estimates provide a more consistent accounting of improvements across different technologies (DOT, 2010; EIA, 2014a; Elgowainy et al., 2013; Plotkin and Singh, 2009), are more readily extended across vehicle sizes (DOT, 2010; Elgowainy et al., 2016, 2013; Plotkin and Singh, 2009), and extend further into the future (Elgowainy et al., 2016, 2013). For details of the assumptions and calculations see the NRC report and its appendix F (NRC, 2013). Additional changes to the LDV segment in the OPT scenario are summarized in Table 2.2, and discussed further in section 2.4.4. Section 2.4.4 also explains how the NRC projections are extrapolated to the other vehicle size classes included in the US9R database.

In addition to the changes made for LDVs, the OPT scenario also incorporates refinements for other sectors as described in the section 2.4.5, Brown (2014), Brown et al. (2014a), Brown et al. (2014b), McLeod (2014), and McLeod et al. (2014). Overall, the changes provide for a more comprehensive treatment of upstream emissions, an expanded set of emissions control options, especially in the industrial sector, and updates and refinements to cost and equipment lifetime estimates in the electricity sector.

Table 2.2. Major changes to LDV sector inputs or constraints for the OPT scenario. See sections 2.4.2 and 2.4.4 for more information.

Parameter/ constraint	**Description of modifications/ changes**
LDV cost	Estimated based on optimistic case of NRC (2013) for gasoline ICEV, HEV, PHEV, BEV, and ethanol vehicle technologies for seven classes of vehicles for the entire time horizon. For example, in 2050 the BEV100 vehicle costs range from 9% to 33% lower than in the BAU scenario.
LDV efficiency	Same as cost. For example, in 2050 the BEV100 vehicle fuel economies range from 30% to 90% higher than in the BAU scenario.
LDV demand	Updated based on 2014 U.S. Census population projections, which results in lower projections for LDV demand. LDV demand is reduced by 2% in 2050 relative to BAU.
Hurdle rate	Assumed to be uniform at 24% for all technologies to reflect a fully competitive market without customer and infrastructure barriers, compared to 18% for ICEVs, 24% for HEVs and 28% for EVs in the BAU scenario.
CAFE constraint	Recalculated based on LHV (Lower Heating Value), which tightens the CAFE representation in the model by 7–9% in each year.
Investment constraints	Removed for years after 2025, except for BEV with 100-mile range. Constraints updated for BEV100, reflecting limited market for shorter-range vehicles.

The fees applied in the GHG fee scenarios are adapted from Marten and Newbold (2012), which provides estimates for the social cost of methane from an integrated assessment model, rather than more simplistic scaling based on global warming potentials (GWPs). Marten and Newbold (2012) projections of social cost of CO_2 (SCC) are almost equal to those reported by the Interagency Working Group (IWG, 2013). The moderate CO_2 (CH_4) fees are 40 2005 U.S.$/metric tonne of CO_2 (1036$/tonne of CH_4) in 2020, escalating to 80 (3107)$/tonne in 2055. High fees are a factor of 1.5 (1.3) times greater, and low fees are 2.9 (1.9) times lower. The full set of values is given in Table 2.6. CO_2-eq is calculated considering CO_2 and methane as the main GHG contributors, using both a 20-year GWP of 84 and a 100-yr GWP of 28 for CH_4 (Myhre and Shindell, 2013) as we are interested in opportunities for reductions over a range of time horizons.

The BAU and OPT scenarios were also run with high and low LDV demand and high and

low oil prices (Table 2.1) to test sensitivity to these assumptions. We also ran six diagnostic cases, listed in Table 2.7, to identify which changes made between the BAU and OPT scenarios most influence the results. One case includes all modifications implemented in the OPT scenario except those specific to the LDV sector while the others isolate separate modifications to the LDV sector.

2.2.4 Well-To-Wheel Emissions Calculation

We use the results from MARKAL to estimate WTW emissions rates for GHG, NO_x, and SO_2, in grams per mile, for ICEV and BEV technologies. WTW estimates focus on the fuel cycle supporting vehicle operation and neglect emissions from vehicle manufacturing and recycling. We calculate WTW emissions using vehicle efficiencies, upstream emission factors, and the electricity mix corresponding to a certain scenario's results in each year. We use a 100-year GWP for methane for calculating WTW GHG emissions. Regional calculations for BEV emissions are estimated using the electricity mix for each particular region in each scenario. For ICEV, regional differences are much less significant, so only national average emissions rates are shown.

2.2.5 Comparison of LDV Efficiencies and Costs

Table 2.3 illustrates how the optimistic efficiencies from the NRC study compare to projections from the original EPA US9R database and other studies, for gasoline ICEV, HEV and BEV (DOT, 2010; Elgowainy et al., 2016; Plotkin and Singh, 2009). For simplicity, comparisons are shown only for the year 2030 and average or full-size vehicles. Comparisons for other years and fuel-technology combinations are included in Figure 2.7. The NRC optimistic case projects higher fuel economies across all vehicle types and sizes than the comparison studies. In particular, the recent Argonne National Laboratory (ANL) study of prospects for LDVs (Elgowainy et al., 2016) projects fuel economies for BEVs and HEVs that are higher than those in the EPA US9R BAU case but lower than those in the NRC optimistic case.

Table 2.4 compares costs for full-size vehicles in 2030 and 2050 between the NRC optimistic case and the original EPA US9R database. The NRC and EPA costs are similar for gasoline ICEV

and HEV technologies in 2030 and 2050. However, for BEV100, the NRC costs are lower than those projected by EPA. For 2030, the NRC's incremental costs for HEV and BEV100 are also relatively low compared to those for similar vehicles in the recent ANL study (Elgowainy et al., 2016). Additional comparisons are provided in Figure 2.6.

Table 2.3. Comparison of projected efficiencies (mpge) for average[a] or full-Size[b] LDVs for model year 2030.

Technology	NRC mid.[c,1]	NRC opt.[1]	EPA US9R	ANL avg.[2]	ANL high[2]	DOT min.[3,a]	DOT max.[3,a]	ANL 2016[4]
ICEV	61	70	53	37	44	31	40	49
HEV	76	88	71	66	83	38	61	76
BEV[d]	180	207	96	144	163	-	-	172

[a] This study focuses on the average vehicle size.
[b] Midsize and large cars are aggregated to the full-size category in the EPA database. We have taken the same approach for the other studies to be able to compare the results. ANL 2016 (Elgowainy et al., 2016) values are for a midsize car.
[c] Estimates from NRC (NRC, 2013) are characterized as midrange (mid.) and optimistic (opt.); from ANL (Plotkin and Singh, 2009) as average (avg.) and high; and from DOT (2010) as minimum and maximum values.
[d] BEV range is 130 miles in NRC (2013); 100 miles in the EPA database, 150 miles in Plotkin and Singh (2009), and 90 miles in Elgowainy et al. (2016).
[1] NRC (2013).
[2] Plotkin and Singh (2009).
[3] DOT (2010).
[4] Elgowainy et al. (2016).

Table 2.4. Comparison of projected cost (thousands 2010 $) for full-size vehicles for model years 2030 and 2050.

	2030		2050	
Technology	**EPA US9R**	**NRC opt.[1]**	**EPA US9R**	**NRC opt.[1]**
ICEV	27.72	28.57	27.74	29.86
HEV	30.85	29.18	30.66	30.45
BEV100	34.95	28.40	32.73	28.01

[1] NRC (2013).

2.2.6 Transition Policies

For contrast with the BAU scenario, our OPT scenario is constructed based on the assumption that customer and market barriers for penetration of EVs have been lowered to make EVs

competitive with gasoline vehicles, in particular after 2025. To get to this point, subsidies or regulations that will lower initial market barriers and encourage increased production volumes are needed. Except for CAFE, these policies are not explicitly represented in our scenarios, but rather they are approximated by the relaxed investment constraints and equalized hurdle rates in the OPT scenario.

2.3 RESULTS AND DISCUSSION

2.3.1 LDV Penetration

Figure 2.1a shows national results for LDV penetration in terms of vehicle stocks for the BAU and OPT scenarios. While gasoline vehicles dominate in the BAU scenario for the entire time horizon, in the OPT scenario BEVs gain a LDV market share of about 15% (all from BEV100) by 2030 and 47% (with 20% share from BEV100 and 27% from BEV200) by 2050. In 2050, these BEVs are mainly in the compact (6% from BEV100 and 21% from BEV200), full (4% from BEV100 and 6% from BEV200), and small SUV (10% from BEV100), size classes, which have relatively high share and lower upfront cost compared to other size classes. HEVs play a negligible role in the BAU scenario, but are adopted to a moderate extent in the midterm in the OPT scenario. Ethanol vehicles account for about 3% of VMT in both scenarios in 2030, but are eliminated by 2050 in the OPT scenario. Diesel vehicles account for a steady 4% in both scenarios.

As noted above, approaching the OPT scenario for EV penetration would require transition policies to lower market barriers. These are not explicitly modeled in this study. That is, our study assumes market barriers for deploying EVs have been conquered, such as charging stations have become widely available. However, the NRC assessment (NRC, 2013) illustrates the level of subsidy that might be required to lower market barriers for EVs. The NRC Committee used the Light-Duty Alternative Vehicle Energy Transitions (LAVE-Trans) model of consumer demand in the transportation sector to explore several transition policy scenarios, including one that assumed optimistic EV technology advances together with EV subsidies. The current $7500 federal tax

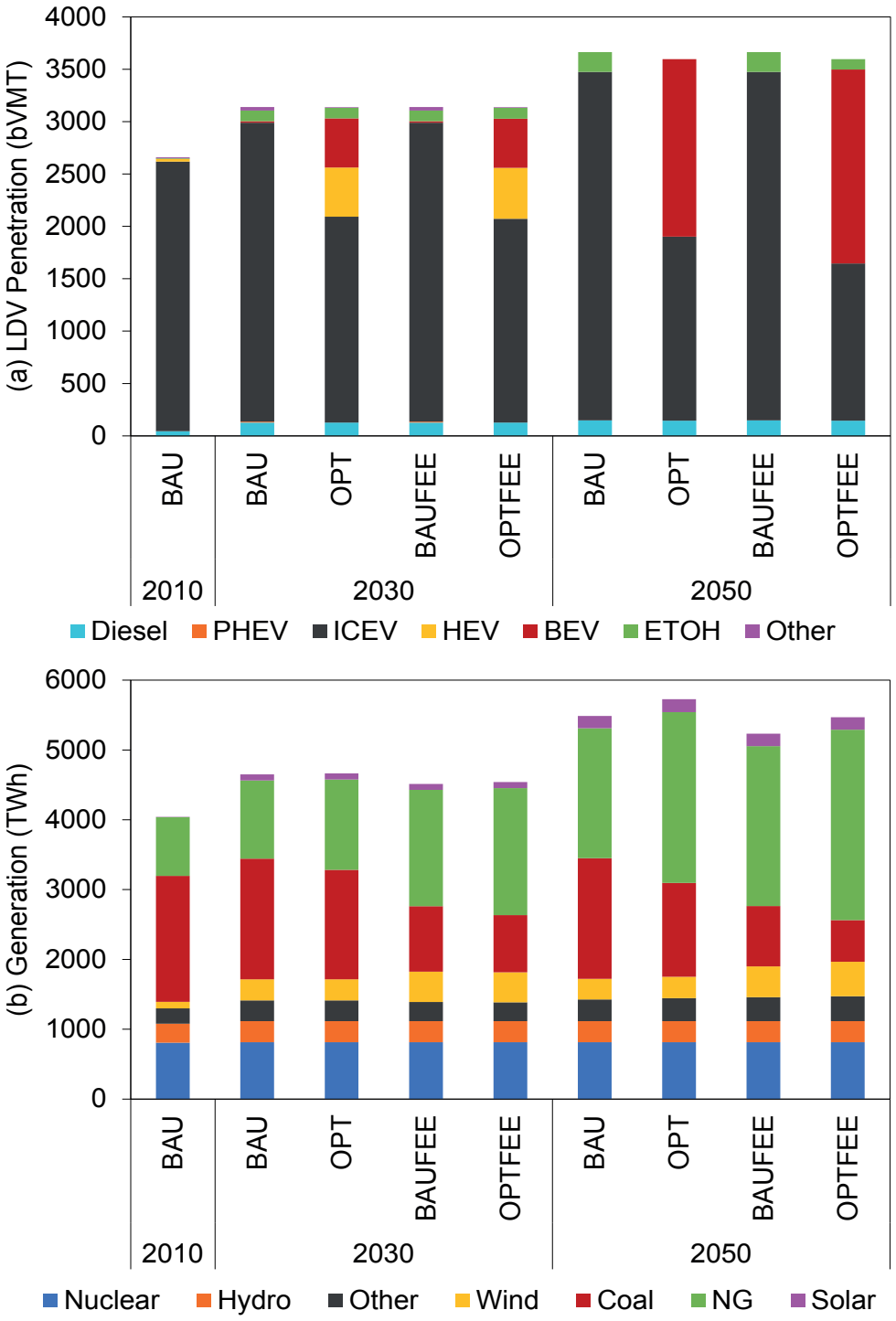

Figure 2.1. U.S. technology mix for (a) LDV and (b) electricity generation by scenario and year. PHEV, ICEV, and HEV are gasoline fueled.

credit for EVs was continued through 2020, briefly increased to $15000 in 2021 and then phased out by ∼2030. This scenario achieved market shares of 8% PHEV and 33% BEV in 2050, with no subsidies provided at that point in time (NRC, 2013). Our OPT case is somewhat more aggressive, achieving about a 15% higher EV market share in 2050.

Regional results (not shown) generally follow the same pattern as the national scale results, except that the ethanol vehicle share varies across the regions. In 2030, it ranges from 0% to 21% for the BAU scenario and from 0% to 16% for the OPT scenario. In 2050, the ethanol share ranges from 0% to 37% for the BAU scenario, but ethanol is not used in 2050 in the OPT scenario. The highest ethanol penetration is in the East North Central region, where corn is relatively abundant and ethanol fuel costs are relatively low. For the OPT scenario, the BEV share is about 15% in 2030 in all regions, but ranges from 40% to 52% across regions in 2050.

Six additional diagnostic cases (see Table 2.7) were run to understand which changes between BAU and OPT were most influential. The results (see Figure 2.9) show that CAFE is the main driving force for HEV penetration in the midterm (case D1). In case D1, HEVs account for 14% of total VMT in 2030, but are not used in 2050. The reason for this is that by 2025–2030, ICEVs are not sufficiently efficient to satisfy CAFE requirements. HEVs are more efficient than ICEVs, and are cheaper than other alternative technologies that could be used to satisfy the standards. However, the database assumes ICEV efficiency will continue to improve and by 2050 they are sufficiently efficient to meet CAFE requirements. The model selects ICEVs over HEVs at this point because ICEVs are less expensive. In isolation, incorporating optimistic LDV cost and efficiency assumptions (case D2) or lowering hurdle rates and investment constraints (D3) do not significantly alter BEV penetration compared to the BAU scenario. However, significant BEV penetration occurs when these changes are combined (cases D4 and D5). Combining these optimistic assumptions reflects a more realistic and consistent scenario than separating them, since if cost and technological barriers of EVs have been addressed, it is expected that hurdle rates would also be lowered. Lastly, modifications outside the LDV sector have negligible impact on the LDV mix (D6).

We also consider results from a variety of scenarios designed to explore the sensitivity of our results to assumptions regarding VMT demand, GHG fees, and oil prices (Table 2.1). In the low (high) LDV demand cases, input LDV demand was reduced (increased) by 12% (5%) in 2030, and by 20% (4%) in 2050 in the BAU scenario, and by 19% (6%) in 2050 in the OPT scenario. With lower demand, the VMT of gasoline cars was reduced by 14% in the BAU scenario and 24% in the OPT scenario in 2030; and by 20% in both scenarios in 2050. In the OPTLODMD case, HEV VMT is 36% higher in 2030 than in the OPT scenario. Increasing LDV demand results in approximately proportional increases in the VMT of gasoline vehicles in both the BAU and OPT scenarios. BEV VMT in the OPTHIDMD scenario also increases in proportion to overall VMT demand. Sensitivity to oil prices was tested using AEO2015 projections (EIA, 2015). These changes had negligible impact on the technology mix in the LDV sector in either the BAU or OPT scenario. This is because, as shown in section 2.4.8, upfront vehicle costs have a much greater effect than fuel costs on the annualized unit cost of vehicle ownership.

To examine how optimistic assumptions about LDV technology advances would alter the response of the energy system to GHG fees, moderate system-wide fees were applied starting in the year 2020 (BAUFEE and OPTFEE). The LDV segment of the transportation sector is able to respond by shifting to more efficient vehicle technologies and/or to fuels with lower in-use and upstream GHG emissions. As shown in Figure 2.1a, with BAU assumptions for LDV efficiency and costs, applying moderate economy-wide GHG fees has little effect on the LDV technology and fuel mix. With OPT assumptions, application of moderate fees increases the share of BEVs by 4.4% in 2050. Some ethanol also enters the vehicle/fuel mix in 2050 in the OPTFEE scenario. Note that there are uncertainties associated with upstream emissions for ethanol that could offset the uptake of CO_2 that is assumed in the model (Crutzen et al., 2008; Hill et al., 2006). Changing the fees as indicated in Table 2.1 produced negligible change in the LDV technology mix in the BAU scenario (results not shown). In the OPT scenario, increasing the fees does not change the share of BEVs in 2050; decreasing the fees reduces the BEV share by 3%. Overall, the influence of GHG emission fees on the LDV technology and fuel mix is limited due to their modest impact on the cost

of vehicle ownership. For all vehicle technologies, the impact of emissions fees in future decades is lower than it would be in the near term due to improvements in vehicle efficiency.

2.3.2 Electricity Mix

Use of an integrated energy system model allows for examination of how changes in the LDV sector might affect energy choices in other sectors, including electricity generation. As shown in Figure 2.1b, while the total electricity generation is equal in the BAU and OPT scenarios in 2030, it is 4% higher in 2050 in the OPT scenario, mainly due to the increased use of BEVs. Electricity generation from natural gas increases over time in both scenarios, whereas generation from existing coal plants declines. Our diagnostic case D6 shows that the extra natural gas generation in the OPT scenario compared to BAU is mainly due to the change we made to the EPA US9R database in limiting the lifetime of existing coal plants to 75 years. In the original database, existing coal plants could be used to the end of the modeled time horizon. Electricity generation from other technologies including wind and solar are similar between the BAU and OPT scenarios, with these two renewable technologies contributing about 9% of generation in 2050. Altering the LDV demand changes the total electricity demand by less than 1% in both low and high demand cases, with either BAU or OPT scenarios.

When moderate GHG fees are applied, total electricity demand in both scenarios decreases by 3% in 2030 and 5% in 2050. Both BAUFEE and OPTFEE utilize more natural gas (49% and 41% in 2030, and 23% and 11% in 2050) and wind (44% and 42% in 2030, and 50% and 61% in 2050) and less coal (46% and 48% in 2030, and 50% and 56% in 2050) than the respective scenarios without fees. Electricity consumption is 5% higher in the OPTFEE scenario in 2050 compared to the BAUFEE scenario, due to greater BEV penetration. For both BAU and OPT, total electricity generation is 1–3% higher in the low fee cases and 1–2% lower in the high fee cases, compared to the corresponding moderate fee scenarios. Carbon capture and sequestration is applied to 4% of generation in 2050 in the BAUHIFEE case and 3% of generation in the OPTHIFEE case.

2.3.3 Crude Oil Consumption

Changes in crude oil consumption in the BAU and OPT scenarios and corresponding fee and sensitivity cases are shown in Figure 2.10. Total crude oil consumption in the BAU scenario decreases by 4% from 2010 to 2030, driven by reductions in gasoline, which are somewhat offset by increases in diesel. The reductions in gasoline consumption correspond to average efficiency improvements of 65% for gasoline ICEV, which offset the 18% increase in LDV VMT demand. The increased diesel consumption is mainly for heavy-duty vehicles (HDV). In 2030, gasoline consumption in OPT is 3% lower than in the BAU scenario, largely because 30% of VMT is met with HEVs and BEVs. From 2030 to 2050, gasoline consumption remains steady in the BAU scenario despite an increase in LDV VMT demand. By 2050, gasoline consumption in the OPT scenario is 62% lower than in the BAU scenario, because BEV provide almost half of LDV VMT. The decrease in gasoline consumption in OPT provides more capacity for other refined products, such as jet fuel and petrochemical feedstock, so the total reduction in crude oil consumption from BAU to OPT is not as large as the reduction in gasoline use. Consumption of imported refined products (including gasoline) is almost five times lower than that of domestically refined products in both scenarios throughout the time horizon.

In the sensitivity tests, increasing the LDV demand results in less than a 1% increase in crude oil consumption in 2030 and 2050 in both the BAUHIDMD and OPTHIDMD cases. However, reducing LDV demand decreases total crude oil consumption by 3% in 2030 in both cases, and by 6% (BAULODMD) and 3% (OPTLODMD) in 2050, mainly from reduced gasoline consumption. With moderate GHG fees, the largest change is seen in 2050, where the total crude oil consumption in the OPTFEE case is about 3.5% lower than in the OPT scenario.

2.3.4 GHG Emissions

Figure 2.2a shows GHG emissions for the BAU and OPT scenarios as CO_2-eq using the 100-year GWP for methane. Results calculated using a 20-year GWP are shown in Figure 2.11

and demonstrate similar patterns. Total GHG emissions decrease from 2010 to 2030 and then increase from 2030 to 2050 in both scenarios. In the BAU scenario, GHG emissions from the LDV sector decline by 53% from 2010 to 2030 and by an additional 21% from 2030 to 2050, due largely to existing CAFE regulations. Correspondingly, in the BAU scenario the LDV share of total emissions is reduced from 21% in 2010 to 10% in 2030 and 7% in 2050. Direct emissions from the LDV sector contribute 9% and 5% of GHG emissions in the OPT scenario in 2030 and 2050, respectively. That is, our OPT scenario results in GHG emissions from LDVs that are 36% lower than in the BAU scenario in 2050.

Total GHG emissions in the OPT scenario are 5% lower than those in the BAU scenario in 2030 and 9% lower in 2050. This is a smaller percentage reduction than that from the LDV sector, because LDV emissions represent a declining share of total emissions and because of intersectoral shifts in emissions. The differences between the OPT and BAU scenarios come from greater reductions from the LDV segment (16% lower in OPT than BAU in 2030 and 36% lower in 2050); other transportation (16% lower in OPT in 2030 and 25% lower in 2050); and from the electric power sector (5% lower in OPT in 2030, and 7% lower in 2050). The Pacific region shows the largest reductions in GHG emissions in the OPT scenario compared to BAU (23% in 2030 and 22% in 2050), and the West South Central region shows the least reductions (2% in 2030, and 4% in 2050).

In diagnostic case D5, with all the OPT improvements in the LDV sector but without modifications in the electric sector, emissions from the electric sector are 2% higher in 2050 than in the BAU scenario, due to greater LDV demand for electricity. The reduction in GHG emissions from the non-LDV segment of the transportation sector in OPT versus BAU is mainly due to a shift to more efficient technologies in freight shipping. Consistent with the results for the LDV mix, LDV emissions are reduced or increased approximately in proportion to LDV demand, for both BAU and OPT scenarios. Similarly, CO_2-eq emissions do not change significantly in sensitivity tests with modified oil prices applied in either the BAU or OPT scenarios.

For both the BAU and OPT scenarios, application of moderate GHG fees reduces total CO_2-eq emissions by 11% in 2030 and by 12% in 2050. In both comparisons, the main reductions are

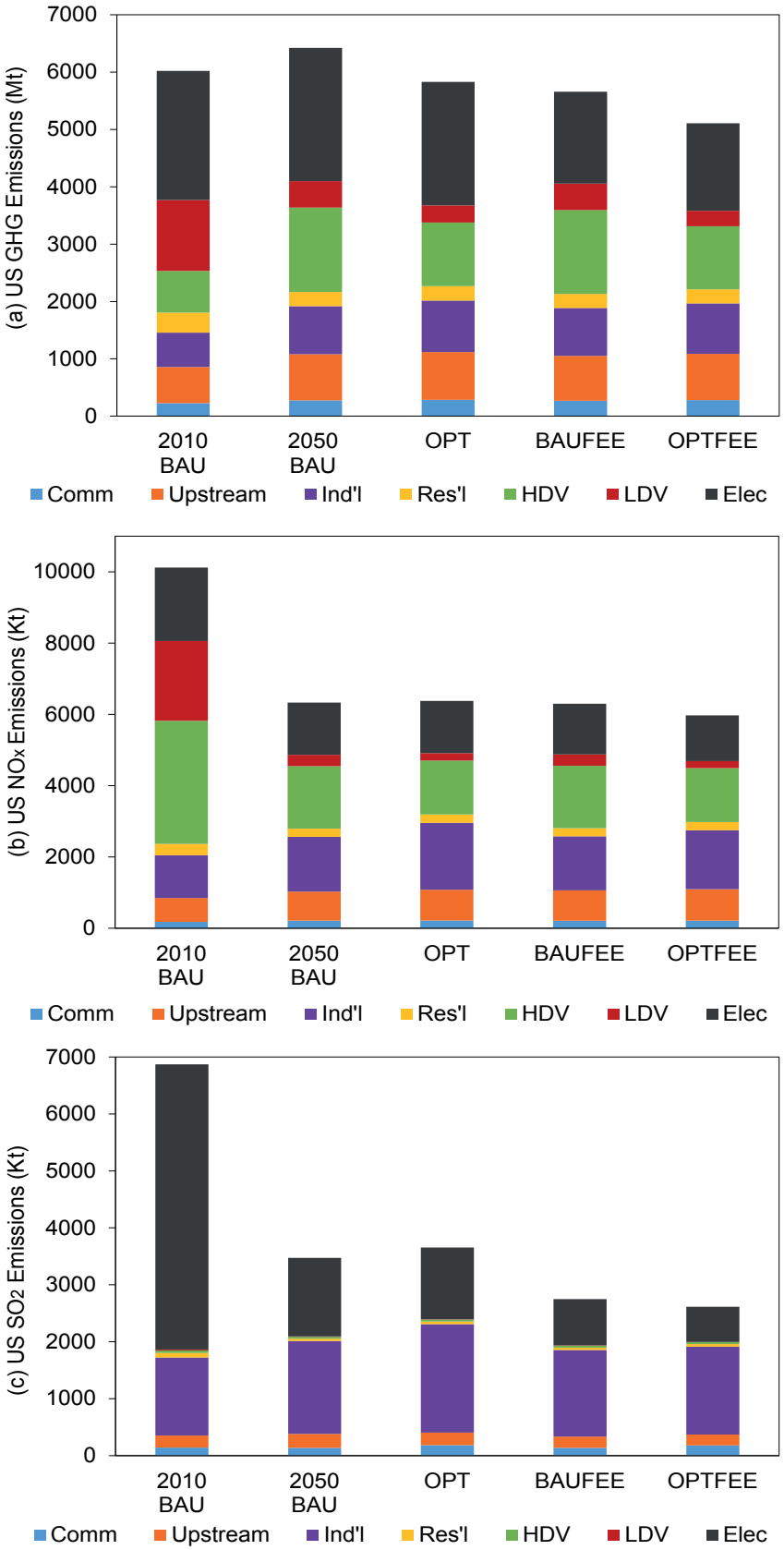

Figure 2.2. U.S. emissions in 2050 compared to BAU2010 emissions (a) GHG (b) NO_x (c) SO_2 by sectors and scenarios; HDV sector includes off-road vehicles.

from the electric power sector, based on increased use of natural gas and some renewables in place of coal. GHG emissions from the electric sector are reduced by about 40% in the BAUFEE and OPTFEE scenarios in 2030 compared to 2005. For BAU and OPT, total GHG emissions are 9–10% higher with low GHG fees and 7–9% lower with high fees compared to the moderate fee results (Figure 2.12), again mainly due to changes in electric sector emissions. For the LDV segment, GHG emissions in 2050 are only 9% lower in OPTFEE than in OPT. Thus, despite using more optimistic assumptions for EV cost and efficiency than used by Rudokas et al. (2015), our results agree with their conclusion that GHG fees would have little effect on LDV emissions. Moreover, over time LDV emissions represent a sharply declining share of total GHG emissions, even without more optimistic technology improvements or fees. On the other hand, the OPT scenario shows that applying energy system-wide GHG fees could help curtail the industrial sector emissions increases that might otherwise occur if widespread use of BEVs induced industrial sector fuel switching.

2.3.5 NO_x and SO_2 Emissions

Figures 2.2b and c show how NO_x and SO_2 emissions compare for the BAU, OPT and corresponding fee scenarios. (Results for VOC emissions are presented in Figure 2.13.) In the BAU scenario, NO_x emissions from LDV decline from about 2 million tonnes in 2010 to 0.4 million tonnes in 2030 and to 0.3 million tonnes in 2050, due to tailpipe emissions limits that have already been promulgated. In the OPT scenario, direct NO_x emissions from LDV are about 0.3 million tonnes in 2030 and 0.2 million tonnes in 2050, which is 35% lower than in the BAU scenario. However, total energy system NO_x emissions are about the same in 2050 in the OPT and BAU scenarios, because industrial sector emissions are 27% higher in the former. In the OPT scenario, the industrial sector shifts from use of electricity to use of combustion-based technologies for heat and power. However, the increase in industrial NO_x emissions in the OPT scenario is partially offset by a decrease in HDV emissions that results from use of more efficient and less polluting technologies in freight shipping, as more diesel is used in the industrial sector. Loughlin et al. (2015) similarly saw a shift in NO_x emissions from the transportation sector to other sectors in their study of NO_x emissions

reduction pathways, including vehicle electrification. Application of GHG emissions fees has little impact on LDV NO_x emissions.

The transportation sector makes a negligible contribution to SO_2 emissions (Figure 2.2c). However, SO_2 is of interest with EVs because of the possibility of increased emissions from the electric sector. In the BAU scenario, SO_2 emissions from electricity generation fall from 5 million tonnes in 2010 to 1.4 million tonnes in 2050 because of existing control requirements and the shift away from coal-fired generation. This reduction is modestly countered in the BAU scenario by an increase in SO_2 emissions from the industrial sector. In the OPT scenario, SO_2 emissions from the industrial sector in 2050 are 20% higher than in the BAU scenario in 2050, due to increased direct fuel use in place of electricity. This change offsets the reductions from the electric sector that result from less use of coal-fired power generation in the OPT scenario. GHG fees reduce total SO_2 emissions in the BAUFEE and OPTFEE scenarios, respectively, by 17% and 22% in 2030, and by 21% and 28% in 2050. Most of the reductions occur in the electric sector in the BAU scenario; in the OPT scenario emissions from the industrial sector are reduced as well.

2.3.6 Well-To-Wheel Emissions

We highlight the impact of potential improvements in LDV efficiency by using our OPT scenario results to calculate WTW GHG emissions from gasoline ICEV and BEV technologies. WTW results for NO_x, and SO_2 were also calculated and are presented in Figures 2.14 and 2.15. On average for 2010, we estimate WTW GHG emissions of 186 and 450 gCO_2-eq mi^{-1} for full-size BEV100 and gasoline-fueled ICEVs in the U.S., respectively. For BEV100, 89% of the emissions are from electricity generation and 11% from upstream fuel sectors. For ICEVs, 88% of emissions are from the use phase, 7% from the refinery, and 5% from fuel production. WTW GHG emissions for full-size BEV100 drop to 94 gCO_2-eq mi^{-1} in 2030 and 62 gCO_2-eq mi^{-1} in 2050. For full-size ICEVs, emissions are 181 gCO_2-eq mi^{-1} in 2030 and 121 gCO_2-eq mi^{-1} in 2050. Thus by 2050, the WTW GHG emissions estimated for both technologies are about one-third of those estimated for 2010. The percentage contributions across WTW stages are relatively constant over time, for

both BEVs and ICEVs. Elgowainy et al. (2016) estimates higher WTW GHG emissions for midsize ICEV, and BEV90 in 2015 and 2030, than our estimations for full-size (combination of midsize and large) cars in those years. Our range for BEV is also slightly higher.

In addition to the WTW GHG emissions estimated based on the average national electricity mix, we also calculated average WTW emissions for each MARKAL region (see Figure 2.16). Regional WTW GHG emissions for full-size BEV100 range from 96 to 219 gCO_2-eq mi^{-1} in 2010, 42 to 121 gCO_2-eq mi^{-1} in 2030, and 35 to 83 gCO_2-eq mi^{-1} in 2050. Thus the highest regional WTW emissions in 2050 are less than the lowest regional WTW emissions in 2010. Across the full time horizon, the lowest BEV WTW GHG emissions correspond to the Pacific region, which has a low share of electricity from coal power plants and high hydropower resources. We find the highest emissions for the West North Central region, which has the highest share of generation from coal (59% in 2030 and 54% in 2050 in the OPT scenario). Our regional rankings for EV WTW emissions in 2015 match those presented by Nealer et al. (2015); however, their study did not consider future scenarios.

Although not directly examined in this study, vehicle cycle emissions are also important in comparing across technologies. Elgowainy et al. (2016) estimated emissions from vehicle manufacturing of about 41 gCO_2-eq mi^{-1} for current midsize ICEV, and about 64 gCO_2-eq mi^{-1} for BEV90 vehicles. In the future, these emissions are expected to decline as electricity sector emissions are reduced and manufacturing processes become more efficient. However, as light duty vehicles generally become more efficient, with lower WTW emissions, the vehicle production cycle will likely comprise an increasing fraction of total life cycle emissions. Thus, in future assessments greater attention needs to be focused on vehicle manufacturing and recycling impacts, as well as on upstream emissions and on the potential for intersectoral shifts.

2.4 SUPPORTING INFORMATION

2.4.1 MARKAL Regions

Figure 2.3 depicts the nine MARKAL regions, which are based on the U.S. Census Divisions, and the states located in each region.

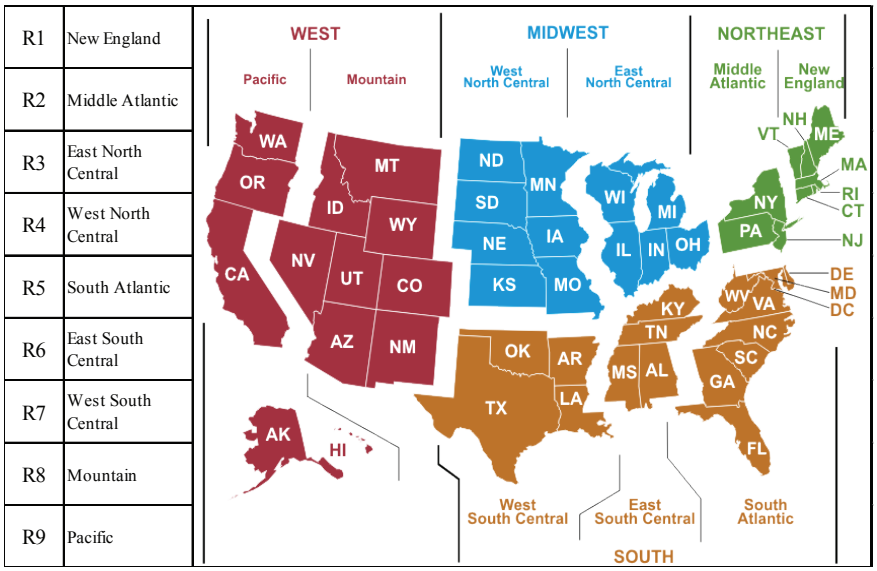

Figure 2.3. Map of U.S. Census Divisions (EIA, 2017b) and the U.S. EPA MARKAL region associated with each Division (Lenox et al., 2013).

2.4.2 Light Duty Vehicle (LDV) Demand

LDV demand applied in the BAU scenario is based on AEO2014 (EIA, 2014a) reference LDV demand projections. The reference demand is modified for the OPT scenario based on the 2014 Census population projections leading to lower demand after 2040 (U.S. Census, 2014). High and low demands for sensitivity analysis are adapted from AEO2014, Figure IF4-2. Figure 2.4 shows how these high and low demands compare with the updated LDV demand in the OPT scenario and original LDV demand in the BAU scenario for the national level. Note that in the MARKAL model, demand is specified separately by region, for each scenario.

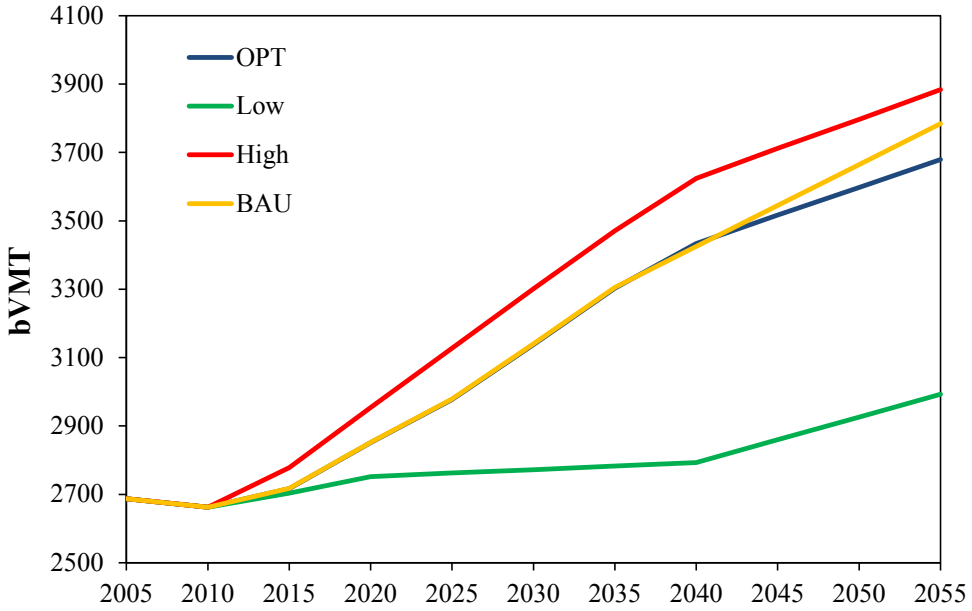

Figure 2.4. National LDV reference (BAU scenario), modified reference (OPT scenario), high, and low demands (for LDV demand sensitivity cases) in billions of vehicle miles travelled (bVMT); values are adapted from AEO2014 (EIA, 2014a).

2.4.3 Oil Prices

The reference oil prices used by EPA and in our BAU scenario are from AEO2014 (EIA, 2014a). High and low oil price projections are adapted from AEO2015, Figure 3 (EIA, 2015). Although domestic and international oil prices have diverged since mid-2010, they have followed similar trends (EIA, 2014b). Accordingly, to impose high or low oil price market conditions in the MARKAL model we apply the same trends to both mining and import supply curves. Oil prices for 2045 to 2055 are estimated by applying price growth factors from the EPA database; moreover, as oil supply curves are defined in five steps we have applied AEO price projections to step 3, as the middle step. Other steps are scaled based on EPA assumptions for supply curves in the BAU. In sensitivity cases with increased or decreased oil prices we have used reference LDV demand projections because demand does not show a very strong correlation with oil prices. Figure 2.5 shows how high and low oil prices compare with the 2014 reference prices in the BAU scenario.

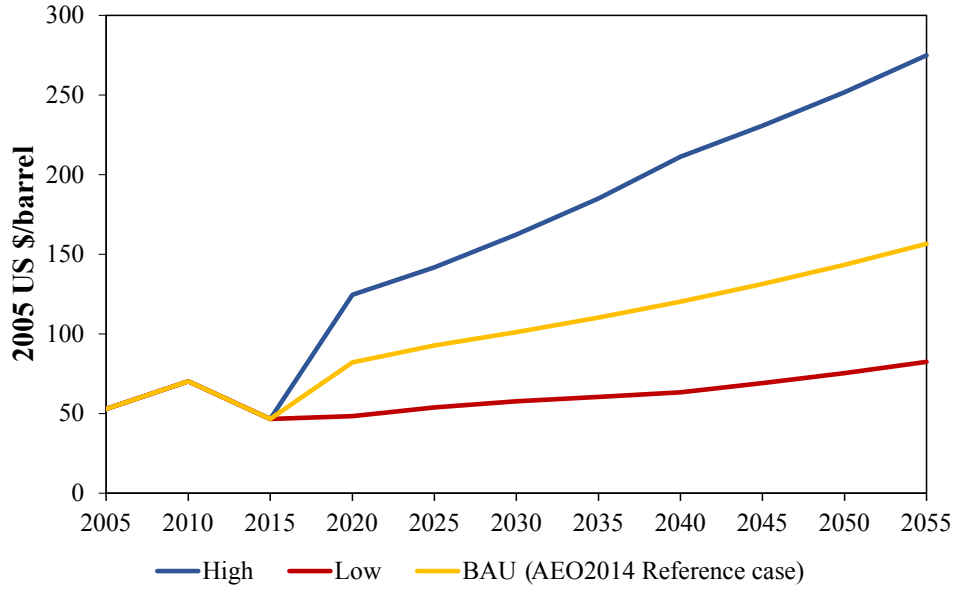

Figure 2.5. Oil Price projections for BAU scenario, and high and low price sensitivity cases. Values are adapted from EIA (2014a) and EIA (2015).

2.4.4 Changes Specific to the LDV Sector

2.4.4.1 Cost and Efficiency Projections of LDV Technologies Based on the Optimistic Case of NRC (2013)

For cost and efficiency projections we have used the NRC (2013) Excel calculation sheet (provided in Appendix F of the report). The report uses a set of base cars, including three cars from compact, midsize, and large sizes (Toyota Yaris, Toyota Camry, and Chrysler 300C, respectively), to draw an average car, and a set of base trucks, including three light trucks from small SUV, minivan, and pick up sizes (Saturn Vue, Dodge Grand Caravan, and Ford F-150, respectively), to draw an average truck. Characteristics of all base cars and trucks match their 2007 models. NRC uses averaged characteristics of these three base cars and three base trucks to represent the characteristics of its average car and truck, respectively. Average incremental costs over the baseline ICE 2010 car and baseline ICE 2010 truck are estimated for the average car and light truck in 2010, 2030, and 2050, for different technologies including ICEs, HEVs, PHEVs, and BEVs. For this study, we have replaced the three NRC base cars (trucks), which are from different size classes,

with three new base cars (trucks) from the same individual MARKAL size classes, to be able to come up with incremental cost estimates for that particular size class. That is, we have provided seven new sets of base cars and trucks, each including three cars or trucks of the same size class. Table 2.5 shows how we mapped each set of base cars and trucks with each of the seven MARKAL size classes. We have modified base cars (trucks) input characteristics, including weight, engine capacity, number of cylinders, fuel consumption, and engine power, according to the characteristics of the new base cars (trucks) in each set. Other parameters that are dependent on the vehicle's size, like battery size, are adjusted or calculated in the model based on the input characteristics in each set. For example, battery size for BEVs are calculated as a function of vehicle's range, depth of charge, battery degradation, and vehicle's efficiency in kWh mi^{-1}. Vehicle efficiency is estimated based on charging efficiency and averaged energy consumption in kWh $100mi^{-1}$, which in turn is calculated based on averaged fuel consumption over the three base cars (trucks) in each set. Further adjustments are also applied to adapt the PHEV and BEV range of 30 and 130 miles, which are NRC default ranges for these technologies, to 20 and 40 miles for PHEVs and 100 and 200 miles for BEVs, which are the default ranges in the EPA database. Baseline prices for different sizes of baseline ICE cars and trucks are extracted from the EPA database. Figure 2.6 shows the projected costs for full-size cars of different technologies and a comparison with EPA database (BAU) projections. Similar graphs are generated for other car and light truck sizes of compact, mini-compact, small SUV, large SUV, minivan, and pickup.

The NRC Committee applied Ricardo's computer simulation models (which are used in the EPA energy audit data), and Meszler Engineering's CAFE Cycle energy audit model in connection with tractive energy estimation, including all load reduction and powertrain improvements, to estimate miles per gallon for base vehicles and the other technologies in 2010, 2030, and 2050 (NRC, 2013). We did not have access to those models, consequently we have extracted scaling factors from the input information to the models for different technologies in different years to estimate improved efficiency of different vehicle sizes. These include scaling factors to project fuel economy in 2010 for the ICE technology to 2030 and 2050, scaling factors to project fuel economy

Table 2.5. Selected vehicle models for sets of base cars and trucks for each MARKAL size class.

MARKAL size class[a]	Model1	Model2	Model3
Mini-Compact	Aston Martin	Lotus Evora	Chevrolet Corvette
Compact	Toyota Yaris	Honda Civic	Chevrolet Cruze
Full-size	Honda Accord	Toyota Camry	Chrysler 300C
Small SUV	Saturn Vue	Jeep Patriot	Honda CR-V
Large SUV	Toyota FJ Cruiser	Ford Explorer	Nissan Armanda
Minivan	Dodge Grand Caravan	Nissan Quest	Toyota Sienna
Pick-up	Ford F-150	Chevrolet Avalanche	Dodge Dakota

[a] EPA aggregates mini-compact and two-seater cars from AEO into mini-compact size class in MARKAL; sub-compact and compact cars into compact; midsize and large cars into full-size; small and large vans into minivan; small and large pickup trucks into pickup.

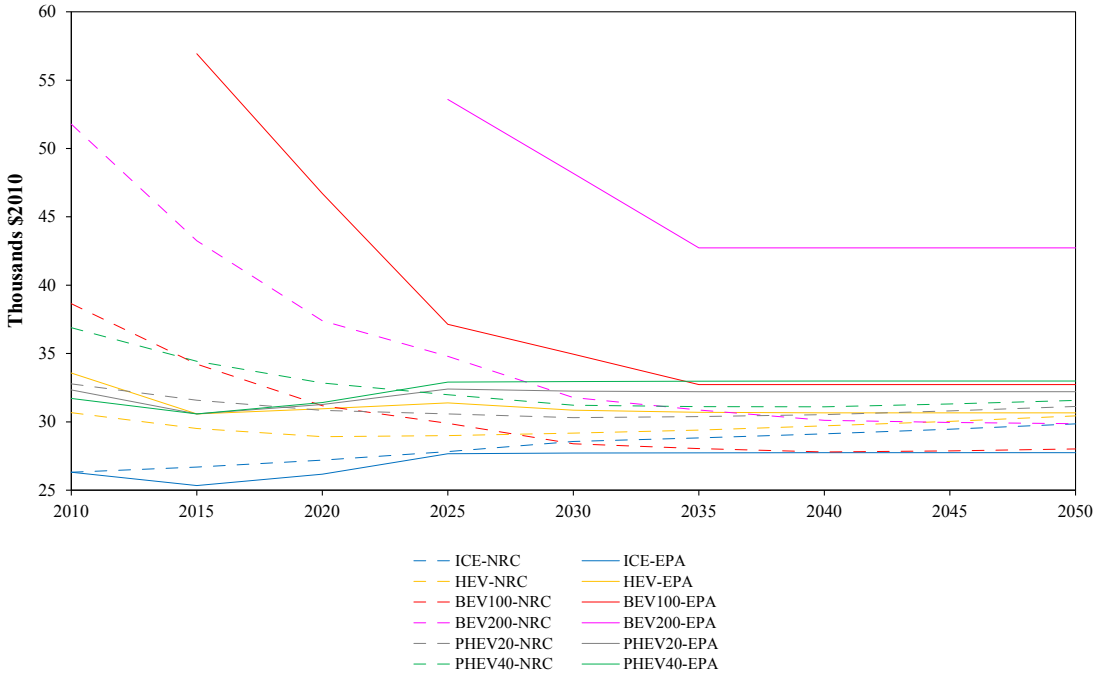

Figure 2.6. Projected cost for the OPT scenario and comparison with BAU cost estimates for full-size cars in U.S. 2010 $; values for the OPT scenario are estimated based on the optimistic case in NRC (2013).

of other technologies in 2010 from ICE in 2010, and scaling factors to project fuel economy of each alternative technology to 2030 and 2050. The fuel economy of the baseline ICE car in 2010 for each technology is estimated from the average fuel economy of the same three sample vehicles used in calculating the cost for each size. A separate scaling factor is calculated from the EPA database

for BEVs to adjust the BEV range to the EPA database defaults. Fuel economy of PHEV vehicles is treated separately as their fuel economy is assumed to be identical to their corresponding BEVs in the charge depleting (CD) mode and to HEVs in the charge sustaining (CS) mode (NRC, 2013). The following equations from Gonder and Simpson (2007) are used for calculation of PHEV fuel economy:

$$mpg_{CD,UF} = \frac{1}{\frac{UF}{mpg_{CD}} + \frac{(1-UF)}{mpg_{CS}}},\ mpg_{cycle} = \frac{1}{\frac{0.5}{mpg_{CD,UF}} + \frac{0.5}{mpg_{CS}}} \tag{2.1}$$

where UF is the utility factor, mpg_{CD} is the fuel economy in the CD mode, mpg_{CS} is the fuel economy in the CS mode, $\text{mpg}_{CD,UF}$ is the fuel economy in the CD mode after applying UF, and mpg_{cycle} is the fuel economy in the full charge and discharge modes cycle.

The Utility Factor (UF) is defined as the ratio of miles driven under CD to the total miles driven (Bradley and Quinn, 2010). There is uncertainty in the Utility Factor (UF) of PHEVs (Elgowainy et al., 2009; Jorgenson et al., 2012; NRC, 2013; Simpson, 2006). Utility factors from the NRC report are used in our study (35%, 46%, and 60% for PHEV20, 30, and 40, respectively). Figure 2.7 shows the projected fuel economy for full-size cars of different technologies and a comparison with EPA database (BAU) projections. Similar graphs are generated for other car and light truck sizes of compact, mini-compact, small SUV, large SUV, minivan, and pickup.

For both cost and efficiency estimations linear interpolation is applied to project the values for the years in between 2010, 2030, and 2050. Also, the 2050 value is applied for 2055 estimations.

2.4.4.2 Representation of CAFE Standards

In the EPA database, CAFE standards are presented as an upper bound constraint on the energy consumption in the LDV sector. The CAFE representation in the model accounts for energy consumption of all LDV technologies including the electricity needed for EVs. EPA converts the average fuel economies for the light duty sector to bVMT/PJ values using energy content (higher heating value, HHV) in each gallon of gasoline. In the current study, we have recalculated bVMT/PJ values based on lower heating value (LHV). This change tightens the CAFE implementations in the model by 7–9% in each year. Figure 2.8 shows the difference between the two calculations.

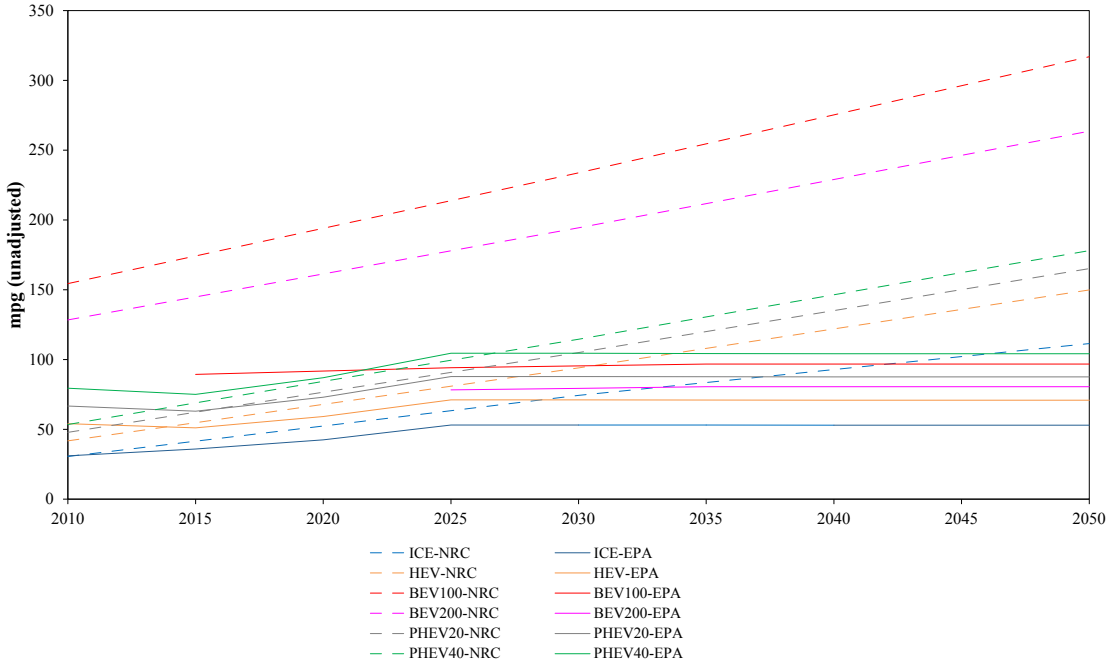

Figure 2.7. Projected unadjusted fuel economy for the OPT scenario and comparison with BAU for full-size cars in mpg; values for the OPT scenario are estimated from the optimistic case in NRC (2013).

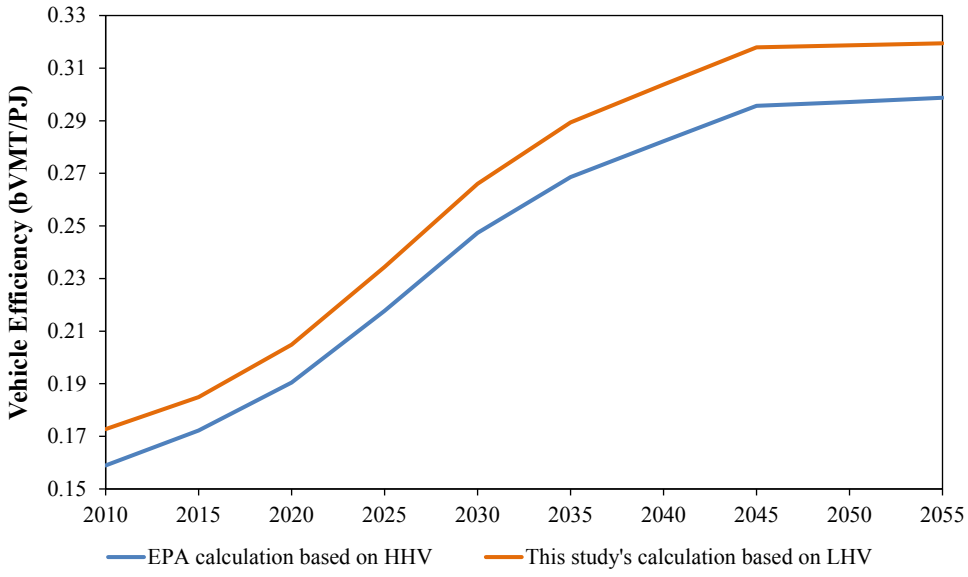

Figure 2.8. CAFE calculation comparison between BAU and OPT scenarios in bVMT/PJ.

The rationale for using LHV instead of HHV is that the energy in the exhaust water vapor is not recovered for the vehicle use therefore vehicles must be more efficient than EPA originally assumed if CAFE standards are to be met. The new calculations are applied after 2010 for the OPT scenario in this study.

2.4.4.3 LDV Investment Constraints

In the EPA database, user-defined technology investment constraints are applied to some LDV technologies like BEVs to limit their adoption rates. Our study assumes that these constraints are removed after 2025, except for the constraint that limits the adoption of BEVs with 100-mile range. This modification helps to build a competitive market for alternative technologies. A constraint should be kept in place for BEV100s, however, as not all consumers are able to adjust their driving habits to short distances. The fractions for BEV100 investments are adapted and updated from Pearre et al. (2011). The reason for choosing this study among the alternatives (Scoffield et al., 2014; Smart et al., 2013; Tamor et al., 2013; Tamor and Milačić, 2015) is that it gives nationwide estimates and uses real field data to study daily driving habits and distances, rather than theoretical formulations or survey responses. Pearre et al. (2011) relate vehicle range to the fraction of vehicles that can be utilized for different numbers of adjustment days. Adjustment days are days when drivers would change their habits (i.e., use another transportation mode, or borrow or rent vehicles) to be able to own vehicles with limited ranges like EVs. We use estimates for "six adjustment days" for the OPT scenario in our study (Pearre et al., 2011).

2.4.5 Changes Applied to the Sectors Other than the LDV Sector

In this section, we provide a summary list of the modifications and corrections applied to sectors other than the LDV sector. These modifications are mainly based on work done by other members of our research group. More details about these changes can be found in Brown (2014); Brown et al. (2014a,b); McLeod (2014); McLeod et al. (2014).

- Treatment of emissions:

  - Upstream emissions, which are not treated completely in the EPA database, are added to the end use sectors including commercial, industrial, and residential sectors; and to the fuel and energy sectors including biomass, coal, electricity, natural gas, and oil.
  - Sector-specific emissions are added to be able to have more detailed output and results on emissions.
  - Modifications are applied to the model to be able to calculate emissions from refinery and hydrogen units separately from the industrial sector.
  - Unreasonably high methane emissions for coal mining technologies, and very low CO_2 emission for biomass IGCC technologies were replaced with estimates from Venkatesh et al. (2011), and Rhodes and Keith (2005), respectively.
  - Modifications are applied to VOC and methane emissions for natural gas production technologies in order to separately account for emissions from shale gas and conventional gas production.

- Treatment of technology:
  - Investment costs of solar PV centralized generation technologies are updated.
  - New technologies and a variety of emission control technologies are added to the industrial sector.
  - CCS technologies are added as a control option for cement plants.
  - Domestic and international electricity trade costs have been modified.

- Treatment of constraints:
  - A constraint is applied to limit the lifetime of coal-fired power plants to 75 years.

2.4.6 GHG Fees

Low, moderate, and high CO_2 and methane fees have been adapted from Marten and Newbold (2012). Table 2.6 presents these fee values in 2005 US $/Metric tonne.

Table 2.6. Social cost of CO_2 and CH_4 applied as economy-wide fees to BAU and OPT scenarios (2005 US $/Metric tonne), years 2020-2055.

	2020	**2025**	**2030**	**2035**	**2040**	**2045**	**2050**	**2055**
CO_2 (Moderate)	40	44	49	55	60	67	73	80
CH_4 (Moderate)	1036	1224	1507	1695	1977	2354	2731	3107
CO_2 (High)	60	67	73	81	89	94	104	113
CH_4 (High)	1412	1601	1883	2166	2542	2919	3296	3672
CO_2 (Low)	12	14	16	19	22	24	27	30
CH_4 (Low)	518	621	753	895	1036	1224	1412	1601

2.4.7 Diagnostic Cases

Table 2.7 shows the list of our six diagnostic cases, which are designed to help understand the effect of each modification on the final results. Diagnostic case 1 (D1) includes only the modifications applied to the CAFE constraints and input LDV travel demand that are described in Table 2.2, with all other parameters kept the same as BAU. The rest of the cases are defined in a similar way, with only the specified modifications in each case applied to the BAU. Results for LDV fuel/technology penetration are shown in Figure 2.9 for each case.

Table 2.7. Description of diagnostic cases.

Diagnostic case	**Description**
1	Incorporates CAFE and LDV demand modifications
2	Incorporates LDV efficiency and cost modifications
3	Incorporates LDV hurdle rate and investment constraints modifications
4	Incorporates Diag.2 and Diag.3 modifications
5	Incorporates all modifications in the LDV sector
6	Incorporates all modifications implemented in the OPT scenario except those specific to the LDV sector

2.4.8 Annualized Unit Cost of Vehicle Ownership

The annualized unit cost of vehicle ownership in a certain year for a particular technology is the sum of the annualized unit upfront cost, unit fuel cost, and unit fixed and variable operation

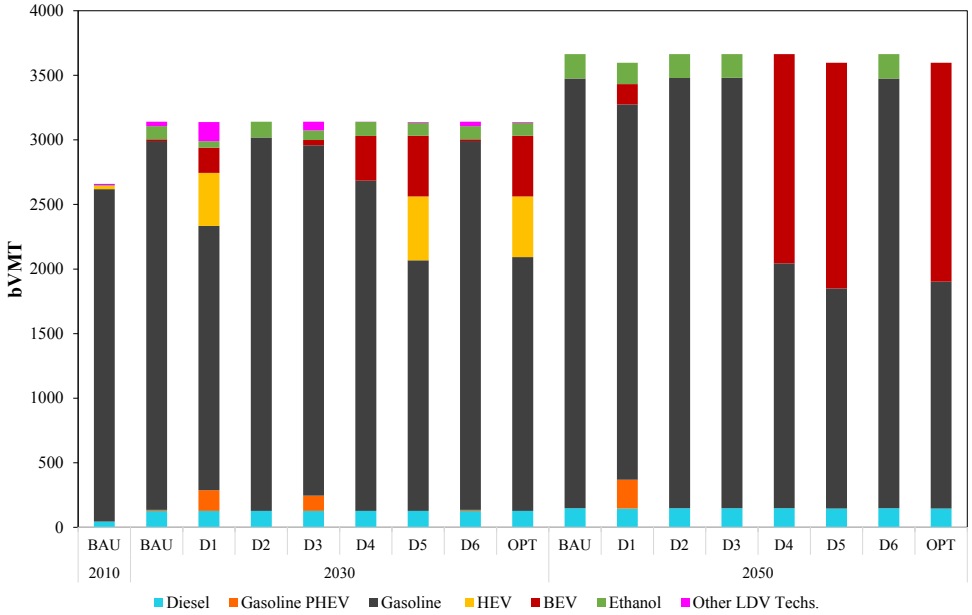

Figure 2.9. Comparison graph of LDV penetration for the six diagnostic cases, BAU, and OPT scenarios.

and maintenance (O&M) costs (Loulou et al., 2004). To convert the costs to the unit costs, EPA assumes 11976 miles for average annual vehicle mileage for the LDV sector. Technology specific hurdle rates (h), which are defined separately in the BAU and OPT scenarios (as mentioned in Table 2.2), are used to convert the lump sum unit investment cost (INVCOST) of a technology to annualized unit investment cost over its lifetime (LIFE) by using (Loulou et al., 2004):

$$ANNUALIZED_{INVCOST} = \frac{INVCOST}{\sum_{j=1}^{LIFE}(1+h)^{-j}} \tag{2.2}$$

2.4.9 Additional Results

2.4.9.1 Crude Oil Consumption

Figure 2.10 shows the total crude oil consumption for BAU, OPT, BAUFEE, and OPTFEE scenarios. The "error bars" show the crude oil consumption for the BAUHIOIL, BAULOOIL, OPTHIOIL, and OPTLOOIL sensitivity cases. In the BAU scenario, gasoline consumption is reduced in 2030 compared to 2010, but remains unchanged in 2050 compared to 2030, despite increased LDV demand. Optimistic assumptions for LDV efficiency and cost in the OPT scenario

result in significant reduction in gasoline consumption in 2030 and 2050 compared to BAU. However, this reduction is offset by increases in other refined products. Application of moderate GHG fees had negligible impact on total crude oil and gasoline consumption in both BAU and OPT scenarios in the entire time horizon.

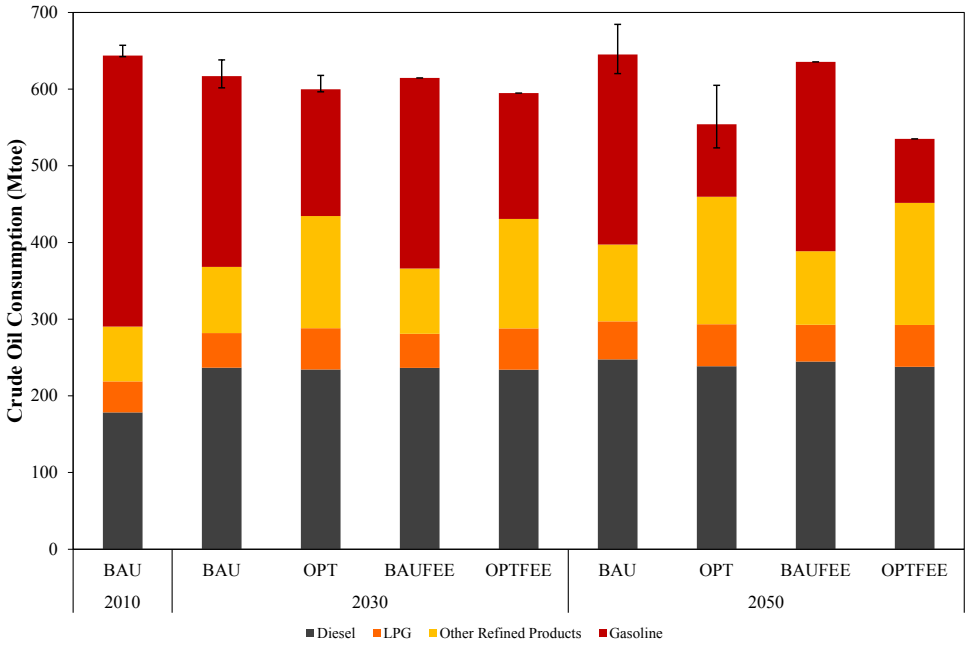

Figure 2.10. Comparison graph of crude oil consumption (Mtoe) for BAU, OPT, BAUFEE, and OPTFEE scenarios. The "error bars" show crude oil consumption for the high and low oil price sensitivity cases.

2.4.9.2 GHG Emissions Calculated Based on GWP_{20}

GHG emissions results with CO_2-eq calculated based on the 20-year GWP for methane are shown in Figure 2.11. The results show the same pattern as those calculated from GWP_{100}, but with a higher magnitude of CO_2-eq emissions. For example, total emissions in 2010 are increased from 6000 Mt CO_2-eq with GWP_{100} to 7000 Mt with GWP_{20}. The main difference comes from the upstream emissions, where methane from coal mining and production of natural gas has a large impact. Methane emissions are not significant in the LDV sector in this study, due to negligible use of CNG vehicles.

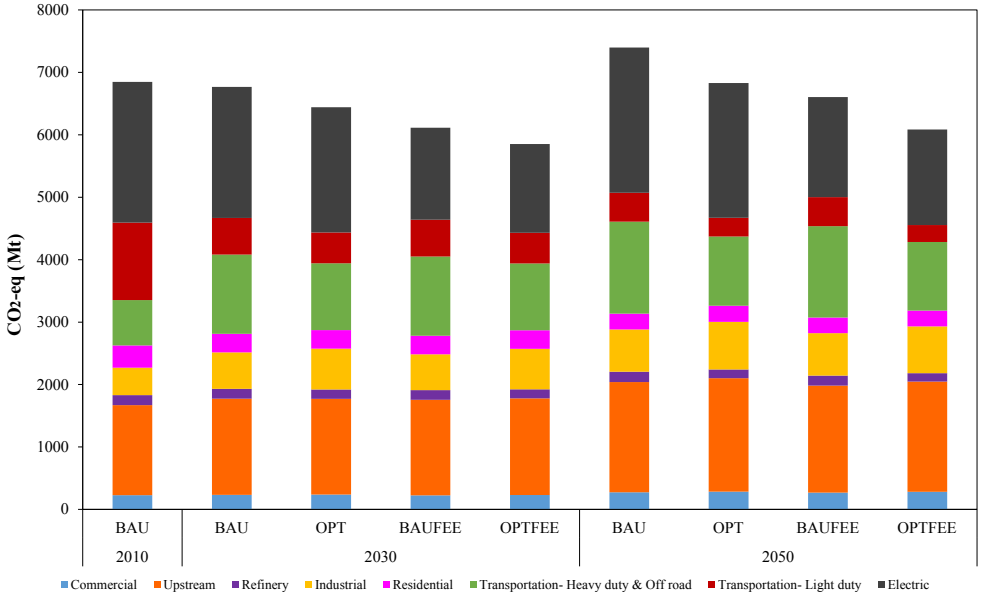

Figure 2.11. Comparison graph of GHG emissions calculated based on GWP_{20} for BAU, OPT, BAUFEE, and OPTFEE scenarios in Mt of CO_2-eq.

2.4.9.3 GHG Emissions for Low and High GHG Fees

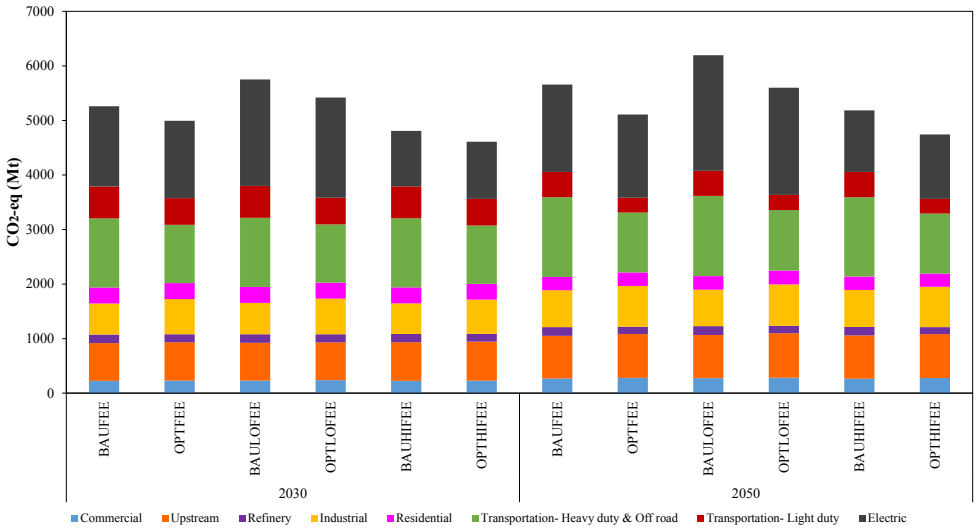

Figure 2.12. Comparison graph of GHG emissions calculated based on GWP_{100} for moderate, high, and low GHG fee cases in Mt of CO_2-eq.

Figure 2.12 compares the impact of high and low GHG fees with that of moderate fees on GHG emissions for both BAU and OPT scenarios in 2030 and 2050. GHG emissions decrease and

increase in response to the high and low fees, respectively, in both BAU and OPT scenarios. The electric sector is the main contributor to the change in GHG emissions. Similar to the moderate fees, low and high GHG fees have little impact on the LDV sector. In both BAUHIFEE and OPTHIFEE cases, 3–4% of GHG emission reductions are achieved through electricity generation from technologies equipped with carbon capture and sequestration.

2.4.9.4 VOC Emissions

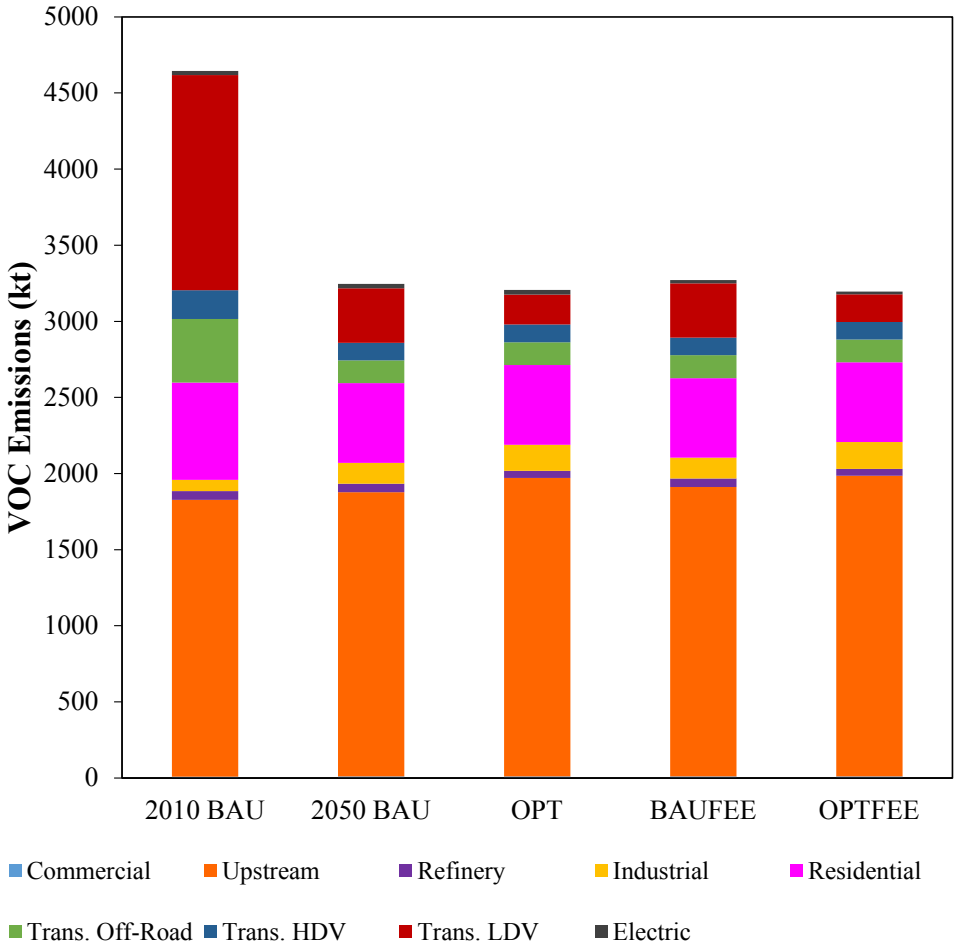

Figure 2.13. VOC emissions in 2050 in kt for BAU, OPT, BAUFEE, and OPTFEE scenarios compared to BAU emissions in 2010.

Figure 2.13 depicts the VOC emissions in the BAU, OPT, BAUFEE, and OPTFEE scenarios

in 2050. In the BAU scenario, VOC emissions from the LDV segment decline sharply from 1.4 million tonnes (30% of the total) in 2010 to about 0.3 million tonnes (11% of the total) in 2030 and 0.4 million tonnes (11% of the total) in 2050. The decline from the LDV sector is partially offset by an increase in upstream emissions. These emissions could be mitigated by additional controls in the oil and gas production sector that are not currently represented in the EPA US9R database. In the OPT scenario, VOC emissions from the LDV segment are about 0.3 million tonnes in 2030 and 0.2 million tonnes in 2050, which is 45% lower than in the BAU scenario. However, total VOC emissions are similar in the BAU and OPT scenarios in 2050, as the 0.1 million tonne reduction in LDV emissions is offset by higher upstream and industrial emissions, due to increased use of natural gas for electricity generation. Application of GHG emissions fees leads to negligible change in total VOC emissions for both BAU and OPT scenarios.

2.4.9.5 Well-To-Wheel Emissions

Figure 2.14 compares the WTW NO_x emissions of full-size BEV100 and gasoline ICEV in 2010, 2030, and 2050. Based on our OPT scenario, national average WTW NO_x emissions from a full-size BEV100 drop from 295 $mgNO_x$ mi^{-1} in 2010 to 143 $mgNO_x$ mi^{-1} in 2030, and to 84 $mgNO_x$ mi^{-1} in 2050. In comparison, WTW emissions from a full-size ICEV are estimated to be 191 $mgNO_x$ mi^{-1} in 2010, 114 $mgNO_x$ mi^{-1} in 2030, and 85 $mgNO_x$ mi^{-1} in 2050. Electricity generation accounts for most of the WTW NO_x emissions for BEV100. In 2010, just over half of WTW NO_x emissions for ICEV come the use phase, with the rest approximately split between upstream production and processing. The share from the use phase increases in later years. In 2010, regional average BEV100 emissions range from 94 $mgNO_x$ mi^{-1} in the Pacific region to 396 in the West North Central region. This range drops to 41 to 218 $mgNO_x$ mi^{-1} in 2030, and to 30 to 133 $mgNO_x$ mi^{-1} in 2050, with the lowest emissions rate occurring in the New England region in 2050.

Figure 2.15 compares the WTW SO_2 emissions of full-size BEV100, and gasoline ICEV in 2010, 2030, and 2050. Under the OPT scenario, we find national average WTW SO_2 emissions

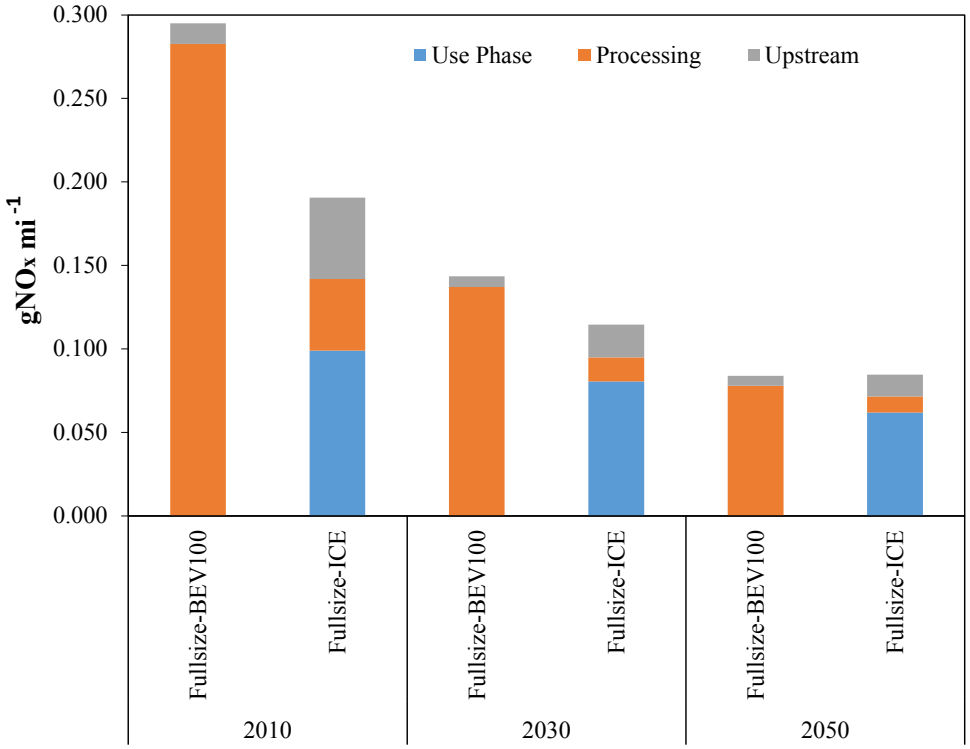

Figure 2.14. Comparison of WTW NO_x emissions from the OPT scenario for full-size BEV100, and ICEV technologies.

for a full-size BEV100 of 435 $mgSO_2$ mi^{-1} in 2010, 203 $mgSO_2$ mi^{-1} in 2030, and 102 $mgSO_2$ mi^{-1} in 2050. In comparison, we find WTW emissions for a compact ICEV of 53 $mgSO_2$ mi^{-1} in 2010, 18 $mgSO_2$ mi^{-1} in 2030, and 13 $mgSO_2$ mi^{-1} in 2050. WTW SO_2 emissions for BEV100 are predominantly (98%) from electricity generation. Those for ICEV come mainly from refineries (70% in 2010 changing to 64% in 2050). Regional WTW emissions for BEV100 in 2010 range from 45 $mgSO_2$ mi^{-1} in the Pacific region to 664 $mgSO_2$ mi^{-1} in the West North Central region. This range is lowered to 20 to 362 $mgSO_2$ mi^{-1} in 2030, and to 5 to 199 $mgSO_2$ mi^{-1} in 2050. The minimum emissions rate occurs in the New England region in 2050. Thus, whether BEV or ICEV have lower WTW emissions of SO_2 and NO_x depends on location, due to sharp regional differences in the electricity mix.

Figure 2.16 compares the WTW GHG emissions calculated for full-size BEV100 for each

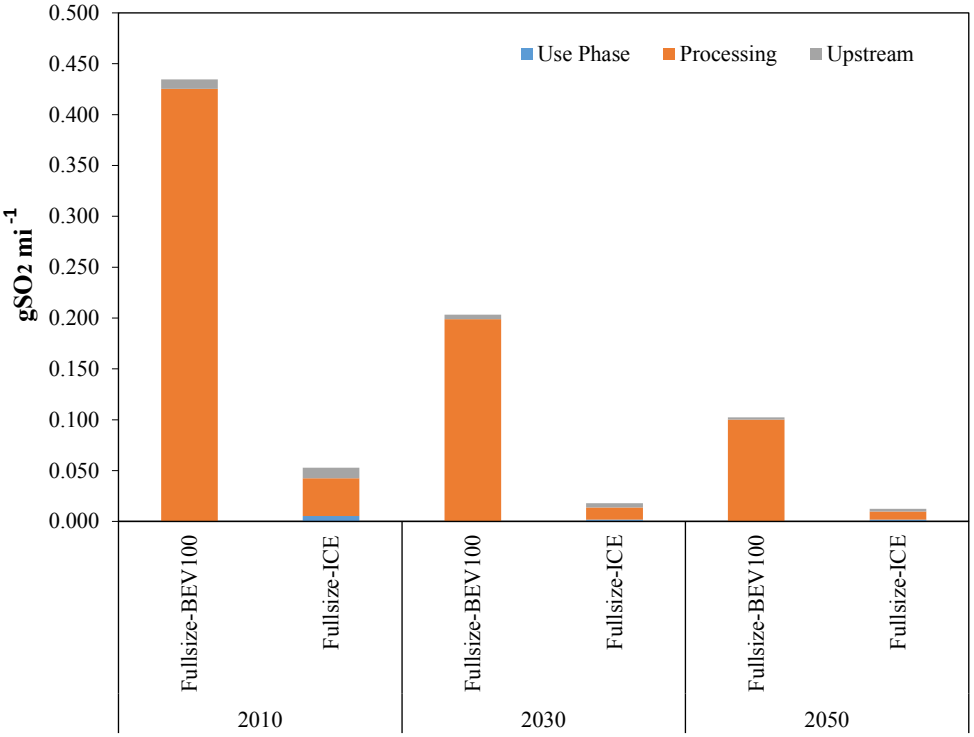

Figure 2.15. Comparison of WTW SO_2 emissions from the OPT scenario for full-size BEV100, and ICEV technologies.

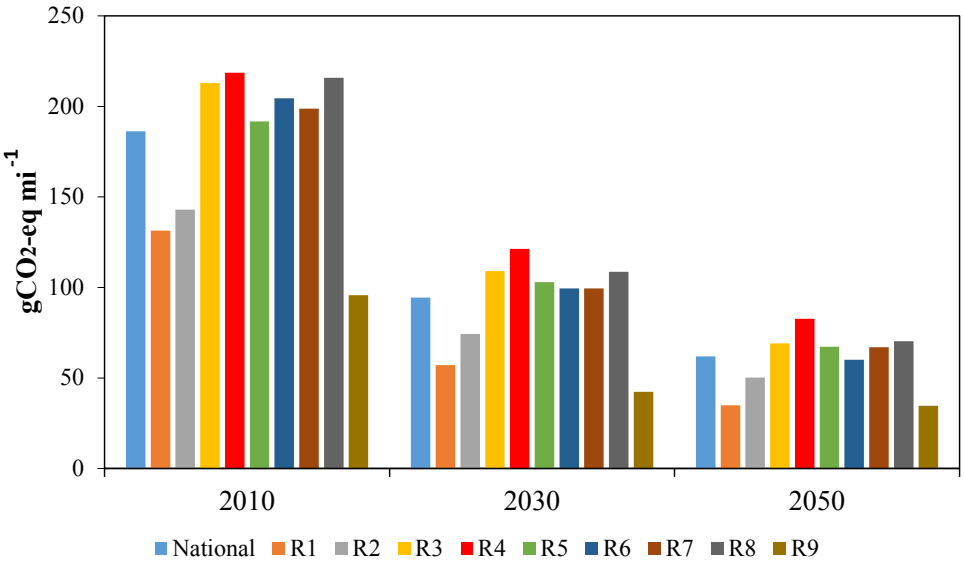

Figure 2.16. Comparison of regional WTW GHG emissions from the OPT scenario for full-size BEV100 technology.

region based on regional electricity mixes from the OPT scenario. The maximum WTW GHG emissions in the entire time horizon correspond to the West North Central region, which has the largest share of electricity generation from coal. The minimum WTW emissions belong to the Pacific region with little generation from coal and with high hydropower resources.

Chapter 3

Cradle-to-Gate Environmental Impacts of Sulfur-Based Solid-State Lithium Batteries for Electric Vehicle Applications[1]

3.1 INTRODUCTION

Recent interest in fleet electrification to mitigate greenhouse gas (GHG) emissions and dependence on oil has motivated research into developing high energy density batteries suitable for electric vehicle (EV) applications, both plug-in hybrid (PHEV) and battery electric vehicles (BEV). Currently, Li-ion batteries (LIBs) are used for EV applications; however, the need for lighter batteries with higher energy densities to provide longer vehicle range has encouraged efforts to develop new chemistries. Lithium batteries offer higher gravimetric and volumetric energy densities than LIBs (Väyrynen and Salminen, 2012). Lithium batteries utilize lithium metal for the anode, whereas graphite or lithium titanate are used in LIBs (Väyrynen and Salminen, 2012). On the other hand, solid-state batteries show potential advantages over those using liquid electrolytes, as they have no electrolyte leakage and vaporization problems; they show very long cycle life, and they enable the use of electrode materials delivering higher energy densities (Takada, 2013). They also are considered a solution for safety issues associated with the flammable organic solvent used in LIBs (Takada, 2013). The safety concerns worsen when the size of the battery increases for EV applications (Takada, 2013). For all of these reasons, solid-state lithium batteries are considered a promising candidate for EV applications.

The biggest disadvantages of solid-state batteries are the low ionic conductivity of the solid

[1] The content of this chapter is from a manuscript in preparation for submission to *Journal of Cleaner Production*

electrolyte, which has prompted ongoing research focusing on the development of solid electrolytes with high conductivity (Takada, 2013). So far, high conductivities have been achieved in several oxide- and sulfide-based electrolytes but not all are compatible with lithium electrodes, whereas one of the main objectives for developing solid-state electrolytes is to enable the use of electrodes with high energy densities (Takada, 2013). Compatibility with lithium anode is seen in the sulfide-based glass electrolytes (Takada, 2013). However, application of lithium anode lowers the cell voltage compared with graphite (Takada, 2013). Moreover, the sulfide-based systems are more convenient for fabricating bulk-type solid-state batteries in contrast to the oxide systems (Takada, 2013). This is because sulfide systems do not necessarily need any sintering process and preparation of electrolyte materials is possible using mechanical milling (Takada, 2013). For all of these reasons, we focus on sulfide systems, which show promise for mass production and EV applications (Goldman Sachs Group Inc., 2017).

In this study, we address the cradle-to-gate environmental impacts of sulfur-based solid-state lithium batteries using a process-based attributional life cycle assessment (LCA) method. We identify the major differences in battery assembly processes and associated environmental impacts of solid-state lithium batteries versus LIBs with the help of a case study of a solid-state pyrite battery. This battery has shown a relatively high theoretical specific capacity of 894 mAh g^{-1} at 60 °C and is in the preparation stage for pilot-scale production by Solid Power (Yersak et al., 2013). Our framework, however, can be applied to any other solid-state lithium batteries, in particular, those with sulfide-based electrolyte.

Some common elements of LIBs are not required for solid-state lithium batteries, such as a negative current collector (Cu), separator (as the solid electrolyte serves as the separator at the same time), cooling system and corresponding thermal management system, formation cycling, and charging for charge retention testing. The solid-state pyrite battery also requires thinner insulation compared to the LIB. These features along with the relatively high specific capacity can offer the environmental benefits over a counterpart LIB. However, the solid-state pyrite battery delivers lower open circuit voltage (OCV) compared to the counterpart LIB (1.80 V vs. 3.95 V at 50%

state-of-charge (SOC)), which results in needing more cells in series to build up the voltage for EV applications (280-400 V) (Dunn et al., 2015b; Nelson et al., 2012; Zackrisson et al., 2010). Moreover, the manufacturing of a sulfide-based solid-state lithium battery demands a larger clean dry-room compared to the current chemistries for LIBs (Goldman Sachs Group Inc., 2017). The energy requirement for the clean dry-room application is considered the most significant contributor to the energy consumption and the environmental burdens of LIBs cell manufacturing (Dunn et al., 2012; Ellingsen et al., 2014; Nelson et al., 2012). These factors potentially offset the environmental benefits of a solid-state pyrite battery (Goldman Sachs Group Inc., 2017).

Previous EV-related LCA studies compared several battery chemistries including LIB chemistries and pre-LIB chemistries such as lead-acid, nickel-cadmium, and nickel-metal hydride batteries, in order to help identify environmentally reasonable choices for EV applications (Matheys and Autenboer, 2005; Sullivan and Gaines, 2010, 2012). Over the past decade, several studies have tried to address the environmental impacts of traction LIBs with different chemistries and performances for EV applications. Peters et al. (2017) have provided a comprehensive review of this literature, including 36 studies, most of which relate to traction batteries for EV applications. We add another study conducted recently by Kim et al. (2016) to the LIB literature. Kim et al. (2016) address the cradle-to-gate emissions from a commercial LIB for a Ford Focus BEV. Six of the EV-focused studies (Amarakoon et al., 2013; Dunn et al., 2015b; Ellingsen et al., 2014; Majeau-Bettez et al., 2011; Notter et al., 2010; Zackrisson et al., 2010) reviewed by (Peters et al., 2017) served as the main sources for LCI data for the rest of the studies. Only a few LCA studies have considered chemistries using Li metal for the anode (Deng et al., 2017; Lastoskie and Dai, 2015; Troy et al., 2016; Zackrisson, 2017). Deng et al. (2017), in particular, focus on Li-S batteries based on the notion that sulfur has a relatively high specific capacity, is abundant, and is known to be less environmentally harmful compared to the heavy metals in LIBs. However, their battery still utilizes a liquid electrolyte. Two recent studies have analyzed the environmental impacts of known Li-ion cathode chemistries with a solid-state electrolyte, again utilizing Li for the anode (Lastoskie and Dai, 2015; Troy et al., 2016). In both studies, the electrolyte is an oxide-based material versus the

sulfur-based electrolyte considered in this study (Lastoskie and Dai, 2015; Troy et al., 2016). Troy et al. (2016) present LCA results for a small lab-scale battery (4.2 g); their study is not particularly focused on the EV applications. Lastoskie and Dai (2015) consider a different battery assembly process (vacuum vapor-deposited thin film) than examined by Troy et al. (2016) and in this study. In summary, we contribute to the literature by investigating the environmental impacts of a pyrite battery that benefits from sulfur-based material, a solid-state electrolyte, and lithium as the anode, all at the same time. We compare our results with the environmental impacts of current traction LIBs and these latter studies.

We conduct a prospective LCA because the pyrite battery is an emerging technology that has been produced only at the lab-scale. We utilize a combination of laboratory data, U.S. patents, thermodynamic and engineering calculations, existing literature and the US-EI 2.2 LCA database to develop a battery manufacturing processing scheme for solid-state batteries and to estimate the battery mass inventory, the energy requirements for battery manufacturing processes and clean dry-room requirements, and the environmental impacts of different materials and processes involved. We also conduct sensitivity analysis to examine the uncertainties associated with some input assumptions, including the effect of cleaner electricity production on environmental impacts of solid-state lithium batteries.

The goal of this study is to provide reasonable insight regarding the environmental impacts of sulfur-based solid-state lithium batteries, suitable for EV applications, in the earlier stages of development and to recognize the major contributors to the environmental burdens of this type of battery. Although prospective LCAs are subject to larger uncertainties compared to the LCAs conducted for mature established products, they can provide reasonable insight and recommendations regarding the environmental burden of a new product before design and mass production schemes are finalized. We use the solid-state pyrite battery for our case study; however, our major conclusions and recommendations can be expanded to other sulfide-based solid-state lithium batteries.

3.2 METHODS

3.2.1 System Boundary

This study is focused on the cradle-to-gate LCA of a solid-state pyrite battery, applicable as a traction battery for EVs. The study focuses on the battery itself; other EV components are outside the system boundary. Our analysis does not include the impacts of manufacturing capital equipment and infrastructure for the battery assembly processes. We further assume no credit from recycling in our analysis, for a few reasons. First, the environmental benefits from recycling can vary depending on the technology and battery chemistry, and no established recycling technology is yet available on a large industrial scale for recycling of new battery chemistries including solid-state pyrite batteries (Peters et al., 2017). Second, it is uncertain if the recycled materials are of adequate grade to be reusable in battery manufacturing. Third, it is also uncertain how energy intensive the recycling steps might be, or whether recycling might offset some environmental benefits from switching to a new chemistry (Peters et al., 2017). Finally, according to Dunn et al. (2015a), if the assembly process comprises up to 60% of battery cradle-to-gate energy consumption, significant energy reduction may not be possible via recycling.

3.2.2 Functional Unit

We define the functional unit as the battery nominal energy capacity (80 kWh). This choice is based on the rationale that the main function of the battery is delivering energy to EVs. Furthermore, this functional unit does not depend on assumptions about the powertrain and includes major battery characteristics such as specific energy capacity, depth-of-discharge (DOD), and charging efficiency (Majeau-Bettez et al., 2011). Presenting the results based on the nominal energy capacity can be useful for a wide range of users, as they can be converted to results based on miles-driven for any powertrain assumptions.

3.2.3 Battery Characterization and Configuration

The battery uses iron pyrite (FeS_2) for the cathode with titanium sulfide (TiS_2) as the conductive material, lithium as the anode, and lithium sulfide (Li_2S) and phosphorous pentasulfide (P_2S_5) for the solid-state electrolyte (Yersak et al., 2013). We consider a battery pack with target 80 kWh energy capacity and 100 kW power, capable of powering a BEV with 200-mile range (BEV200) on the U.S. Environmental Protection Agency (EPA) Corporate Average Fuel Economy (CAFE) test cycle. The battery energy requirement for a specified BEV range is adapted from estimates developed by the National Research Council (NRC) Committee on Transition to Alternative Vehicles and Fuels (NRC, 2013). NRC (2013) estimated the required efficiency (kWh mi^{-1}) for driving a BEV with a certain range in two steps. First, they estimated the traction energy that is delivered to the wheels of a vehicle and is required to navigate the CAFE test cycle. In the second step, they estimated the required energy input to the vehicle (fueling rate) by working backward from the wheels to the vehicle engine and considering various energy transfer mechanisms and their associated losses (NRC, 2013). The NRC Committee estimated efficiencies for an average car and an average truck with a 130-mile range. Our previous work presents how we project these efficiencies for seven vehicle size classes and other BEV ranges including BEV200 (Keshavarzmohammadian et al., 2017). We utilize the efficiencies estimated for model year 2010. The pack energy requirement is estimated by applying 80% depth of discharge (DOD), and 10% battery deterioration over the battery cycle life (NRC, 2013). The cycle life of the pyrite battery is not determined yet; however, our study assumes that the battery lasts the life of an EV. The battery pack contains four modules in a row, each including 53 cells (212 cells per pack). This battery pack configuration assumes no parallel cells and modules. According to the documentation of Argonne National Laboratory (ANL) BatPac model, moving to cells with higher capacities and with only series connections reduces the cost of the battery (Nelson et al., 2012). Based on these battery characteristics and configuration, the average battery mass is estimated at 440 kg (358–554 kg). Accordingly, the specific energy of the pyrite battery is estimated as 182 Wh kg^{-1} (144–223 Wh

kg^{-1}). This is higher than the specific energy of current LIB chemistries, including lithium nickel cobalt manganese oxide (NCM), advanced lithium nickel cobalt manganese oxide (LMR-NCM), lithium cobalt oxide (LCO), LMO, lithium iron phosphate (LFP), lithium nickel cobalt aluminum oxide (NCA), and lithium nickel cobalt oxide (LCN), which are reported to range from 52–175 Wh kg^{-1} (Kim et al., 2016; Peters et al., 2017). However, it is lower than those which are reported by Lastoskie and Dai (2015) for solid-state batteries with NCA, LMO, NCM, and LCO chemistries (ranging from 220–300 Wh kg^{-1}); by Dunn et al. (2015a) for LMR-NCM with SiC anode (200 Wh kg^{-1}); by Li et al. (2014) for NCM with silicon nanowire anode (360 Wh kg^{-1}); and by Deng et al. (2017) for a Li-S battery (220 Wh kg^{-1}). See also Table 3.4 in the results section. The pyrite battery has only been produced at the lab scale. Section 3.4.1 explains how the mass of the battery pack is estimated from the lab composition.

3.2.4 Battery Manufacturing and Assembly Process

The starting point for the manufacturing processes description for the pyrite battery is the LIB production practices described in the BatPac documentation (Nelson et al., 2012). Adjustments have been made for the pyrite battery based on personal correspondence with staff at Solid Power, accounting for the different cell chemistry and structure from those of LIBs. Figure 3.1 illustrates a simplified diagram of the pyrite battery assembly. Cathode components (positive active material, the conductive material, binder, and solvent) are mixed to make the cathode paste. In LIBs, this process is also done for the anode. However, Li serves as the anode for lithium batteries and this process is eliminated. Accordingly, no copper current collector is needed. The cathode is then coated on both sides of the aluminum foil (positive current collector) through the coating, drying (the solvent), and calendering processes. While in LIBs the electrolyte is in the liquid form and is added to the cell at the latter stages of the cell assembly, before the cell closure, here electrolyte is treated in a similar way as the cathode. That is, the electrolyte paste (electrolyte materials, binder, and solvent) is prepared through a mixing process and then is coated on the cathode-coated foil through the same processes as those for the cathode. The electrolyte serves as the separator, as well.

The coated foil undergoes a slitting and stacking process (during which the anode is also attached) similar to the LIBs. Cell assembly is completed by laminating the cell, welding of cell terminals to the electrodes, and enclosing the cell in a pouch. In LIBs, the pouch serves as the container for the liquid electrolyte. The solid-state electrolyte does not actually need a sealed pouch; however, we assume an enclosure is needed to avoid cell exposure to the air. Also, an enclosure is required when the cell assembly is done in a different location than the module and pack assembly. Therefore, we assume the same pouch as for LIBs is used for the pyrite battery (as is current common practice). For the LIBs, the cells undergo formation cycling and charge retention testing before they are sent to the module assembly units. The solid-state pyrite battery does not need formation cycling. This chemistry presents in the fully-charged state initially, as opposed to LIBs with discharged initial status. This feature eliminates the charging process needed before the charge retention testing for the pyrite battery.

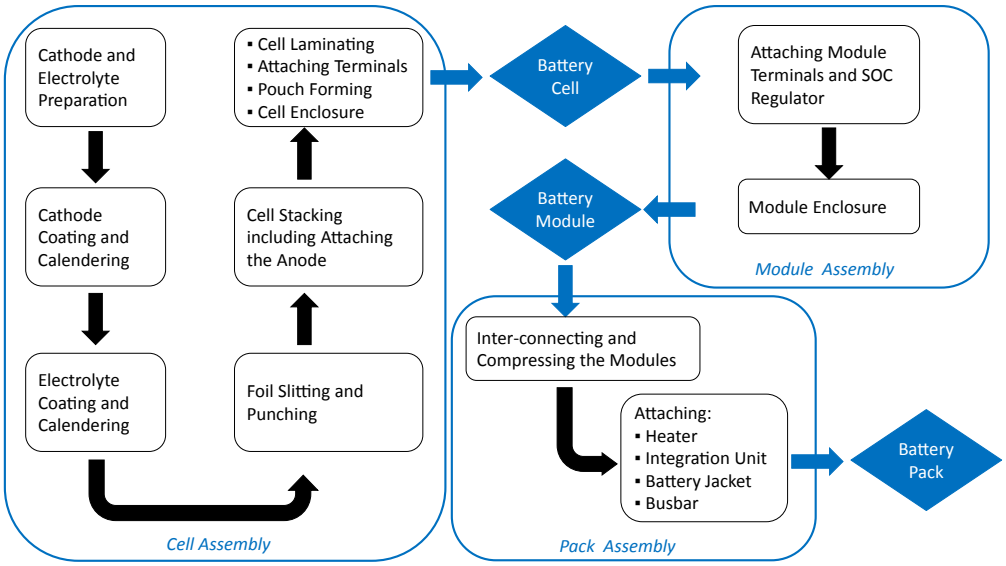

Figure 3.1. Simplified diagram for pyrite battery manufacturing

In the module assembly unit, the adjacent cells are connected via laser-welding, and the module is assembled by welding the module terminals, attaching the SOC regulator, and enclosing the module in its casing, using fasteners (Nelson et al., 2012). Note that the pyrite battery does not need a cooling system or a spacer for gas release. Accordingly, all the required trays, radiators,

and the coolant are eliminated for this battery.

For the pack assembly, the modules are compressed using compression plates and straps (Nelson et al., 2012). A busbar is needed if the modules are arranged in one row (Nelson et al., 2012). Battery heater and battery management system (BMS), are attached and the battery jacket encloses the pack (Nelson et al., 2012). BMS measures the pack current and voltage, balances the module voltages, estimates SOC and state-of-health (SOH) for both module and pack, and monitors and signals the battery thermal management (Nelson et al., 2012). The pyrite battery does not need a cooling system, which in turn can reduce the mass of BMS, also it needs thinner insulation compared to the LIBs. However, we conservatively assume the same mass for BMS and the same thickness of the insulation as those for LIBs, due to the uncertainty in the final design of the solid-state pyrite battery.

3.2.5 Impact Assessment

The energy requirements per unit mass, area, or stroke of the individual processes are estimated based on the energy requirements of laboratory equipment. To estimate the energy requirements for the clean dry-room, we choose the average climate design data of Reno, Nevada, with average annual temperature and relative humidity of 12.1 °C and 45.6%, respectively (Weatherbase, 2017). Clean rooms demand higher air change rates (ACH) compared to general-purpose buildings (ASHRAE, 2015). We adapt the ACH from the American Society of Heating, Refrigerating and Air-Conditioning Engineers (ASHRAE) recommendations for clean spaces (ASHRAE, 2015). Section 3.4.2 details how we estimate the energy requirement for the clean dry-room and the related assumptions. The requirement of clean dry-room conditions for battery manufacturing could impose a high energy demand for keeping the area dry and clean at the same time. Sulfur-based solid-state lithium batteries need larger dry rooms compared to LIBs, for the same production capacity (Goldman Sachs Group Inc., 2017).

To estimate the environmental impacts of the materials and the manufacturing processes, we utilize the US-EI 2.2 database, which is one of the databases accessible from the Ecoinvent Center,

and the Tool for the Reduction and Assessment of Chemical and other environmental Impacts (TRACI 2.1_1, V1.02) for the impact assessment. The ten midpoint impact categories available in TRACI 2.1_1 are ozone depletion potential (ODP), 100-year global warming potential (GWP100), photochemical smog formation (PSF), acidification (ACD), eutrophication (EUT), carcinogenics (CAR), non-carcinogenics (NCA), respiratory effects (RPE), ecotoxicity (ECO), and fossil fuel depletion (FFD). We also add cumulative energy demand (CED) to the list of impacts. For the description of these categories see Section 3.4.3.

Pyrite is an abundant mineral and can be found in different types of rocks, as well as coal beds (Klein et al., 1993; Uni Of Minnesota, 2017). It is rarely mined for its direct use (Uni Of Minnesota, 2017). Recently, however, pyrite has received attention due to its potential for cathode applications (Kim et al., 2007; Yersak et al., 2013) and its significant share in the solid-waste from coal mining (Oliveira et al., 2016). In the US-EI 2.2 database, the data for pyrite is approximated from iron mining, lime crushing, and lime mining. This is due to a lack of information for production processes of pyrite. See also Section 3.4.4.

For materials that are not found in the database (Li_2S, P_2S_5, and TiS_2) or are not commercially available (TiS_2), we use information in U.S. patents for the possible chemical reactions and processes leading to that particular product from the precursor materials for which LCI data are available (Jacob and Brown, 1978; Taylor, 1965; Wainer, 1958). We estimate the energy requirements for the associated heating processes for material production based on the thermodynamic calculations (Section 3.4.4). Our calculation assumes 100% reaction yield. To examine the uncertainty associated with this assumption we conduct a sensitivity case, described in the "Sensitivity Analysis" section, below. For the processes that are similar to those for LIBs, we select the same processes from the database as proposed by Ellingsen et al. (2014) (Section 3.4.4).

For battery manufacturing processes in the U.S., we adapt the medium voltage electricity mix based on the US-EI 2.2 database. This mix assumes 46% generation from coal, 21% nuclear, 20% natural gas, 8% hydropower, 3% wind and solar, and 2% generation from other resources. We examine the sensitivity of our results to a scenario with cleaner electricity production (see

"Sensitivity Analysis" section).

The location of a solid-state pyrite battery factory in the U.S. is not defined yet, therefore, we adapt the average distances and transportation modes from assumptions made by the U.S. Environmental Protection Agency (EPA) (Amarakoon et al., 2013). Section 3.4.4 presents the main assumptions about primary and secondary materials and transportation distances. To examine the uncertainties associated with the assumptions regarding the shipping and transport distances, we conduct a sensitivity analysis case (see "Sensitivity Analysis" section). Section 3.4.4 also presents the detailed inventories of the battery pack components and processes and the corresponding impact entries from the US-EI 2.2 database.

3.2.6 Sensitivity Analysis

To understand the impact of uncertainties associated with our input assumptions we examine the sensitivity of our results to the reaction yields for TiS_2, Li_2S, and P_2S_5 production, shipping and transport distances, and cleaner electricity mix. Table 3.1 lists the sensitivity cases and the assumptions that distinguish them from the original calculations.

Table 3.1. Sensitivity cases in this study.

Sensitivity case	**Description**
Reaction yield	Assumes reaction yields for TiS_2, Li_2S, and P_2S_5 productions are reduced to 50% vs. the original calculation assuming 100% reaction yields.
Shipping and transport distances	Assumes the shipping distance by oceangoing vessels from China to California remains the same as the original calculation, but the transport distances are doubled vs. the original calculation. This case assumes shipping distance of 7300 miles by oceangoing vessels from China to California and an average distance of 520 miles for 5% of loads (by mass) transported by trucks and 1706 miles for 95% of loads (by mass) transported by railcars for the domestic transport.
Cleaner electricity generation mix	Assumes generation from coal is halved, generation from natural gas is doubled, and generation from wind and solar is increased by 10% vs. the original calculation. This case assumes 23% generation from coal, 13% from nuclear, 41% from natural gas, 5% from hydropower, 13% from wind and solar, and 5% from other generation technologies.

3.3 RESULTS AND DISCUSSION

In this section, we present and discuss the battery mass inventory and total impact of battery production for cumulative energy demand and for the ten midpoint impact categories, analyzed by TRACI 2.1_1 (V1.02) based on the battery nominal energy capacity (kWh^{-1}) functional unit. We also present the contribution of each battery assembly stage to the total impacts for each category. In addition, we present the sensitivity of our results to reaction yields, shipping and transport distances, and a cleaner electricity generation mix.

3.3.1 Mass Inventory

Table 3.2 summarizes the mass of different elements used for a 440 kg battery pack with 80 kWh energy capacity. Table 3.6 provides a complete version of this table; it also presents the mass inventory for the estimated maximum and minimum battery mass of 554 and 358 kg, respectively.

Table 3.2. Estimated mass inventory of a pyrite battery cell, module, and pack with 80 kWh energy capacity.

Element	**Mass**
Cell(g)	
Positive active material (FeS_2)	470
Cathode conductive material (TiS_2)	470
Negative active material (Li)	109
Electrolyte (Li_2S)	184
Electrolyte (P_2S_5)	259
Positive current collector foil (Al)	98
Terminals	84
Binder (PMMA)	73
Cell container (PET-Al-PP)	84
Total Cell	**1833**
Module (g)	
Cells	97125
Module hardware	994
Total Module	**98120**
Pack (kg)	
Modules	392.5
Pack hardware	47.5
Total Pack	**440**

According to this estimation, battery cells comprise 88% of the total mass of the battery pack mass. Kim et al. (2016) argue that in their study and also based on Ellingsen et al. (2014)'s study of commercial batteries, the cells comprise about 60% of the total mass of the battery pack for LIBs, while in the studies that are not based on primary manufacturer data, cells account for more than 80% of total mass of the battery pack. In our study, this share increases compared to LIBs, partly due to the elimination of some pack elements such as the cooling system and trays. In the pyrite battery, cathode paste and positive current collector comprise 52.5% of total pack mass, anode share is 5%, the share of electrolyte paste is 22.5%, and the share of the rest of the battery components is about 20%. These numbers are different across studies even with the same chemistry. Ellingsen et al. (2014) and Deng et al. (2017) present 25.7% and 49.16% for aggregated cathode paste and current collector shares, respectively; 23.2% and 8.44% for aggregated anode paste and negative current collector shares, respectively; 10.8% and 15.85% for aggregated electrolyte and separator shares, respectively; finally, 40.3% and 26.55% for the shares of the rest of the components, respectively. Shares from Kim et al. (2016) study are 40% for all electrodes and current collectors, 12% for electrolyte and separator, and 48% for the rest of the components. Note that Ellingsen et al. (2014) and Kim et al. (2016) both utilize NCM LIB battery chemistry based on primary data and Deng et al. (2017) utilize Li-S chemistry with liquid electrolyte.

Figure 3.3 shows the breakdown of the mass composition by material. Pyrite and TiS_2 (cathode active and conductive materials, respectively) have equal shares of the total battery mass, 23% each. Li_2S and P_2S_5 (electrolyte) comprise 9% and 12% of total battery mass, respectively. Lithium metal comprises 5% of total pack mass. In our battery, the shares of aluminum and plastics are slightly lower (by 3%) than those reported by Ellingsen et al. (2014), but the shares of copper and steel are significantly lower (by 9% and 12%, respectively). This is mainly because the pyrite battery does not have a copper current collector or cooling system. The share of pyrite is almost equal to the share of cathode paste in the NCM battery studied by Ellingsen et al. (2014). That is, part of the energy-intensive metal extraction associated with cathode production in LIBs chemistry is replaced with pyrite, which is abundant and less energy-intensive to extract (see also "Energy

Use" section).

3.3.2 Energy Use

We present the direct energy requirements for manufacturing of a pyrite battery cell and pack, as well as cradle-to-gate CED for the battery. We normalize the energy requirements by capacity to facilitate comparison with other studies. The major processes in the cell manufacturing with considerable energy consumption include different mixing processes, coating and calendering, pouch forming, and the clean dry-room applications. We estimate 735 MJ kWh^{-1} for the cell manufacturing direct energy requirements. The detailed energy requirements of each individual process are listed in Table 3.16. The energy requirement for clean dry-room applications comprises 96% of cell manufacturing direct energy requirements, assuming Reno, Nevada, for the location of the factory and annual production of 28125 packs each having 80 kWh capacity. The total direct energy requirement for the pack production is 736 MJ kWh^{-1}, conveying the fact that cell production is the major contributor to the direct energy requirements of total pack production. Although direct energy requirements for battery assembly may be different for different battery chemistries, due to mixing requirements and size of dry-room, CED is a more instructive impact category for overall comparison of different chemistries. CED shows the life cycle energy requirements, accounting for differences in embedded energy for production of different materials. We estimate the total CED of about 3300 MJ kWh^{-1} for the pyrite battery. An estimated 72% of CED is from fossil fuels, 23% from nuclear, and 5% from biomass, wind, solar, geothermal, and water (hydropower). Dry-room has the biggest share of the total CED (75%), followed by the cathode paste (10%) (Figure 3.2). Mining of pyrite has a negligible contribution to the CED impacts of cathode paste. Xylene is the biggest contributor (56%) to the CED impacts of cathode paste, followed by TiS_2 (30%).

Dunn et al. (2015a) estimate about 0.8 MJ $mile^{-1}$ (0.5 MJ km^{-1}) CED for production of an electric vehicle excluding the battery. Our estimation of CED for pyrite battery production is 2.2 MJ mi^{-1}, assuming 120000 miles for vehicle life. This is higher than CED for production of other parts than battery. In our estimation for 80 kWh battery capacity, we utilized adjusted efficiency of

35 kWh per 100 miles for BEV200 from our previous work (Keshavarzmohammadian et al., 2017), adapted from NRC (2013). Assuming 90% charging efficiency and 35% average power generation efficiency results in about 4.0 MJ mi^{-1} energy consumption for the use phase of an electric vehicle. This compares at 2.2 MJ mi^{-1} for production of battery.

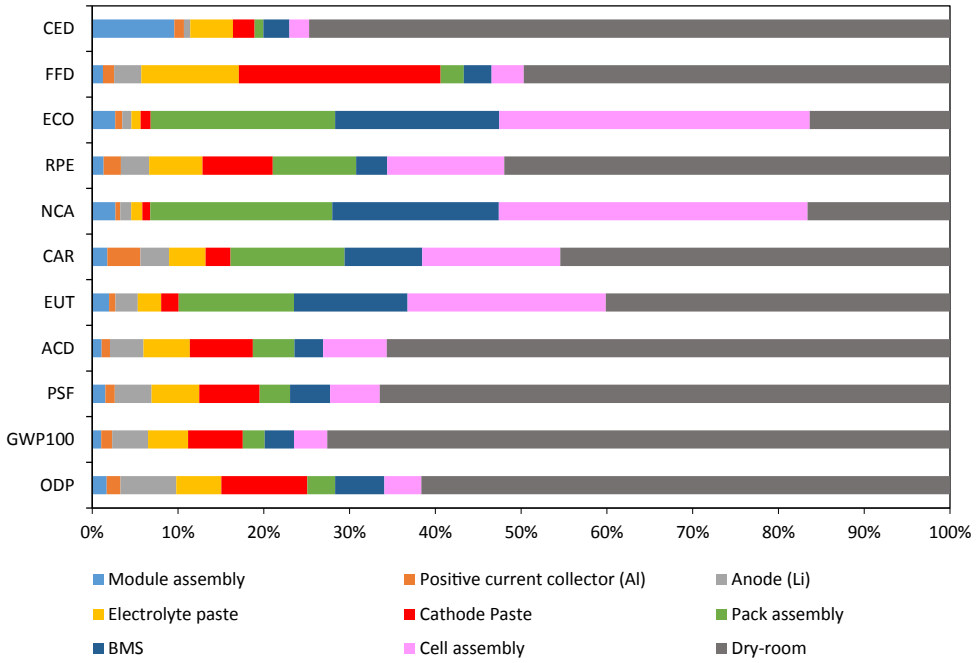

Figure 3.2. Share of different battery stages to the battery production impacts for the average battery weight. ODP: Ozone depletion potential; GWP_{100}: global warming potential, calculated based on 100-year; PSF: photochemical smog formation; ACD: acidification; EUT: eutrophication; CAR: carcinogenics; NCA: non-carcinogenics; RPE: respiratory effects; ECO: ecotoxocity; FFD: fossil fuel depletion; CED: cumulative energy demand.

3.3.3 Environmental Impacts

Table 3.3 shows total impacts of battery production based on the nominal energy capacity functional unit. Figure 3.2 details the contribution of each battery stage to the total impacts for the average weight. The numerical values for impacts of each stage are presented in Table 3.17.

As shown in Figure 3.2, the impacts of dry-room energy requirements are the biggest contributor to the total GWP_{100} and PSF impacts (73% and 66%, respectively), followed by cathode paste

Table 3.3. The total impacts of production for a pack with a nominal capacity of 80 kWh. The impacts are normalized by this nominal capacity

Impacts[a]	**Units**	
ODP	kg CFC-11 eq kWh^{-1}	1.02×10^{-05}
GWP_{100}	kg CO_2 eq kWh^{-1}	1.99×10^{02}
PSF	kg O_3 eq kWh^{-1}	9.81×10^{01}
ACD	kg SO_2 eq kWh^{-1}	1.16×10^{00}
EUT	kg N eq kWh^{-1}	1.12×10^{00}
CAR	CTU_h kWh^{-1}	1.63×10^{-05}
NCA	CTU_h kWh^{-1}	1.51×10^{-04}
RPE	kg $PM_{2.5}$ eq kWh^{-1}	8.66×10^{-02}
ECO	kg CTU_e kWh^{-1}	3.68×10^{03}
FFD	kg MJ surplus kWh^{-1}	1.87×10^{02}

[a] ODP: Ozone depletion potential; GWP_{100}: global warming potential, calculated based on 100-year; PSF: photochemical smog formation; ACD: acidification; EUT: eutrophication; CAR: carcinogenics; NCA: non-carcinogenics; RPE: respiratory effects; ECO: ecotoxocity; FFD: fossil fuel depletion.

(6% and 7%, respectively) and electrolyte (5% and 6%, respectively). Cell assembly has the same share of total PSF impacts as electrolyte (6%). Dry-room energy requirements are also the biggest contributor to the total RPE impacts (52%), followed by cell assembly (14%) and pack assembly (10%). Overall, dry-room energy requirements are the biggest contributor to the impacts of eight categories out of ten (ranging from 40% for EUT to 73% for GWP100), except for NCA (17 %) and ECO (16%). Cell assembly has the biggest share of total impacts for NCA and ECO (36% both). Impacts of cathode paste are also significant in ODP, ACD, and FFD categories. Similarly, the impacts of pack assembly are significant in ECO, NCA, CAR, and EUT categories; those of BMS are significant in ECO, NCA, EUT and ODP categories; finally, the impacts of electrolyte are significant in FFD.

Dry room, cathode paste, and electrolyte are the stages that contribute most to GWP_{100} impacts, with the share from cathode paste coming mainly from TiS_2 and xylene (40% each). Li_2S is the main contributor (31%) to GWP_{100} impacts of electrolyte. However, P_2S_5 and xylene show a comparable share to those from Li_2S (28% and 26%, respectively). Similarly, dry room, cathode

paste, electrolyte, and cell assembly are the stages that contribute most to PSF impacts, with the share from cathode paste coming mainly from TiS_2 (46%). Li_2S is the main contributor (42%) to PSF impacts of electrolyte and cell terminal production is the main contributor (49%) to PSF impacts of cell assembly. Finally, cell assembly and pack assembly are the stages that contribute most to RPE impact, with the share from cell assembly coming mainly from cell terminal production (80%). Production of busbar is the main contributor (56%) to the RPE impacts of pack assembly. For the major contributors to the impacts of each stage and category see Table 3.18.

The GWP_{100} and FFD impacts of xylene are considerable for both cathode and electrolyte pastes. It should be noted that in theory, the solvent is dried off completely in the drying step after each round of coating and is recovered in solvent recovery units for reuse. That is, a certain amount of solvent should be enough for mass scale production. However, as is common practice in Li-ion LCAs, the solvent is considered for each pack individually. Other options of solvent for the pyrite battery can be tetrahydrofuran (THF) and heptane. For all ten impact categories, THF generates more impacts per kg than xylene (Figure 3.5). Heptane generates more impact than xylene for eight categories out of ten, except for FFD and GWP_{100} (Figure 3.5).

Our results show that the energy requirements of clean dry-rooms are significant. This conveys that significant attention should be paid to the location of the factory, with preference given to locations with dry weather conditions, and to the dehumidification system design. Shifting the location of the facility from Reno, Nevada (Section 3.4.2) to Sugar Land, Texas increased the GWP_{100} impacts of the dry-room from 146 kg CO_2 eq kWh^{-1} to 196 kg CO_2 eq kWh^{-1} (by 34%, proportional to the energy requirements). Other impacts of dry-room are also increased by the same factor.

In our study, we do not address the impacts of capital equipment including the HVAC system. Downsized HVAC equipment also helps to reduce those impacts. We also do not address the impacts of capital equipment for capture and oxidation of CO, which is the by-product of the suggested reaction for production of TiS_2 (Section 3.4.4.2). Production of each pyrite pack with 80 kWh energy capacity results in about 50 kg of CO emissions, assuming 100% reaction yield. Assuming

28125 annual pack production, which is a moderate level, results in CO annual emission of 1403 metric ton, so a control device may be required to oxidize CO to CO_2.

We estimate the GWP100 impact of about 133 g CO_2 eq mi^{-1} for each pyrite pack with 80 kWh energy capacity, assuming 120000 miles for vehicle life. As we explained in the methods section, this battery can power a BEV200 on the EPA CAFE test cycle. In our previous work, we estimated well-to-wheel (WTW) GHG emissions of a full-size BEV200 and a full-size gasoline vehicle (GV) in 2010 as 224 and 450 g CO_2 eq mi^{-1}, respectively (Keshavarzmohammadian et al., 2017). These values are derived based on efficiencies and fuel economies adapted from the same NRC report as that utilized here for sizing the battery (NRC, 2013). The efficiencies and fuel economies used in WTW GHG emissions calculations are adjusted values (Keshavarzmohammadian et al., 2017). Thus, GWP_{100} of pyrite battery pack production is lower than use phase impacts of both technologies. Moving toward more efficient vehicles would reduce the impacts of use phase for both technologies. WTW GHG emissions for the optimistic (OPT) scenario in 2030 from our previous work are 114 g CO_2 eq mi^{-1} for BEV200 and 181 g CO_2 eq mi^{-1} for gasoline vehicle (GV) (Keshavarzmohammadian et al., 2017). This scenario adapts the EV and GV efficiencies from the optimistic case in the NRC report and assumes shorter life for coal power plants (Keshavarzmohammadian et al., 2017; NRC, 2013). These results show that with improved vehicles' efficiencies, the GWP100 impacts of pyrite battery production becomes comparable with those from operation of BEV200s and GVs.

Previous studies have estimated higher GHG emissions from BEV manufacturing compared to the counterpart GV, where the difference mainly comes from the GHG emissions from the battery manufacturing (ANL, 2016; Dunn et al., 2012; Hawkins et al., 2013; Kim et al., 2016; Majeau-Bettez et al., 2011; Nealer et al., 2015; Notter et al., 2010). They also estimate lower GHG emissions from battery production compared to the rest of the BEV components (ANL, 2016; Dunn et al., 2012; Hawkins et al., 2013; Kim et al., 2016; Majeau-Bettez et al., 2011; Nealer et al., 2015; Notter et al., 2010). The estimated GHG emissions from BEV manufacturing excluding battery manufacturing (which is almost equal to GHG emissions from GVs production) in these studies range from 50–75 g

CO_2 eq mi^{-1}, assuming 120000 miles vehicle life. The GWP_{100} impacts of pyrite battery production (133 g CO_2 eq mi^{-1}) are higher.

Comparison of ACD impacts of battery production with WTW SO_2 emissions is also instructive, although not all ACD impacts come from SO_2 emissions. Thus, our comparison assumes SO_2 emissions are the major contributor to the ACD impacts of battery production. In our previous work, we estimated WTW SO_2 emissions of a full-size BEV200 and a full-size GV in 2010 as 511 and 37 mg SO_2 mi^{-1}, respectively (Keshavarzmohammadian et al., 2017). We estimate ACD impacts of about 733 mg SO_2 mi^{-1} for production of the pyrite battery. This is higher than WTW SO_2 emissions from vehicle use phase.

3.3.4 Sensitivities

Our sensitivity analysis with respect to the reaction yield for TiS_2, P_2S_5, and Li_2S shows that assuming 50% reaction yield increases total impacts of all ten categories by amounts ranging from 1.7% for ECO impacts to 13.5% for ODP. The increases come from the cathode and electrolyte pastes. The increase in the impacts of cathode paste ranges from 25.8% for FFD to 88.1% for ODP. Those for electrolyte paste range from 27.2% for FFD to 91.1% for NCA. A reaction yield normally is under 100%, due to losses, impurities in reactants, side reactions, and incomplete reaction.

The share of transportation to the total impacts ranges from 0.1% for EUT to 2.3% for PSF in the original calculations. Doubling the transport distances increases the shares of transportation impacts ranging from 0.2% for ECO to 4.5% for PSF.

The cleaner electricity generation mix, which assumes halved generation from coal, doubled generation from natural gas, and a 10% increase in generation from wind and solar compared to the original electricity mix, reduces impacts in nine out of ten categories, ranging from a 6.6% reduction in NCA to a 29.4% reduction in ACD. The reductions are due to the reduction in impacts of cell assembly (ranging from 0.6% in ECO to 19.6% ODP) and dry-room operation (ranging from 14.4% in GWP_{100} to 46.8% in EUT). FFD is increased by 35.6%, again due to an increase in impacts of cell assembly (28.9%) and dry-room (68.6%).

3.3.5 Comparison with Other Studies

Peters et al. (2017) compare CED for pack production of LIBs with different chemistries and manufacturing modeling approaches (top-down versus the bottom-up approach) across 36 studies and estimate an average value of 1182 MJ kWh^{-1} ranging from 100 MJ kWh^{-1} to 2500 MJ kWh^{-1}. The top-down approach historically has resulted in higher energy estimates compared to the bottom-up approach, (Ellingsen et al., 2014; Peters et al., 2017) possibly due to the risk of inclusion of inhomogeneous products in top-down models and the risk of missing processes in bottom-up models (Ellingsen et al., 2014). Kim et al. (2016) estimate CED of 1500 MJ kWh^{-1} for a Ford Focus LIB battery. Their estimate is also in the range summarized by Peters et al. (2017). Our estimate of CED for pyrite battery falls on the upper side of this range (3300 MJ kWh^{-1}). However, it should be noted that the energy requirements of dry-room and production of TiS_2 (which is not commercially available) are both uncertain; more optimized design for dehumidification process and TiS_2 production can possibly reduce the CED of the pyrite battery. Moreover, continued research and development (R&D) on pyrite battery has shown that TiS_2 can be possibly eliminated.

Energy requirements and impacts of battery assembly process is the most uncertain part of battery LCAs, mainly due to the lack of primary data (Kim et al., 2016; Peters et al., 2017). In our study, we apply a bottom-up approach and we estimate energy use of 735 MJ kWh^{-1} for cell production. This value is lower than the value estimated for LIB by Zackrisson et al. (2010) (793 MJ kWh^{-1}) and the average value for LIB found by Ellingsen et al. (2014) (2318 MJ kWh^{-1}), but it is higher than their lower-bound value (586 MJ kWh^{-1}), which is a representative of mass production in their study, and that found by Deng et al. (2017) for a Li-S battery (275 MJ kWh^{-1}). Our battery does not need charging for charge retention testing and formation cycling but needs a bigger dry-room area. As shown in values by Ellingsen et al. (2014), increased annual production for the same dry-room area reduces the cell manufacturing energy requirements. Zackrisson et al. (2010) and Ellingsen et al. (2014) use bottom-up models utilizing manufacturers' data; but in their studies, it is not clear what portion of energy estimated is from formation cycling and charge retention

testing, what is the area of dry-room in their facility, and what is the level of annual production. Deng et al. (2017) use a bottom-up model and estimate the dry-room energy requirements in kWh per kg of the cell through measuring and modeling of a pilot-scale dry-room facility of Johnson Controls Inc. over 21 days. Based on their estimation, dry-room energy requirement comprises 42% of cell manufacturing energy requirements which compares to a 96% share in our study. However, their study does not detail the corresponding annual production to the assumed dry-room area. Like the pyrite battery, a Li-S battery does not need any charging before charge retention testing (Deng et al., 2017). On the other hand, there are different sources of uncertainty in our estimation, which also makes the detailed comparison hard. First, we estimate the energy requirements for the processes from the lab scale facilities. The manufacturing processes get more efficient in large-scale production, compared to the small scale and energy input generally scales with the process costs. The cost of process equipment is correlated with size or capacity following the formula $Cost_B = Cost_A \left(\frac{Capacity(size)_B}{Capacity(size)A}\right)^b$, where b varies from 0.5–0.8 and will average between 0.6–0.7 for many types of equipment (Cooper and Alley, 2002; Peters et al., 1968). That is, with doubled capacity and assuming b=0.6, the cost would be increased by 50% rather than doubled. However, it would not be possible to get 100% yield and turn all input materials to the final products in the large-scale production compared to the lab scale. Argonne assumes 90–98% yield factors for different cell materials including current collector foils, 5% lost for solvent recovery, and 5% lost in cells rejected after charge retention testing in annual production (ANL, 2017). Second, due to the process-level approach and the emerging feature of the new chemistry, it is likely that some energy flows are neglected in this estimation. Finally, the location of the factory would affect the energy requirements of dry-room applications.

Comparison of environmental impacts across LCA studies is often difficult. Different studies report results for different impact assessment systems which may utilize different impact categories, units, or characterization factors. Even within the same impact assessment system, only a high-level comparison would be possible, due to the differences in electricity mixes (in different locations), the year in which a study is conducted, and the focused chemistry. GWP_{100} has been the most

common impact category for comparison. Our estimate for GWP_{100} impacts of battery production (199 kg CO_2 eq kWh^{-1}) is higher than average LIB value estimated by Peters et al. (2017) (110 kg CO_2 eq kWh^{-1}, ranging from 40–350 kg CO_2 eq kWh^{-1}), and that estimated by Kim et al. (2016) (140 kg CO_2 eq kWh^{-1}), but our value is in the range of average LIBs (Peters et al., 2017). Our estimate is lower than that estimated by Deng et al. (2017) (234 kg CO_2 eq kWh^{-1}). As we assume larger impacts from dry-room applications compared to those studies, this can be related to the elimination of some elements in the pyrite battery compared to the Li-S battery such as current collector foils, separator, and cooling systems. In our study, cell production accounts for 93% of total battery manufacturing GWP_{100} impacts. Based on Ellingsen et al. (2014) estimates, GWP_{100} for cell manufacturing comprises 62% of the total GWP_{100} impacts of battery manufacturing in the lower-bound case (87% in the average case), Zackrisson (2017) and Deng et al. (2017) estimate 53% and 60% for the same share, respectively.

Table 3.4 compares the GWP_{100} for each stage of pyrite battery manufacturing with Ellingsen et al. (2014)'s lower-bound case for a NCM chemistry and with results from Deng et al. (2017) for a Li-S chemistry. We chose these studies, since Ellingsen et al. (2014) is one of the most detailed recent LCAs for LIB chemistry based on primary data and it is also the reference for impact assessment of some components in our study; Deng et al. (2017) study a sulfur-based lithium battery, but with liquid electrolyte. Both these studies break the stages almost similar to our study.

Table 3.4 shows that GWP_{100} impacts for most stages of pyrite battery are in the same order as Ellingsen et al. (2014) lower-bound value, which is representative of mass scale production. Note that their average estimation is higher than this lower-value. We expect that GWP_{100} impacts of the pyrite battery would be lowered by switching from the lab-scale production to the mass-scale production. Deng et al. (2017) estimate more impacts from cathode paste and anode (including current collectors) and lower impacts for BMS, and packaging than our study and also Ellingsen et al. (2014). Our estimate for aggregated GWP_{100} impacts of electrolyte paste, cell assembly, and dry-room matches those estimated by Deng et al. (2017) but is higher than lower-bound value by Ellingsen et al. (2014).

Table 3.4. GWP_{100} comparison of different stages of battery manufacturing.

This Study		Ellingsen et al. (2014)		Deng et al. (2017)	
Stage	**GWP_{100} (kg CO_2-eq kWh^{-1})**	**Corresponding stage**	**GWP_{100} (kg CO_2-eq kWh^{-1})[a]**	**Corresponding stage**	**GWP_{100} (kg CO_2-eq kWh^{-1})**
Cathode paste, positive current collector	15	Cathode paste, positive current collector	18	Cathode paste, positive current collector	45
Anode	8	Anode, negative current collector	10	Anode, negative current collector	20
Electrolyte paste, cell assembly, dry-room	162	Manufacturing of battery cell, other battery cell components	111	Electrolyte, separator, cell container, cell manufacturing	161
BMS, Module and pack assembly	14	BMS, packaging, battery assembly	29	BMS, module packing, pack packing	6
Cooling system	0 (not applicable)	Cooling system	4	Cooling system	2
Total	199	Total	172	Total	234

[a] Values correspond to the lower-bound case.

It should be noted that to be able to fairly compare the impacts of pyrite battery with the LIBs, other impact categories should be also compared. That is because, for example, negative current collector (Cu), which is not required for the pyrite battery, does not contribute significantly to GWP_{100} but it is the main contributor to EUT (fresh water and terrestrial), toxicity (freshwater, marine, and human), and metal depletion in LIB production (Ellingsen et al., 2014). Its contribution to the impacts of photo-oxidation formation, particulate matter formation, and ACD is also considerable (Ellingsen et al., 2014). However, the cross comparison across studies is not feasible when they differ in the impact assessment system. For example, we cannot compare our results with Deng et al. (2017), Ellingsen et al. (2014), and most of the studies listed in the review study by Peters et al. (2017), as these studies use other impact assessment systems (such as ReCiPe Midpoint) than TRACI, which is used in this study. EPA's (2013) study (Amarakoon et al., 2013)

is one of the few studies that utilizes the TRACI 2.0 impact assessment system; this enables us to compare five impact categories (including GWP_{100}) from their study directly to those from our study (Table 3.5). Table 3.5 presents a cross comparison between our study and average impacts of LMO, NCM, and LFP chemistries for a 40 kWh BEV battery or a 11.6 kWh PHEV battery (Amarakoon et al., 2013).

Table 3.5. Comparison of battery pack impacts between pyrite battery (this study) and average LMO, NCM, and LFP LIB chemistries (Amarakoon et al., 2013). The values for this study are presented excluding dry-room impacts.

Impacts[a]	Units[b]	This study[c]	EPA (2013)[d]
ODP	kg CFC-11 eq kWh^{-1}	3.91×10^{-06}	4.73×10^{-06}
GWP_{100}	kg CO_2 eq kWh^{-1}	5.46×10^{01}	1.12×10^{02}
PSF	kg O_3 eq kWh^{-1}	3.29×10^{00}	9.96×10^{00}
ACD[I]	kg SO_2 eq kWh^{-1}	4.00×10^{-01}	1.59×10^{00}
EUT	kg N eq kWh^{-1}	6.69×10^{-01}	7.64×10^{-02}

[a] ODP: Ozone depletion potential; GWP_{100}: global warming potential, calculated based on 100-year; PSF: photochemical smog formation; ACD: acidification; EUT: eutrophication.
[b] Normalized by cycle capacity.
[c] EPA study does not include the impacts of dry-room applications. Thus, for the purpose of comparison, numbers presented here exclude those impacts.
[d] Amarakoon et al. (2013).
[I] Units in EPA study (kg H^+ Mole eq) are converted to SO_2 eq for the purpose of this comparison.

Pyrite battery impacts are lower than average LIB values in the EPA (2013) study (Amarakoon et al., 2013) except for EUT. EUT is lower by a factor of 10 in EPA's study than ours. In the pyrite battery, the contribution of cathode paste to the EUT impacts is negligible, and cell assembly is the largest contributor (39%), followed by module and pack assembly (22% each). The impacts of cell assembly is in turn dominated by material production for positive and negative terminals (aluminum and copper). In EPA's study, however, these terminals are not modeled. Throughout the whole comparison here, it should be note that despite using a primary data set, EPA estimate a factor of 10 lower energy requirements for cell production compared to studies such as Ellingsen et al. (2014). In EPA's study, the cathode is the biggest contributor to the ODP impacts (36.3%), followed by pack manufacturing (33.8%). The cathode is also the biggest contributor to the PSF

impacts (42.3%), ACD impacts (52.6%) and EUR impacts (98%). Similarly, in the pyrite battery cathode paste is the biggest contributor to ODP, but with a lower share. The share of cell assembly to the total ACD impacts of pyrite battery is similar to the cathode (22%). The reduced share of the cathode to the impacts of different categories in the pyrite battery compared to average LIBs in EPA's study is due to the use of pyrite as the cathode active material. As described before, the impacts of cathode in pyrite battery are mainly dominated by production of TiS_2, which can be possibly eliminated based on the results of further R&D on the material structure of pyrite battery.

Our study shows that the energy requirements of clean dry-room applications are not well understood, whereas it has a significant share of the impacts of battery production. Future work quantifying those energy requirements and optimizing dry-room energy consumptions could improve the LCA of battery production with different chemistries.

This paper focuses on the impacts of battery production only. Whereas, one advantage of solid-state batteries over LIBs would be their potentially longer cycle life (Takada, 2013); another potential advantage of solid-state batteries would be their lower use-phase impacts than LIBs. Lastoskie and Dai (2015), show that use-phase impacts of BEVs with solid-state electrolyte are 5–6% lower than their counterpart LIBs, utilizing the same cathode chemistry and cycle life. They related this conclusion to the higher cell energy density of solid-state structure which results in lower battery mass and higher vehicle efficiency. The cycle life of pyrite battery is not defined yet, also there are uncertainties in the mass inventory of a pyrite battery pack for EV applications. Addressing these questions would help to understand the use phase benefits of solid-state lithium pyrite battery over the LIB chemistries.

3.4 SUPPORTING INFORMATION

3.4.1 Mass Inventory for a Pyrite Battery Pack with 80 kWh Energy Capacity

The Pyrite battery exists only in the lab-scale. We develop a simple model, based on the results from the lab experiments and reasonable assumptions from the Argonne National Laboratory

(ANL) BatPac model (ANL, 2017; Nelson et al., 2012) and the literature, to estimate the mass of the battery pack. The BatPac model is a bottom-up cost model designed to estimate battery costs (applicable to transportation) based on the material chemistry, battery design, and processes (ANL, 2017; Nelson et al., 2012). However, we do not directly utilize this model in our study, as the current version of the model focuses on the known chemistries for the liquid lithium-ion batteries. Therefore, significant research and modification are needed to be able to adjust the model for the solid-state lithium batteries. We take assumptions from the BatPac model wherever they are applicable and relevant to our study. We start our estimation by calculating the cell mass, and add the mass of necessary elements for modules and packs.

First, we estimate the mass of positive and negative active materials (FeS_2 and lithium, respectively) in each cell. In our study, the battery pack has 80 kWh energy capacity and is designed for EV applications. The battery voltage for EV applications ranges from 280–400 V (Dunn et al., 2015b; Nelson et al., 2012; Zackrisson et al., 2010). We choose 380 V for the purpose of our calculation. This choice is similar to the ANL default assumption in the BatPac model (ANL, 2017). These assumptions result in a battery pack capacity of 211 Ah. Assuming no parallel modules and no parallel cells, which helps to minimize the number of cells in this battery pack and reduce the cost of the battery (Nelson et al., 2012), results in 211 Ah module and cell capacities. Based on laboratory experiments, the specific capacity is 448 mAh g^{-1} (350–560) for positive active material (cathode) and 2557 mAh g^{-1} (2000–3200) for negative active material (anode). Accordingly, the mass of positive and negative active materials can be estimated using cell capacity and the corresponding specific capacity. Based on the laboratory data, the mass calculation for the anode assumes 20% excess anode to assure the same charging capacity for anode and cathode and assumes 10% negative space (Table 3.6).

Next, we estimate the mass of cathode conductive material (TiS_2), the binder for cathode paste (PMMA), and positive current collector foil (Al). Note that unlike Li-ion batteries the pyrite battery does not need a negative electrode paste or a negative current collector (Cu). According to laboratory data, the mass composition for the cathode is 47.5%, 47.5%, and 5% for FeS_2, TiS_2,

and binder, respectively (equal to 95% for active and conductive materials). Using the FeS_2 mass from the earlier calculations and these compositions, the masses of TiS_2 and binder are estimated (Table 3.6). To estimate the mass of current collector foil we match the lab cathode compositions for the pyrite battery with the default cathode compositions for the Li-ion chemistries in the BatPac model. ANL assumes 89% positive active material, 6% conductive material (carbon), and 5% binder, respectively (equal to 95% for active and conductive materials) (ANL, 2017). Including aluminum foil in this composition (9%) results in 81% positive active material, 5% carbon (equal to 86% active and conductive material), and 5% binder (ANL, 2017). We use the same compositions (but with equal shares for active and conductive material) to estimate the mass of Al current collector (Table 3.6).

Unlike the Li-ion batteries, the electrolyte in our battery is treated in a similar way as the cathode. That is, it is produced by making a slurry paste and is coated on the cathode foil. We estimate the mass of electrolyte (Li_2S and P_2S_5) using the lab-scale cell composition (28% (FeS_2), 12% (Li_2S), 17% (P_2S_5), 28% (TiS_2), 4.5% total binder for both cathode and electrolyte (PMMA), and 10.5% (Li)) and the mass of FeS_2, TiS_2, binder for cathode, and Li from the earlier calculations (Table 3.6). The mass of binder for electrolyte is estimated from the electrolyte composition of 39.5% (Li_2S), 55.5% (P_2S_5), and 5% (PMMA) from the lab experiments and the electrolyte mass (Table 3.6).

For terminals (positive and negative) and cell container (PET-Al-PP), we adapt their share out of the total cell compositions from BatPac model. BatPac assumes 1% for positive terminal, 3% for negative terminal, and 4% for the cell container (92% for the rest of elements) (ANL, 2017). We adjust these percentages to our battery (1%, 3%, and 5%, respectively) by excluding the separator and copper current collector.

The components that comprise the module mass include cells (53 in each module), module terminals, state-of-charge (SOC) regulator, and module enclosure (Table 3.6). Note that the pyrite battery does not need a cooling system and the spacer for gas release. We adapt the calculations for the module elements from the BatPac model. The BatPac model assumes terminal heating and

Table 3.6. Estimated mass inventory of a pyrite battery cell, module, and pack with 211 Ah capacity.

Element	**Mass**		
	Average	Min	Max
Cell (g)			
Positive active material (FeS_2)	470	376	602
Negative active material (Li)	109	87	139
Cathode conductive material (TiS_2)	470	376	602
Binder (PMMA) for cathode	50	40	63
Positive current collector foil (Al)	98	79	126
Electrolyte (Li_2S)	184	147	236
Electrolyte (P_2S_5)	259	207	331
Binder (PMMA) for electrolyte	23	19	30
Positive terminals	21	17	27
Negative terminals	63	50	81
Cell container (PET-Al-PP)	84	67	108
Total Cell	**1833**	**1464**	**2343**
Module (g)			
Cells	97125	77613	124181
Terminals	62	62	62
SOC regulator	424	424	424
Module enclosure including fasteners	508	444	589
Total Module	**98120**	**78545**	**125257**
Pack (kg)			
Modules	392.5	314.2	501.0
Module inter-connects	0.4	0.4	0.4
Compression plates and steel straps	2.6	2.1	3.3
Battery jacket	34.0	30.5	38.4
Busbar	6.5	6.5	6.5
Heater	0.2	0.2	0.2
BMS	4.0	4.0	4.0
Total Pack	**440**	**358**	**554**

resistance factors of 0.019 W g^{-1} and 0.00054 A-ohm cm^{-1}, respectively (ANL, 2017). The masses of module terminals are estimated from terminal heating and resistance factor, and maximum current at full power (ANL, 2017). The maximum current at full power (A) is estimated from target battery power, 100 kW for our study, cell OCV at full power or OCV at 20% SOC, 1.3 V for our study, and target % OCV, 80% (ANL, 2017; Nelson et al., 2012). % OCV sets the battery beginning of life voltage at rated power and shows the fraction of the OCV at which the rated

power is achieved (Nelson et al., 2012). ANL suggested a minimum % OCV of 80% (Nelson et al., 2012). ANL assumes each SOC regulator weighs 8 g. ANL assumes 1mm for module enclosure thickness. For the module casing, we choose the same material, acrylonitrile butadiene styrene (ABS) with 1.1 g cm^{-3} density, as Ellingsen et al. (2014). This choice is also consistent with the ANL assumptions in the BatPac model, which uses 1.1 g cm^{-3} for a non-aluminum casing (ANL, 2017). We assume that module fasteners comprise 4.8% of total module mass, based on the assumptions from Ellingsen et al. (2014).

The components that comprise the battery pack mass include modules (4 in each pack), battery jacket, module inter-connects, module compression plates and steel straps, busbar (if there is one row of modules, in our case), battery heater, and battery management system (BMS) (Table 3.6). No coolant and coolant space is required for the pyrite battery. We adapt the calculations from the BatPac model. ANL assumes each module interconnect is 5-cm long (ANL, 2017). The mass of each module interconnect is calculated in a similar way to the module terminals using the same heating and resistance factor, and maximum current at full power as those used for module terminals (ANL, 2017). We assume the same thickness as the BatPac model (1.5 mm) for steel compression plates. The battery pack jacket is made of aluminum with insulation. ANL assumes a total thickness of 14 mm for the pack's jacket (ANL, 2017). Although the pyrite battery theoretically requires less insulation, we have assumed the same thickness as the default value in the BatPac model (10 mm) for Li-ion batteries (ANL, 2017). ANL assumes the insulation is made of a light-weight high-efficiency material, sandwiched between two aluminum layers, 2 mm thick each (Nelson et al., 2012). However, it does not specify a particular insulation material. We assume the insulation is made of polyurethane with an average density of 0.032 g cm^{-3} (ANL, 2017; Pode, 2004). The busbar is made of copper and is subject to 0.030 V voltage drop (ANL, 2017). To estimate the battery heater mass, we also use the ANL assumptions for heater unit mass (0.2 kg kW^{-1}) and heater power (1.0 kW) (ANL, 2017). ANL assumes the BMS weighs 4.0 kg. We utilize the same value in our estimation (ANL, 2017).

Figure 3.3 provides the battery mass composition by material. Detailed inventory can be

found in Section 3.4.4

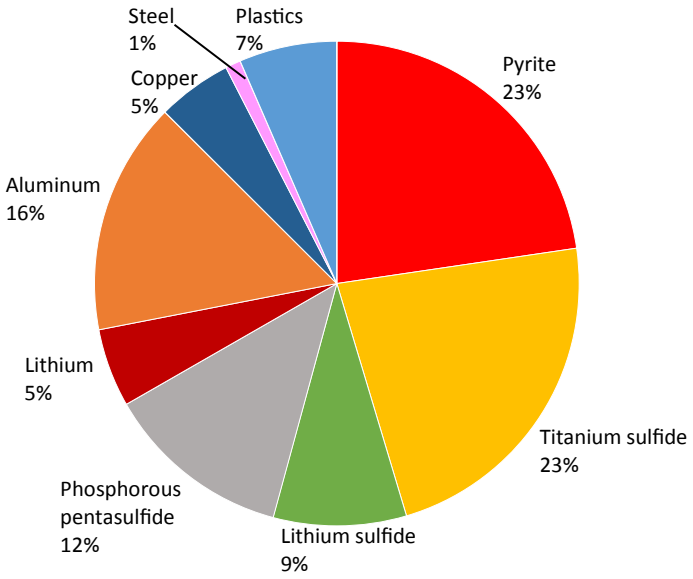

Figure 3.3. Mass composition of a 440 kg pyrite battery pack by material.

3.4.2 Estimation of Energy Requirements for the Clean Dry-room

To estimate the energy requirements for a clean dry-room application, we assume a dehumidification process from the outdoor air condition to the dry condition with dew point of –50 °C (informed by Solid Power) and the relative humidity of 100%. We consider this dehumidification process is followed by a heating process with constant humidity ratio to heat-up the temperature to the room temperature of 70 °F (21 °C). Figure 3.4 shows the schematic of the related psychometric processes. We assume that the room pressure is the same as atmospheric pressure. However, in the real applications, the room pressure is kept positive to avoid air infiltration. To accommodate cleanroom requirements, we adapt the air change rate per hour (ACH) from the American Society of Heating, Refrigerating and Air-Conditioning Engineers (ASHRAE) recommendations for the clean spaces (ASHRAE, 2015). According to the ASHRAE handbook, the following equation is used for defining ACH:

$$ACH = \frac{V}{H} \tag{3.1}$$

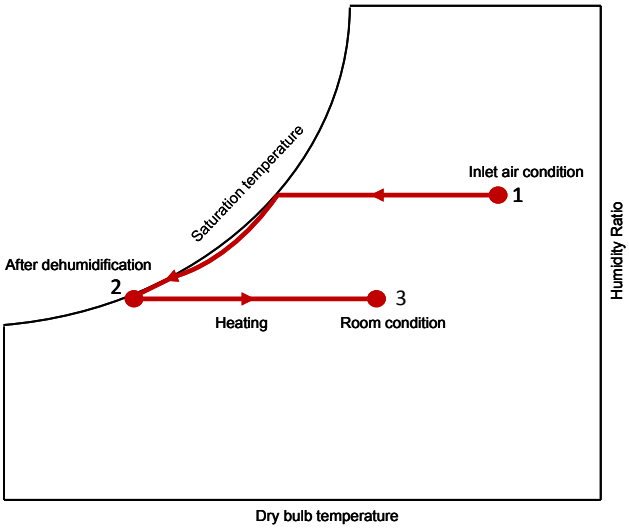

Figure 3.4. Typical psychometric processes for dehumidification

In equation 3.1, ACH is the air change rate per hour, V is the room air velocity (m hr^{-1}) through the room horizontal plane, and H is the room height (m). According to the Solid Power inputs, we assume a clean dry-room with about 8160 m^2 area and 3 m height for annual production of 28125 packs with 80 kWh. According to the Cleanroom Construction Associates' (CCA) and Cleanroom Technology websites, lithium-ion battery plants are categorized as Class 6 or Class 7 according to the International Standard Organization (ISO) classifications (ASHRAE, 2015; CCA, 2017; Cleanroom Technology, 2017). According to ASHRAE handbook, the velocity of room air ranges from 0.12–0.18 m s^{-1} for Class 6 and 0.04–0.08 m s^{-1} for Class 7 (ASHRAE, 2015). We use the Class 7 requirements with the room air velocity of 0.04 m s^{-1} in our calculation. That is, we apply an ACH of 48 in our calculation.

The location of pyrite battery manufacturing facilities is not defined yet. The inlet air condition may be subject to significant spatial, seasonal and diurnal variations. For the purpose of our calculation, we choose Nevada (Reno) as one of the reasonable locations for battery production with dry climate conditions. We choose the average climatic design information to estimate the annual energy consumption for clean dry-room applications from weatherbase website (Weatherbase, 2017). That is, we assume average annual temperature and relative humidity of 12.1 °C and 45.6%, respectively (Weatherbase, 2017). The standard pressure is 14.68 psi (101.21 kPa) (ASHRAE,

2013). Equations 3.2 and 3.3 show the formula for calculating dehumidification $\dot{Q}_d$ and heating $\dot{Q}_h$ loads, adapted from Çengel and Boles (2011). We utilize the Engineering Equation Software (EES) to conduct the energy requirement estimation.

$$\dot{Q}_d = \dot{m}_{air}(h_1 - h_2) - \dot{m}_{condensate} h_{condensate} \tag{3.2}$$

$$\dot{Q}_h = \dot{m}_{air}(h_2 - h_3) \tag{3.3}$$

In equations 3.2 and 3.3, $\dot{Q}_d$ and $\dot{Q}_h$ are the dehumidification and heating loads (kJ s^{-1}), respectively, $\dot{m}_{air}$ and $\dot{m}_{condensate}$ are the mass flowrate (kg s^{-1}) of entering air and condensate generated during the humidification process, respectively, h_1, h_2, h_3 and $h_{condensate}$ are enthalpy (kJ kg^{-1}) for point 1, 2, 3 and the condensate, respectively, shown in Figure 3.4.

According to the ASHRAE handbook, different types of dehumidifiers are available for manufacturing applications including dehumidifying coils and desiccant dehumidification (ASHRAE, 2016). Different systems may differ in the psychometric processes and they may need a cooling process after the dehumidification process instead of a heating process (ASHRAE, 2016). For highly dry applications (low dewpoints) and large factories, like our case, field built-up systems are designed utilizing different equipment. Accordingly, it would be hard to predict which sources of inefficiencies are introduced and what combination of energy sources are used. To simplify the impact assessment, we assume the main energy source of energy for dehumidification systems is electricity. Table 3.15 shows the dry-room energy requirement for a pack.

3.4.3 Description of Impact Categories

In this study, we utilize the Tool for the Reduction and Assessment of Chemical and other environmental Impacts (TRACI 2.1_1, V1.02), developed by the U.S. Environmental Protection Agency (EPA) for the impact assessment (Hischier et al., 2010). This methodology utilizes input parameters that are consistent with U.S. locations (Hischier et al., 2010). Currently, TRACI 2.1_1 includes ten midpoint impact categories: ozone depletion potential (ODP), 100-year global warming potential (GWP100), photochemical smog formation (PSF), acidification (ACD), eutrophica-

tion (EUT), carcinogenics (CAR), non-carcinogenics (NCA), respiratory effects (RPE), ecotoxicity (ECO), and fossil fuel depletion (FFD). The TRACI tool does not include the land use and water use impact categories, as further research is needed for these categories (Hischier et al., 2010). ODP, expressed in kg CFC-11 eq, calculates the relative importance of substances that contribute significantly to the breakdown of the stratospheric ozone layer, based on chemical's reactivity and lifetime (EPA, 2012b; Hischier et al., 2010). GWP100, expressed in kg CO_2 eq, calculates the potency of greenhouse gases (GHGs) relative to CO_2 over the 100-year time horizon, based on the GHGs' radiative forcing and lifetime (EPA, 2012b; Hischier et al., 2010). PSF, expressed in kg O_3 eq, measures the maximum incremental reactivity (MIR) values, which quantify relative ground-level ozone impacts of different volatile organic compounds (VOCs) (EPA, 2012b). Ground level ozone is formed following the reaction between nitrogen oxides (NO_x) and VOCs in the presence of sunlight (EPA, 2012b). ACD, expressed in kg SO_2 eq, is the increasing concentration of hydrogen ion within a local environment and shows the potential to cause wet or dry acid deposition through the addition of substances (such as sulfuric acid and ammonia) that increase the acidity of the environment (EPA, 2012b; Hischier et al., 2010). Eutrophication, expressed in kg N eq, is the enrichment of an aquatic ecosystem with nutrients such as nitrates and phosphates that accelerate biological productivity of algae and weeds (EPA, 2012b). CAR and NCA, expressed in Comparative Toxic Unit (CTU_h), calculate the potential of chemicals to cause human cancer and non-cancer health impacts, respectively (Huijbregts et al., 2010). CTU_h is equal to the number of cases per kg of emissions (Huijbregts et al., 2010). RPE, presented in kg $PM_{2.5}$ eq, is a measure of exposure to criteria air pollutants including NO_x, $PM_{2.5}$, and SO_2 from point and mobile sources (Hischier et al., 2010). ECO, expressed in CTU_e, calculates the potential of chemicals to cause ecological harm (Hischier et al., 2010). CTU_e (PAF m^3 day kg^{-1} of emissions) is equal to ecological effect factor (EF), which reflects the change in the Potentially Affected Fraction (PAF) of species due to the change in concentration (PAF m^3 kg^{-1}), multiplied by the fate factor (FF), which represents the persistence of the chemical in the environment in days (Huijbregts et al., 2010). FFD, expressed in MJ surplus, measures the damage to fossil fuel resources and is expressed as the surplus energy

needed for future extraction of fossil fuels as a result of lower quality resources (PRé, 2015). This definition is based on the rationale that people always extract the best resources first and leave the lower quality ones for future, demanding more effort for extraction. The extra effort is presented as "surplus" energy (PRé, 2015). We also add cumulative energy demand (CED) to the list of the impacts. CED demonstrates the energy use throughout the life cycle of a product or service, including the direct and indirect energy consumptions, such as raw materials (Hischier et al., 2010).

3.4.4 Detailed Inventory and Corresponding Impact Entry in the US-EI 2.2 Database

In this section, we present the assumptions about primary and secondary materials, and transportation distances; as well as the detailed inventory of the elements of the battery with an average mass of 440 kg and the corresponding entries in the US-EI 2.2, used for the impact assessment. We also explain the basis for the main assumptions and estimations whenever applicable.

3.4.4.1 Assumptions about Materials and Transportation Distances

Our calculations assume 70% primary and 30% secondary copper, respectively. These percentages are adapted from Annual Data for 1996–2016 developed by Copper Development Association Inc. (2017). We use the default assumptions for primary and secondary aluminum production as US-EI 2.2 (68% from primary resources, 21.6% from new scraps, 10.4% from old scrap). US-EI 2.2 assumes no primary sulfur production for the U.S. We find this assumption reasonable as according to the U.S. Geological Survey (USGS), there is no primary sulfur production in the U.S., partly due to the sulfur removed from the transportation fuels (Ober, 2001). The U.S. elemental sulfur is also imported from Canada and Mexico, both with no primary sulfur production (Ober, 2001).

We assume all materials and products are or can be produced in the U.S., except for battery grade graphite and tin, which are assumed to be imported from China (Amarakoon et al., 2013; USGS, 2017). EPA assumes a shipping distance of 7300 miles by oceangoing vessels from Shenzhen

in China to Long Beach in California (Amarakoon et al., 2013). For domestic transport, EPA assumes that 5% and 95% (by mass) of load are transported for an average distance of 260 and 853 miles by trucks and railcars, respectively (Amarakoon et al., 2013). EPA has adapted these values from Bureau of Labor Statistics data for Hazmat Shipment by Mode of Transportation (Bureau of Labor, 2013). To examine the uncertainties associated with the assumptions regarding the shipping and transport distances, we conduct a sensitivity analysis case (see "Sensitivity Analysis" section).

3.4.4.2 Cathode Paste

The energy requirement for the cathode paste include the energy requirement for material productions of positive active material (FeS_2), conductive material (TiS_2), solvent (xylene), and binder (PMMA); the energy requirement for the mixing process, which is a high shear mixing according to the lab experiments; and the energy requirement for the transportation (Table 3.7)

Pyrite is an abundant mineral and can be found in igneous, sedimentary and metamorphic rocks; it also exists in coal beds and is a solid-waste of coal mining (Klein et al., 1993; Uni Of Minnesota, 2017). It is rarely mined for its direct use; it used to be mined as a source of sulfur and sulfuric acid, but pyrite is not valued in the modern industry (Uni Of Minnesota, 2017). Recently, pyrite has got attention due to its potential for cathode applications (Kim et al., 2007; Yersak et al., 2013). Oliveira et al. (2016) propose beneficiation of pyrite from coal mining to help reducing their solid-wastes with the rational that pyrite can be used as a precursor for production of other products such as sulfur, sulfuric acid, fertilizers and ferrous sulfate. In US-EI 2.2 database, the data for pyrite is approximated from iron mining, lime crushing, and lime mining. This is due to the lack of information for production processes of pyrite.

TiS_2 is not commercially available and we could not find the characterization of TiS_2 production in the US-EI 2.2 database. We estimate the energy requirements for TiS_2 production based on the U.S. patent for Ti production (Wainer, 1958). This patent shows that TiS_2 is the intermediate product of Ti production and can be produced by heating TiO_2 in an atmosphere of carbon disulfide (CS_2) at temperatures (T) higher than 1500 °C (Equation 3.4) (Wainer, 1958).

$$CS_2 + TiO_2 + C \rightarrow TiS_2 + 2CO \qquad (at\ T \geq 1500^{\circ}C) \tag{3.4}$$

We estimate the energy requirements for the heating process based on the energy requirements for heating CS_2 from a standard temperature of 25 °C to 1500 °C. CS_2 is a liquid at standard temperature and pressure (STP) with a boiling point of 46 °C. Hence, it undergoes a phase change during the process. TiO_2 with a melting point of 1843 °C and a boiling point of 2972 °C, and C with vapor point of 4027 °C remain in the solid state during the process. We assume no change in the boiling point of CS_2, which may happen due to the presence of solid TiO_2 and C particles. For CS_2, we use the specific heat capacity of 1.04 J g^{-1} K^{-1} and 0.60 J g^{-1} K^{-1} for the liquid and gas phases, respectively, and latent heat value of 363.15 J g^{-1}. Our calculation assumes 100% reaction yield. See also the "Sensitivity Analysis" section for a lower reaction yield.

Table 3.7. Detailed inventory and corresponding impact entry from US-EI 2.2 for the cathode paste.

Component	**Quantity**[a]	**Unit**	**US-EI 2.2 Entry**
Cathode paste			
Positive active material (FeS_2)	470	g	Intral, at plant/US
Conductive material (TiS_2)	470	g	
TiO_2	336	g	Titanium dioxide, production mix, at plant/US
CS_2	320	g	Carbon disulfide, at plant/GLO
C	50	g	Graphite, at plant/US
Heating process	0.40	MJ	Heat, unspecific, in chemical plant/US
Solvent (xylene)	1189	g	Xylene, at plant/US
Binder (PMMA)	50	g	Polymethyl methacrylate, beads, , at plant/US
Mixing process	0.52	kWh	Electricity, medium voltage, production UCTE*, at grid/UCTE
Transportation by truck	243.1	tkm	Transport, Lorry >28t, fleet average/US
Transportation by railcar	42.0	tkm	Transport, freight, rail, diesel/US
Shipping by oceangoing vessel	125.7	tkm	Transport, transoceanic freight ship/OCE

[a] The quantities are for one cell.

3.4.4.3 Positive Current Collector

The positive current collector is made of aluminum. We assume the same proxy process as that assumed by Ellingsen et al. (2014) for the foil production (Table 3.8)

Table 3.8. Detailed inventory and corresponding impact entry from US-EI 2.2 for the positive current collector.

Component	Quantity[a]	Unit	US-EI 2.2 Entry
Positive current collector			
Aluminum	98	g	Aluminium, production mix, at plant/US
Current collector foil production	98	g	Sheet rolling, aluminium/US
Transportation by truck	16.60	tkm	Transport, Lorry >28t, fleet average/US
Transportation by railcar	2.87	tkm	Transport, freight, rail, diesel/US

[a] The quantities are for one cell.

3.4.4.4 Anode

In the pyrite battery, the anode is made of Li metal. Li is normally produced in the ingot form. For battery applications, Li foil is used. We were not able to find the characterization of lithium sheet rolling in the US-EI 2.2 database. We use aluminum sheet rolling as the proxy for lithium sheet rolling. Lithium is a softer metal than aluminum and is expected to have lower energy requirement for the sheet rolling process. Table 3.9 details the inventories for the anode.

Table 3.9. Detailed inventory and corresponding impact entry from US-EI 2.2 for anode.

Component	Quantity[a]	Unit	US-EI 2.2 Entry
Anode			
Negative active material (Li)	109	g	Lithium, at plant/GLO
Lithium foil production	109	g	Sheet rolling, aluminium/US
Transportation by truck	18.3	tkm	Transport, Lorry >28t, fleet average/US
Transportation by railcar	3.2	tkm	Transport, freight, rail, diesel/US

[a] The quantities are for one cell.

3.4.4.5 Electrolyte Paste

The energy requirements for the electrolyte paste include the energy requirements for material production of Li_2S, P_2S_5, solvent (xylene), and binder (PMMA); the energy requirements for different mixing processes (including high shear and normal mixing) according to the lab experiments; and the energy requirements for transportation (Table 3.10). We could not find the characterization of Li_2S and P_2S_5 production in the US-EI 2.2 database.

We estimate the energy requirements for Li_2S production based on the U.S. patent for producing high purity lithium sulfide (Jacob and Brown, 1978). This patent shows that Li_2S is produced by reacting lithium carbonate powder with hydrogen sulfide at 500<T<700 °C (Equation 3.5) (Jacob and Brown, 1978).

$$Li_2CO_3 + H_2S \rightarrow Li_2S + H_2CO_3 \qquad (at\ 500 < T < 700^{\circ}C) \tag{3.5}$$

We estimate the energy requirements for the heating process based on the energy requirements for heating up Li_2CO_3 from 25 °C to 700 °C. H_2S is passed through when Li_2CO_3 is heating up or after (Jacob and Brown, 1978). Li_2CO_3 is in the powder form and has a melting point of 723 °C and boiling point of 1310 °C, therefore it does not undergo phase change during the heating process. We use the specific heat capacity of 1.32 J g^{-1} K^{-1} for the solid phase. Our calculation assumes 100% reaction yield. See also the "Sensitivity Analysis" section for results assuming a lower yield.

We estimate the energy requirements for P_2S_5 production based on the U.S. patent for producing phosphorous pentasulfide (Taylor, 1965). This patent shows that P_2S_5 is produced by reacting liquid sulfur at 300 °F (149 °C) with liquid phosphorous at 190 °F (88 °C) (Equation 3.6) (Taylor, 1965).

$$2P + 5S \rightarrow P_2S_5, \quad (at\ S : T = 149^{\circ}C,\ P : T = 88^{\circ}C) \tag{3.6}$$

We estimate the energy requirements for the heating process based on the energy requirements for heating sulfur and phosphorous from 25 °C to 149 °C and 88 °C, respectively. S and P have

Table 3.10. Detailed inventory and corresponding impact entry from US-EI 2.2 for the electrolyte paste.

Component	Quantity[a]	Unit	US-EI 2.2 Entry
Electrolyte paste			
Li_2S	184	g	
Li_2CO_3	296	g	Lithium carbonate, at plant/GLO
H_2S	137	g	Hydrogen sulphide, H_2S, at plant/US
Heating process	0.26	MJ	Heat, unspecific, in chemical plant/US
P_2S_5	259	g	
P	72	g	Phosphorus, white, liquid, at plant/US
S	187	g	Secondary sulphur, at refinery/US
Heating process	0.03	MJ	Heat, unspecific, in chemical plant/US
Solvent (xylene)	560	g	Xylene, at plant/US
Binder (PMMA)	23	g	Polymethyl methacrylate, beads, at plant/US
Mixing process	0.34	kWh	Electricity, medium voltage, production UCTE*, at grid/UCTE
Transportation by truck	144.8	tkm	Transport, lorry >28t, fleet average/US
Transportation by railcar	25.0	tkm	Transport, freight, rail, diesel/US

[a] The quantities are for one cell.

melting points of 115 °C and 44°C, respectively. We use the specific heat capacity of 0.71 J g^{-1} K^{-1} and 0.77 J g^{-1} K^{-1} for the solid phase of S and P, respectively; 1.10 J g^{-1} K^{-1} and 0.85 J g^{-1} K^{-1} for the liquid phase, respectively; and latent heat value of 39.2 J $g^{-1}$and 21.1 J g^{-1}, respectively. Our calculation assumes 100% reaction yield. See also the "Sensitivity Analysis" section for results with a lower yield.

3.4.4.6 Cell Assembly

The energy requirement for cell assembly includes the energy requirements for all processes for manufacturing a cell, as well as the energy requirement for the production of cell terminals and container (PET-Al-PP pouch). Energy requirements for cell assembly processes are estimated based on the energy consumption by lab equipment. We assume the same proxy processes as utilized by Ellingsen et al. (2014) for cell terminal and container production (Table 3.11).

Table 3.11. Detailed inventory and corresponding impact entry from US-EI 2.2 for cell assembly.

Component	**Quantity**[a]	**Unit**	**US-EI 2.2 Entry**
Cell Assembly			
Coating and drying	1.71	kWh	Electricity, medium voltage, production UCTE*, at grid/UCTE
Calendering	0.17	kWh	Electricity, medium voltage, production UCTE*, at grid/UCTE
Slitting	0.01	kWh	Electricity, medium voltage, production UCTE*, at grid/UCTE
Electrode punching	0.003	kWh	Electricity, medium voltage, production UCTE*, at grid/UCTE
Cell stacking	0.01	kWh	Electricity, medium voltage, production UCTE*, at grid/UCTE
Hydraulic pressing	0.003	kWh	Electricity, medium voltage, production UCTE*, at grid/UCTE
Cell Terminals			
Aluminum	21	g	Aluminium, production mix, at plant/US
Al tab production	21	g	Sheet rolling, aluminium/US
Copper, primary	44	g	Copper, primary, at refinery/RNA
Copper, secondary	19	g	Copper, secondary, at refinery/US
Cu tab production	63	g	Sheet rolling, copper/US
Welding the terminals	0.01	kWh	Electricity, medium voltage, production UCTE*, at grid/UCTE
Pouch material	84	g	
Aluminum	42	g	Aluminium, production mix, at plant/US
PET	7	g	Polyethylene terephthalate, granulate, amorphous, at plant/US
Nylon 6	7	g	Nylon 6, at plant/US
PP	27	g	Polypropylene, granulate, at plant/US
LDPE (dry lamination)	2	g	Packaging film, LDPE, at plant/US
Pouch production			
Al sheet rolling	42	g	Sheet rolling, aluminium/US
Injection molding	40	g	Injection moulding/US
Pouch forming	0.44	kWh	Electricity, medium voltage, production UCTE*, at grid/UCTE
Pouch sealing	0.001	kWh	Electricity, medium voltage, production UCTE*, at grid/UCTE
Transportation by truck	32.0	tkm	Transport, lorry >28t, fleet average/US
Transportation by railcar	5.5	tkm	Transport, freight, rail, diesel/US

[a] The quantities are for one cell.

3.4.4.7 Module Assembly

The energy requirement for module assembly includes the energy requirements for welding of adjacent cells by a laser welding method, and welding of module terminals, as well as the energy requirement for the production of module terminals, casing, fasteners, and SOC regulator. We assume the same proxy processes as utilized by Ellingsen et al. (2014) for production of module terminals, casing, fasteners, and SOC regulator (Table 3.12).

Table 3.12. Detailed inventory and corresponding impact entry from US-EI 2.2 for module assembly.

Component	**Quantity**[a]	**Unit**	**US-EI 2.2 Entry**
Module Assembly			
Welding of adjacent cells	5.72	kWh	Electricity, medium voltage, production UCTE*, at grid/UCTE
Module Terminals	62	g	
Aluminum	14	g	Aluminium, production mix, at plant/US
Al tab production	14	g	Sheet rolling, aluminium/US
Copper, primary	33	g	Copper, primary, at refinery/RNA
Copper, secondary	14	g	Copper, secondary, at refinery/US
Cu tab production	48	g	Sheet rolling, copper/US
Welding the terminals	0.03	kWh	Electricity, medium voltage, production UCTE*, at grid/UCTE
Module casing	483	g	
ABS	483	g	Acrylonitrile-butadiene-styrene copolymer, ABS, at plant/US
Injection molding	483	g	Injection moulding/US
Module fasteners	24	g	
Nylon 6	1	g	Nylon 6, at plant/US
Steel, low-alloyed	23	g	low-alloyed, at plant/US
Steel product manufacturing	23	g	Steel product manufacturing, average metal working/US
Injection molding	1	g	Injection moulding/US
Module SOC regulator	424	g	Printed wiring board, through-hole mounted, unspec., Pb free, at plant/GLO
Transportation by truck	107.1	tkm	Transport, lorry >28t, fleet average/US
Transportation by railcar	18.5	tkm	Transport, freight, rail, diesel/US

[a] The quantities are for one module.

3.4.4.8 Battery Management System

BMS measures the pack current and voltage, balances the module voltages, estimates SOC and state-of-health (SOH) for both module and pack, and monitors and signals the battery thermal management (Nelson et al., 2012). ANL assumes BMS weighs 4 kg. However, it does not provide details for the BMS subcomponents. We adapt the mass fractions for BMS subcomponents from Ellingsen et al. (2014). Ellingsen et al. (2014) defines battery module boards (BMBs), integrated battery interface system (IBIS), IBIS fasteners, and a high voltage system and a low voltage system as the subcomponents of BMS. It should be noted that BMB is equivalent to the SOC regulator in the BatPac model and is already counted for in the module inventory (Table 3.12). Therefore, we adjust the mass fractions from Ellingsen et al. (2014) to our study by excluding BMB. Accordingly, IBIS, IBIS fasteners, high voltage system, and low voltage system comprise 52.6%, 0.3%, 32.9%, and 14.2% of the mass of BMS, respectively. The mass fraction for subcomponents of IBIS, IBIS fasteners, high voltage system, and low voltage system, as well as the material and processes for BMS production, are also adapted from Ellingsen et al. (2014). Table 3.13 details the inventory of BMS.

Table 3.13. Detailed inventory and corresponding impact entry from US-EI 2.2 for battery management system (BMS).

Component	Quantity[a]	Unit	US-EI 2.2 Entry
BMS			
IBIS	2.10	kg	
Integrated circuit	0.04	g	Integrated circuit, IC, logic type, at plant /GLO
Connectors	44	g	Connector, clamp connection, at plant/GLO
Printed board	231	g	Printed wiring board, through-hole mounted, unspec., Pb free, at plant/GLO
Steel components	1787	g	Steel, low-alloyed, at plant/US
Brass parts	12	g	Brass, at plant/US
Nylon parts	4	g	Nylon 6, at plant/US
ABS	0.42	g	Acrylonitrile-butadiene-styrene copolymer, ABS, at plant/US
PET	14	g	Polyethylene terephthalate, granulate, amorphous, at plant/US

Continued on next page

Table 3.13 – *Continued from previous page*

Component	Quantity	Unit	US-EI 2.2 Entry
Steel product manufacturing	1787	g	Steel product manufacturing, average metal working/US
Casting brass	12	g	Casting, brass/US
Injection molding	19	g	Injection moulding/US
IBIS fasteners	13	g	
Steel components	13	g	Steel, low-alloyed, at plant/US
Steel product manufacturing	13	g	Steel product manufacturing, average metal working/US
High voltage system	1.31	kg	
Copper, primary	249	g	Copper, primary, at refinery/RNA
Copper, secondary	107	g	Copper, secondary, at refinery/US
Polyphenylene sulfide	42	g	Polyphenylene sulfide, at plant/GLO
Tin	21	g	Tin, at regional storage/US
Steel components	2	g	Steel, low-alloyed, at plant/US
Aluminum components	158	g	Aluminium, production mix, at plant/US
Nylon parts	58	g	Nylon 66, at plant/US
PET	75	g	Polyethylene terephthalate, granulate, amorphous, at plant/US
Synthetic rubber	5	g	Synthetic rubber, at plant/US
Copper product manufacturing	356	g	Copper product manufacturing, average metal working/US
Metal product manufacturing	21	g	Metal product manufacturing, average metal working/US
Steel product manufacturing	2	g	Steel product manufacturing, average metal working/US
Aluminum product manufacturing	158	g	Aluminium product manufacturing, average metal working/US
Injection molding	180	g	Injection moulding/US
Cables	591	g	Cable, ribbon cable, 20-pin, with plugs/GLO at plant/GLO
Low voltage system	570	g	
Nylon parts	17	g	Nylon 66, at plant/US
Electronic components	553	g	Electronic component, active, unspecified, at plant/GLO
Injection molding	17	g	Injection moulding/US
Transportation by truck	2.3	tkm	Transport, lorry >28t, fleet average/US
Transportation by railcar	0.4	tkm	Transport, freight, rail, diesel/US
Shipping by oceangoing vessel	0.2	tkm	Transport, transoceanic freight ship/OCE

[a] The quantities are for one pack.

3.4.4.9 Pack Assembly

The energy requirement for the pack assembly includes the energy requirements associated with production of module copper interconnections, module compression plates and straps, busbar, battery heater, and battery jacket. We assume the insulation is made of polyurethane (Pode, 2004). Table 3.14 details the inventory for the pack assembly.

Table 3.14. Detailed inventory and corresponding impact entry from US-EI 2.2 for pack assembly.

Component	**Quantity**[a]	**Unit**	**US-EI 2.2 Entry**
Pack Assembly			
Copper interconnections	310	g	
Copper, primary	216	g	Copper, primary, at refinery/RNA
Copper, secondary	94	g	Copper, secondary, at refinery/US
Copper product manufacturing	310	g	Copper product manufacturing, average metal working/US
Compression plates and steel straps	2.6	kg	
Steel components	2.6	kg	Steel, low-alloyed, at plant/US
Steel product manufacturing	2.6	kg	Steel product manufacturing, average metal working/US
Busbar	6.5	kg	
Copper, primary	4.5	kg	Copper, primary, at refinery/RNA
Copper, secondary	2.0	kg	Copper, secondary, at refinery/US
Copper product manufacturing	6.5	kg	Copper product manufacturing, average metal working/US
Heater	0.2	kg	
Resistor	0.2	kg	Resistor, unspecified, at plant/GLO
Resistor production	0.2	kg	Production efforts, resistors/GLO
Battery Jacket	34	kg	
Aluminum	33	kg	Aluminium, production mix, at plant/US
Insulation	1	kg	Polyurethane, rigid foam, at plant/US
Al sheet rolling	33	kg	Sheet rolling, aluminium/US
Injection molding	1	kg	Injection moulding/US
Transportation by truck	34.4	tkm	Transport, lorry >28t, fleet average/US
Transportation by railcar	5.9	tkm	Transport, freight, rail, diesel/US

[a] The quantities are for one pack.

3.4.4.10 Dry-room

The estimation method for energy requirement of a clean dry-room is presented in section 3.4.2. Table 3.15 shows the energy requirement for one pack assuming 8160 m^2 floor area for the clean dry-room for annual production of 28125 packs with 80 kWh (estimated by Solid Power). We assume the same medium voltage electricity profile as other battery assembly processes explained in the earlier sections.

Table 3.15. Detailed inventory and corresponding impact entry from US-EI 2.2 for clean dry-room.

Component	**Quantity**[a]	**Unit**	**US-EI 2.2 Entry**
Clean dry-room energy requirements	15652	kWh	Electricity, medium voltage, production UCTE*, at grid/UCTE

[a] The quantities are for one pack.

3.4.4.11 Energy Requirements of Each Battery Assembly Process and Dry-room

Table 3.16 summarizes the energy requirements of each battery assembly process and the dry-room from the earlier tables (3.7–3.15).

Table 3.16. Energy requirements of each battery assembly process and dry-room in MJ.

Process	**Quantity**[a]
Mixing	654
Coating and drying	1305
Calendering	130
Slitting	5
Electrode punching	3
Stacking	4
Cell laminating	2
Tab welding	5
Pouch forming	339
Pouch sealing	0.6
Welding the adjacent cells	82
Welding the module terminals	0.5
Dry-room	56347

[a] The quantities are for one pack.

3.4.5 Additional Results

Additional results are presented in this section. Table 3.17 shows the numerical results for the environmental impacts of each battery stage. Table 3.18 represents the major contributor to the environmental impacts of each stage for each impact category. Figure 3.5 compares the environmental impacts of different solvent options.

Table 3.17. Environmental impacts of each battery production stage for the average weight. The impacts are normalized by nominal energy capacity.

Impacts[a]	**Units**	**Cathode paste**	**Positive current collector (Al)**	**Anode (Li)**	**Electrolyte paste**	**Cell assembly**	**Module assembly**	**BMS**[b]	**Pack assembly**	**Dry room**
ODP	kg CFC-11 eq kWh^{-1}	1.02×10^{-06}	1.64×10^{-07}	6.63×10^{-07}	5.36×10^{-07}	4.40×10^{-07}	1.73×10^{-07}	5.84×10^{-07}	3.29×10^{-07}	6.28×10^{-06}
GWP_{100}	kg CO_2 eq kWh^{-1}	1.27×10^{01}	2.55×10^{00}	8.33×10^{00}	9.32×10^{00}	7.69×10^{00}	2.10×10^{00}	6.83×10^{00}	5.07×10^{00}	1.45×10^{02}
PSF	kg O_3 eq kWh^{-1}	6.89×10^{-01}	1.07×10^{-01}	4.19×10^{-01}	5.47×10^{-01}	5.68×10^{-01}	1.52×10^{-01}	4.60×10^{-01}	3.48×10^{-01}	6.52×10^{00}
ACD	kg SO_2 eq kWh^{-1}	8.54×10^{-02}	1.14×10^{-02}	4.54×10^{-02}	6.29×10^{-02}	8.64×10^{-02}	1.29×10^{-02}	3.90×10^{-02}	5.64×10^{-02}	7.65×10^{-01}
EUT	kg N eq kWh^{-1}	2.29×10^{-02}	8.26×10^{-03}	2.91×10^{-02}	3.04×10^{-02}	2.58×10^{-01}	2.21×10^{-02}	1.48×10^{-01}	1.50×10^{-01}	4.48×10^{-01}
CAR	CTU_h kWh^{-1}	4.72×10^{-07}	6.23×10^{-07}	5.44×10^{-07}	6.94×10^{-07}	2.62×10^{-06}	2.89×10^{-07}	1.47×10^{-06}	2.16×10^{-06}	7.38×10^{-06}
NCA	CTU_h kWh^{-1}	1.40×10^{-06}	8.56×10^{-07}	1.90×10^{-06}	1.97×10^{-06}	5.44×10^{-05}	4.10×10^{-06}	2.93×10^{-05}	3.20×10^{-05}	2.51×10^{-05}
RPE	kg $PM_{2.5}$ eq kWh^{-1}	7.08×10^{-03}	1.75×10^{-03}	2.84×10^{-03}	5.39×10^{-03}	1.18×10^{-02}	1.16×10^{-03}	3.14×10^{-03}	8.42×10^{-03}	4.50×10^{-02}
ECO	CTU_e kWh^{-1}	4.29×10^{01}	2.96×10^{01}	3.98×10^{01}	3.92×10^{01}	1.33×10^{03}	9.87×10^{01}	7.03×10^{02}	7.90×10^{02}	6.01×10^{02}
FFD	MJ surplus kWh^{-1}	4.41×10^{01}	2.45×10^{00}	5.95×10^{00}	2.13×10^{01}	7.03×10^{00}	2.35×10^{00}	6.05×10^{00}	5.08×10^{00}	9.31×10^{01}
CED	MJ kWh^{-1}	3.16×10^{02}	3.76×10^{01}	2.41×10^{01}	1.64×10^{02}	8.41×10^{01}	3.36×10^{01}	1.00×10^{02}	7.95×10^{01}	2.47×10^{03}

[a] ODP: ozone depletion potential; GWP100: global warming potential, calculated based on 100-year; PSF: photochemical smog formation; ACD: acidification; EUT: eutrophication; CAR: carcinogenics; NCA: non-carcinogenics; RPE: respiratory effects; ECO: Ecotoxicity; FFD: Fossil Fuel Depletion; CED: cumulative energy demand.

[b] BMS: battery management system.

Table 3.18. Major contributor and percent contribution of the related sub-elements to the environmental impacts of each stage. For anode (Li) and positive current collector (Al), the metal production is the main contributor to each stage. Dry-room is a single element stage. These stages are not shown in the table.

Impacts[a]	**Cathode paste**		**Electrolyte paste**		**Cell assembly**		**Module assembly**		**BMS**[b]		**Pack assembly**	
	contributor	%	contributor	%	contributor	%	contributor	%	contributor	%	contributor	%
ODP	TiS_2	86	Li_2S	55	Pouch material production & Coating and drying	33 each	SOC	59	Low voltage system	94	Battery Jacket production	78
GWP_{100}	TiS_2 & Xylene	40 each	Li_2S	31	Coating and drying	44	SOC	72	Low voltage system	93	Battery Jacket production	79
PSF	TiS_2	46	Li_2S	42	Terminal production	49	SOC	61	Low voltage system	93	Battery Jacket production	46
ACD	TiS_2	67	P_2S_5	46	Terminal production	63	SOC	70	Low voltage system	89	Busbar production	49
EUT	TiS_2	76	Li_2S	60	Terminal production	93	SOC	80	Low voltage system	93	Busbar production	81
CAR	TiS_2	46	Li_2S	60	Terminal production	80	SOC	79	Low voltage system	90	Busbar production	47
NCA	TiS_2	76	Li_2S	66	Terminal production	98	SOC	80	Low voltage system	92	Busbar production	85
RPE	TiS_2	64	P_2S_5	53	Terminal production	80	SOC	71	Low voltage system	83	Busbar production	56
ECO	TiS_2	68	Li_2S	52	Terminal production	97	SOC	79	Low voltage system	92	Busbar production	84
FFD	Xylene	66	Xylene	64	Coating and drying	31	SOC	59	Low voltage system	91	Battery Jacket production	77

[a] ODP: ozone depletion potential; GWP_{100}: global warming potential, calculated based on 100-year; PSF: photochemical smog formation; ACD: acidification; EUT: eutrophication; CAR: carcinogenics; NCA: non-carcinogenics; RPE: respiratory effects; ECO: Ecotoxicity; FFD: Fossil Fuel Depletion.

[b] BMS: battery management system.

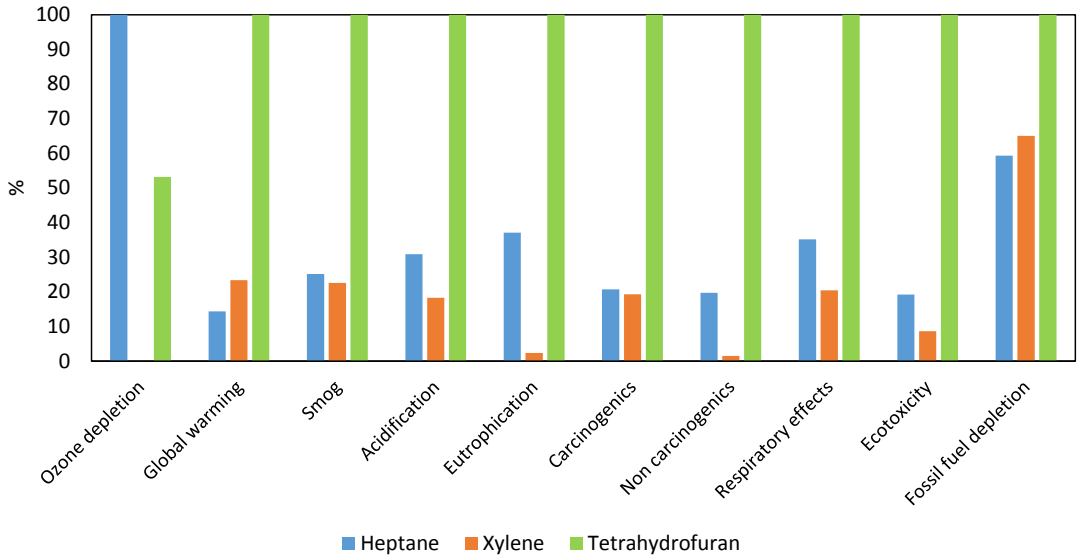

Figure 3.5. Comparison of environmental impacts of heptane, xylene, and tetrahydrofuran (THF). In each category, the largest value is set as 100%.

Chapter 4

Regionally Targeted Subsidies for Electric Vehicles based on Ownership Costs and Air Quality and Climate Benefits[1]

4.1 INTRODUCTION

Electric vehicles (EV) are increasingly receiving attention in the U.S. due to their potential for reducing oil consumption and greenhouse gas (GHG) and other air pollutant (including precursors of ozone and $PM_{2.5}$) emissions (DOE, 2017b; NRC, 2013). Although EVs can offer savings to purchasers in the form of reduced fuel costs, the higher capital cost of EVs compared to their gasoline vehicle (GV) counterparts is the most significant barrier to wider adoption (Krupa et al., 2014). Additional barriers include concerns about vehicle range, access to charging stations, limited numbers of EV models on offer, and lack of familiarity with EV technology (Deloitte Consulting LLC, 2010; Egbue and Long, 2012; Krupa et al., 2014; Sierzchula et al., 2014; Tran et al., 2012).

A variety of financial incentives and policies have been proposed, and some implemented, to reduce EV capital costs and increase their market penetration, which in turn can lower manufacturing costs via learning by doing and economies of scale (Deloitte Consulting LLC, 2010; Egbue and Long, 2012; Krupa et al., 2014; NRC, 2013; Sierzchula et al., 2014; Tran et al., 2012). The U.S. government offers federal tax credits of up to $7500 for purchase or lease of qualifying plug-in hybrid and battery EVs (PHEVs and BEVs), including passenger cars and light trucks. Reflecting the program's intent of helping manufacturers lower costs by achieving economies of scale, the credits are phased out when a given manufacturer sells 200,000 qualifying vehicles for use in the

[1] The content of this chapter is from a manuscript submitted to *Energy Policy* journal.

U.S. (DOE, 2017a). More than a dozen states in the U.S. offer additional vehicle purchase or lease incentives, such as state tax credits, rebates, and sales tax exemptions. As of August 2017, California's Clean Vehicle Rebate Program has distributed more than $300 million for purchase or lease of approximately 120,000 BEVs, for an average rebate of about $2570 (CARB, 2017).

U.S. federal income tax credits for EV purchases are offered uniformly throughout the country (as long as EVs are marketed in a particular location). Some researchers have questioned their efficiency because they fail to reflect variations in potential social benefits or costs associated with EV operations in different locations (Holland et al., 2016; Skerlos and Winebrake, 2010). Skerlos and Winebrake (2010) argued that differentiated tax credits based on location of purchase could achieve higher social benefits than a uniform subsidy for PHEVs. They suggested that larger credits should be given in regions with higher net benefits of PHEV use, i.e., regions with higher pollution levels and larger population exposure, low-carbon electricity generation, and greater miles traveled per vehicle. However, they left the quantification of the differentiated social benefits and corresponding credits for future research. Holland et al. (2016) proposed that optimal regionally differentiated subsidies should be equal to the differences between damages over the lifetime of a GV and an EV. Based on current vehicle technology and the 2011–2012 electricity generation mix, and accounting for local air pollution and GHG impacts, they estimated that this difference ranges from –$5000 to +$5000 for regions across the U.S. They found that in some regions EVs would impose more environmental damages than GVs do, so that in those regions subsidies for EVs could not be justified solely on current environmental externalities. Recent studies of other clean energy and transportation technologies have similarly found that their environmental externalities and private costs vary significantly across regions (Rhodes et al., 2017; Tamayao et al., 2015; Vaishnav et al., 2017; Yuksel et al., 2016).

As demonstrated by Holland et al. (2016), consideration of pollution externalities as a basis for subsidy designs highlights the importance of local factors, because benefits or damages differ by location. The transportation sector contributes to ground level ozone, $PM_{2.5}$, and CO_2 emissions and their associated health and environmental impacts. EVs reduce tailpipe emissions but those

emissions reductions are offset by varying amounts depending on fuel sources and technologies used to generate electricity for charging EVs in different locations. Moreover, shifting the energy source to the electric sector correspondingly shifts emissions from mobile sources operating at ground level to more remote power plants with tall stacks that distribute the emitted compounds further downwind. In the case of secondary pollutants (ozone and secondary $PM_{2.5}$), background concentrations of precursors and variable atmospheric conditions affect the level of formation and removal of these pollutants, further contributing to different levels of damages across the country. Thus, the magnitude of avoided air pollution damages from the transportation sector and offsetting damages from the electric sector vary across the country depending on the level of emissions, miles driven per vehicle, and for air quality factors the location of sources and size of the exposed population.

Holland et al. (2016) consider EV subsidies only for the purpose of addressing current externalities, neglecting their potential value in helping bring down future EV costs. On the other hand, a key aim of EV purchase and leasing incentive programs in the U.S. is to increase production experience in order to reduce costs of this new technology along a learning curve. Focusing on this latter aim, Herron and Williams (2013) proposed a cascading diffusion model to estimate optimal subsidies required to achieve specified levels of penetration for a new technology. They demonstrate the model with the example of residential solid oxide fuel cells, considering consumers' direct willingness-to-pay (WTP) for the new technology along with the technology's projected learning curve. Herron and Williams (2013) recognize that WTP can vary in different sub-markets due to differences in economic performance. Targeting initial subsidies toward sub-markets with the most favorable economic conditions helps advance production levels along the learning curve to reduce costs, making the technology more competitive in additional regions. Matteson and Williams (2015) suggest that the cascading diffusion model could be applied for EVs, but leave the application for future research.

The aim of this study is to show how consideration of regionally differentiated WTP and pollution externalities affects the minimum level of subsidies required to achieve a target level of

EV production in the U.S. For illustrative purposes, we target a level of 12 million BEVs. We adapt the model of Herron and Williams (2013) for cascading diffusion of EVs across regionally defined sub-markets in the U.S., accounting for cost reductions from EV production across international markets. We augment the cascading diffusion model by considering whether the subsidies advance current social welfare by reducing external damages. We go beyond previous studies by considering EV learning curves and direct WTP along with environmental externalities from deploying EVs in place of GVs across nine U.S. regions. Externalities for each region are estimated by monetizing premature mortalities associated with exposure to $PM_{2.5}$ and O_3, adapted from Dedoussi and Barrett (2014) and Pappin et al. (2015), as well as utilizing social cost of carbon (SCC) (Marten and Newbold, 2012). Climate impacts of species other than long-lived GHGs are not considered. We utilize global EV learning curves in our analysis since cumulative global sales are almost doubling annually (Nykvist and Nilsson, 2015). That is, the cost of battery technology and BEVs is decreasing based on global production levels and not merely based on the U.S. production. Therefore, in addition to the U.S. regional markets, we also analyze the U.S. market within the international market. The overall framework developed here can be applied to any group of sub-markets as well as to other technologies such as PHEV, fuel cell vehicles or photovoltaic panels.

4.2 METHODS

4.2.1 Minimum Subsidy Based on the Cascading Diffusion Model

The cascading diffusion model is based on the notion that the subsidy needed to make a new technology competitive can be minimized by introducing it first in sub-markets with more favorable economic conditions, i.e.; those with the highest consumer WTP (Herron and Williams, 2013). The sub-markets are sorted in descending order, from the highest WTP to the lowest, and the model assumes sequential adoption in favorable sub-markets (Herron and Williams, 2013). In the case of BEVs, when the vehicle cost is higher than the WTP, the minimum subsidy (Equation 4.1) for a target level of production is calculated from the area between the learning curve for BEV

cost and the WTP in each successive sub-market (Figure 4.1) (Herron and Williams, 2013). The learning curve shows how the future cost of a technology declines as the cumulative production level increases and follows the power law formula (Equation 4.2).

$$Minimum\ Subsidy(P_t) = \int_{P_i}^{P_t} \{C(P) - WTP(P)\} dP,\ C(P) > WTP(P) \tag{4.1}$$

$$C(P) = C_i \left(\frac{P}{P_i}\right)^b,\ b = \frac{log(LR)}{log(2)},\ LR = 1 - PR,\ P > P_i \tag{4.2}$$

In equations (4.1) and (4.2), P_t is the target level of production, $C(P)$ is the production cost per vehicle at a cumulative level of P units, $WTP(P)$ is the descending staircase function for WTP in different sub-markets up to the target level of production P_t , P_i is the initial level of production, P is the further level of production, C_i is the cost of initial production, b is the learning coefficient, LR is the learning rate, and PR is the progress ratio, which quantifies the fractional cost reduction every time the cumulative production doubles. The overall market is deemed to be competitive when subsidies in subsequent markets are not required.

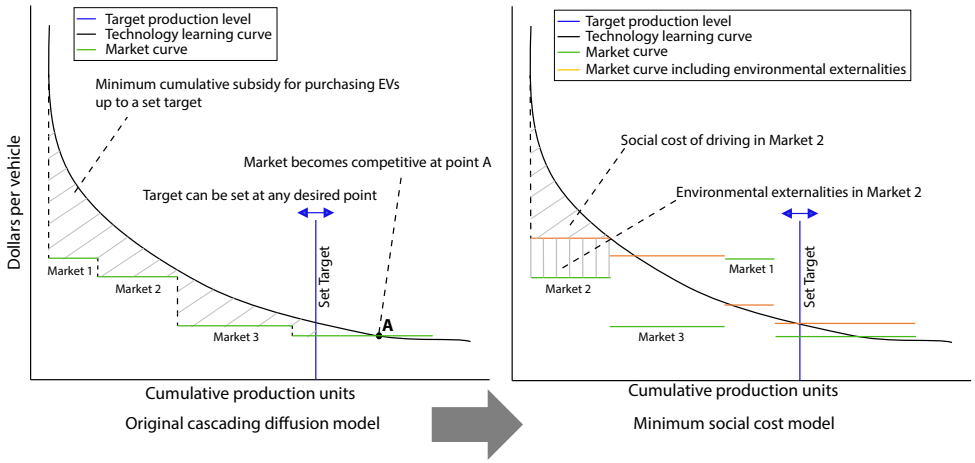

Figure 4.1. Original cascading diffusion model (left) and MSC model (right). Social cost is defined as subsidy less external benefits (or plus external damages) with EVs.

The minimum subsidy designed based on the cascading diffusion model actually estimates the lower bound for the amount of cumulative subsidies required to fill the gap between the cost of BEVs and WTP, due to two main reasons. First, the subsidies calculated based on the technology

learning curve assume continuous tapering while in the real world, subsides need to be tapered in discrete steps to make their implementation feasible from an administrative standpoint. This increases the amount of required cumulative subsidies compared to continuous tapering (Matteson and Williams, 2015). Second, the cascading diffusion model assumes sequential adoption across sub-markets, which is not likely to happen in the real world. Parallel adoption in different sub-markets potentially increases the amount of required cumulative subsidies. This study uses this lower bound formulation as the basis for examining how consideration of externalities might impact regionally differentiated subsidies.

4.2.2 Minimum Social Cost

In this study, we modify the cascading diffusion model to account for external costs of vehicle air pollution. The objective is altered to minimize the social cost, which for purposes of this study is defined as the subsidy less the environmental benefits (or plus the damages) associated with the target level of EV penetration (Equation 4.3). This definition incorporates the net air quality and climate benefits or damages associated with emissions from operation of BEVs in place of GVs in each U.S. region (Figure 4.1).

$$MinimumSocialCost(P_t) = \int_{P_i}^{P_t} [\{C(P) - WTP(P)\} - EE(P)]dP \tag{4.3}$$

In equation (4.3), $\{C(P) - WTP(P)\}$ is the subsidy and $EE(P)$ is the environmental externalities associated with driving P units of BEVs in place of GVs. $EE(P)$ has a positive value if EVs provide net environmental benefits and a negative value if EVs provide net environmental damages. Estimation of externalities is described in Section 4.2.6.

4.2.3 Model Implementation

Our study focuses on the market diffusion of BEVs in different U.S. regions; however, we also analyze the U.S market within the international market, since the cost of BEV technology can also drop following the global learning curve. Thus, we generate international market curves using

the original cascading diffusion model, and the U.S. regional market curves using both the original model and the minimum social cost (MSC) model that accounts for environmental externalities. We analyze how considering the U.S. as a part of an international market reduces the level of subsidies required for the U.S. to hit a specified EV penetration target. For illustrative purposes, we choose a 12 million EV penetration target for both the international and U.S. regional markets. This target spans most of the international market based on other countries' stated EV targets (Cazzola et al., 2016) (Table 4.15). It also helps to illustrate the sequence in which subsidies would be targeted across different U.S. regions by encompassing multiple regional markets. The modeling framework could equally be applied for other target levels.

The analysis is conducted for BEV technology with a 200 mile-range, assumed to be available in seven size classes of mini-compact, compact, full-size, small SUV, large SUV, minivan, and pickup. We originally generated optimistic, reference, and pessimistic EV market curves based on the reference, low, or high fuel price conditions in each sub-market. The optimistic market curves correspond to high gasoline and low electricity prices. Our analysis showed that in the case of pessimistic market curves, corresponding to low gasoline and high electricity prices, both the international and U.S. market curves are far below the EV cost learning curves, so they are excluded from presentation of our results. We also generate optimistic and pessimistic cost learning curves for BEV200 using the estimated upper and lower bound progress ratios for the battery technologies that are applicable to BEV200s. The base year in our study is 2015 with all monetary values presented in 2015 U.S. dollars (USD). Deflator factors from the Department of Commerce Bureau of Economic Analysis have been applied to adjust dollars of other years to 2015 dollars.

4.2.4 Market Curves

Market Curves combine WTP curves with the market size for each sub-market (Herron and Williams, 2013). Here, we explain the assumptions and input parameters used for generating international and U.S. regional market curves for BEV200.

4.2.4.1 Willingness-to-pay

WTP for BEV200 in each sub-market, S, is equal to the net present value (NPV) of the difference between the future annual fuel expenses (A) for the operation of an average BEV200 compared to that for an average GV in that sub-market, where the future annual fuel costs are discounted over the life of vehicle ownership (Equations 4.4–4.6).

$$WTP_S = NPV_{DR,LIFE}(A_{GV,S} - A_{BEV200,S}) \tag{4.4}$$

$$A_{GV,S} = \frac{M_S}{G_S} F_S \tag{4.5}$$

$$A_{BEV200,S} = M_S E_S(\alpha F_{off-peak,S} + (1-\alpha) F_{peak,S}) \tag{4.6}$$

In equation (4.4), DR is the discount rate and $LIFE$ is the term of vehicle ownership. In equation (4.5), M_S is the annual miles per vehicle, G_S is the fuel economy (mpg) of an average GV, and F_S is the gasoline cost (\$ gallon^{-1}). In equation (4.6), E_S is the efficiency (kWh mi^{-1}) of an average BEV200, α is the fraction of charging that happens off-peak, and $F_{off-peak,S}$ and $F_{peak,S}$ are the off-peak and peak electricity prices (\$ kWh^{-1}), respectively. In equations (4.4)–(4.6), fuel costs, vehicle size mix, fuel economy or efficiency, and vehicle mileage are differentiated by sub-market (S).

We assume the annual fuel cost remains constant in each year over the life of vehicle ownership. In our base calculation, we assume 10 years of vehicle ownership and a 5% discount rate. Ten years is selected based on the average age of passenger cars and light trucks currently in the fleet, 10.8 years, according to Kelley Blue Book (KBB, 2012) and 11.6 years, according HIS Markit (2016). Although BEVs are expected to have lower maintenance costs than GVs (INL, 2017), we assume equal maintenance costs for both technologies, mainly because unanticipated malfunctions are arguably more likely with the new technology. For our base calculation, we assume no battery replacement over the years of vehicle ownership and no peak charging for BEVs with the notion that consumers make rational decisions to maximize their benefits. To address the uncertainties associated with the assumptions made in our base calculation, we examine the sensitivity of our

results to the discount rate, years of vehicle ownership, peak charging, and battery replacement (see Section 4.2.7). We note that this WTP calculation ignores other factors that might influence the purchase decision such as marketing (Deloitte Consulting LLC, 2010; Eppstein et al., 2011; Krupa et al., 2014), styling (Deloitte Consulting LLC, 2010; NRC, 2013; Sierzchula et al., 2014), the social influences of observing others' purchases (Eppstein et al., 2011; Krupa et al., 2014; NRC, 2013; Sierzchula et al., 2014), and preferences for "green" or advanced technology (Deloitte Consulting LLC, 2010; Egbue and Long, 2012; Eppstein et al., 2015; Krupa et al., 2014).

For the international market, different countries serve as the sub-markets (Section 4.6.1). For the U.S. market, we define the regions (as sub-markets) based on the nine U.S. Census Divisions (Lenox et al., 2013) shown in Figure 4.4. The U.S. regions are New England (R1), Middle Atlantic (R2), East North Central (R3), West North Central (R4), South Atlantic (R5), East South Central (R6), West South Central (R7), Mountain (R8), and Pacific (R9). Section 4.6 details the annual fuel cost calculations for GVs and BEV200s in both international and U.S. regional markets.

For the international market, we generate two sets of market curves, one that includes gasoline taxes in the gasoline prices, and a second that excludes them (Section 4.6.1). For the U.S.-only analysis we exclude gasoline taxes from the gasoline prices based on the rationale that with significant EV penetration in the U.S. market, current fuel tax policies may change to avoid lost revenues for road infrastructure and maintenance (U.S. Congress, 2014).

4.2.4.2 Market Size

Market size is defined based on the potential market for BEVs in each sub-market. For the international analysis, we define the market size in each country based on their targets for EV stocks, presented in the Global EV Outlook (Cazzola et al., 2016) for most of the countries in our study (section 4.6.2.1). For the U.S. market, we assume the market size in each region is 25% of the regional new vehicle sales projections to 2020, from the U.S. Annual Energy Outlook (AEO) (EIA, 2017a) (Table 4.16). In comparison, the EV stock target for the U.S. that is utilized in the international market curves (about 1 million vehicles) equates to 7% of total new sales in 2020 or

about 1% of total new sales from 2015–2025. The total U.S. market size considered here is thus much larger than in the international market analysis because, with the rationale similar to that used for setting the overall production target, this market size helps to illustrate the sequence in which subsidies would be targeted across different U.S. regions by encompassing multiple regional markets.

4.2.5 Learning Curves

We generate the incremental learning curves of average BEV200, applied to both the international and U.S. markets, from battery learning curves. The term "incremental" refers to the difference between the upfront cost of an average BEV200 and a comparable GV. The average is calculated from seven vehicle size classes. We adapt the battery learning curves from Nykvist and Nilsson (2015), who estimated an initial battery cost of 300 \$ kWh^{-1}, corresponding to 5.2 GWh cumulative production in 2014, and a progress ratio of 6–9%. We assume the initial values apply for 2015. The progress ratios of 6% and 9% correspond to our pessimistic and optimistic learning curves, respectively. Section 4.6.3 provides a detailed explanation for how the battery learning curves are converted to incremental cost learning curves for BEV200s. In brief, we add the incremental costs, other than the battery costs, of an average BEV200 over an average GV to the battery learning curve. We assume these costs also benefit from learning by doing and economies of scale and consequently decline following the power law.

4.2.6 Environmental Externalities

To estimate the environmental externalities from deploying BEV200s in place of GVs in each U.S. region, we assume BEV200s generate annual environmental benefits from removing the GV tailpipe emissions and reducing the corresponding air pollution exposure, but these benefits are potentially offset by a shift in emissions to the electric sector. The net environmental benefits or damages are aggregated over the life of the vehicle as:

$$Net\ EE_S = \sum_{t=1}^{LIFE} \frac{AEE_S}{(1+DR)^t} \tag{4.7}$$

where EE_S and AEE_S (calculated from Equation 4.8) are the cumulative ($/vehicle) and annual ($/vehicle/year) environmental externalities in sub-market S, respectively. We assume a discount rate (DR) of 5% and 10 years of vehicle ownership ($LIFE$). Our calculation assumes that AEE_S remains constant over the years of vehicle ownership.

$$AEE_S = \sum_{j=1}^{3} AEB_{road,S} - \sum_{k=1}^{5} AED_{electric,S} \tag{4.8}$$

where $AEB_{road,S}$ and $AED_{electric,S}$ are annual environmental benefits and damages from the road and electric sector ($/vehicle/year), respectively, with $j = CO_2$, NO_x, and primary $PM_{2.5}$ and $k = CO_2$, NO_x, primary $PM_{2.5}$, SO_2, and NH_3. In our study, we include NO_x and primary $PM_{2.5}$ as the precursors of $PM_{2.5}$ for the road sector, and additionally consider SO_2 and NH_3 for the electric sector. SO_2 and NH_3 emissions from GVs in the light duty vehicle (LDV) sector are assumed negligible. NO_x is the only ozone precursor considered. Our calculations ignore the impacts of VOC emissions on ozone, as NO_x has been shown to be the most important contributor to ozone mortality (Pappin and Hakami, 2013). In our study, we focus on the direct emissions from the road and electric sectors, neglecting upstream emissions such as those associated with fuel extraction, processing, and delivery. Estimation of annual environmental externalities for each of these pollutants is described in more detail in the following sections.

4.2.6.1 Annual Environmental Externalities from $PM_{2.5}$

$PM_{2.5}$ consists of a mixture of solid and liquid particles, some of which are directly emitted to the atmosphere (primary $PM_{2.5}$) and some formed from gaseous precursors through accumulation processes such as condensation on existing particles. Toxicological evidence and epidemiological studies establish the link between long-term exposure to $PM_{2.5}$ and premature mortality (WHO, 2006).

To estimate AEE_S from $PM_{2.5}$ for each region, we first calculate the annual number of avoided deaths per unit of emission reduction (kg) from the road and electric sectors, in each

region (Table 4.18). To perform this task, we aggregate the grid-cell level numbers of deaths per annual emission of each species, from Dedoussi and Barrett (2014), in each region for each sector. Dedoussi and Barrett (2014) study focuses only on premature deaths. This assumption is justified because human health-related damages contribute up to 95% of the total damages from $PM_{2.5}$, including premature deaths, morbidity, reduced timber and crop yields, materials damage, and reduced visibility and recreation usage (Muller and Mendelsohn, 2009). Moreover, mortality is the largest contributor to the monetized health impacts of improving air quality (EPA, 2011). Dedoussi and Barrett (2014) apply the GEOS-Chem adjoint model to calculate the number of deaths in the U.S. due to annual emissions of each species in each model grid cell. They use baseline all-cause death rates for adults over 30 years old, and a concentration response function (CRF) derived by EPA (2011). The CRF assumes a 1% increase in all-cause deaths for every 1 μg m^{-3} increase in annual average $PM_{2.5}$. The baseline values of all-cause deaths for adults over 30 are estimated from the World Health Organization Global Burden of Disease (Mathers, 2008). They use population data from the Global Rural-Urban Mapping Project (GRUMP) 2006 database (Balk et al., 2006). The resolution of the three-dimensional GEOS-Chem grid is $\sim$50 km E-W $\times$ $\sim$50 km N-S, with 47 vertical layers extending to 80 km. For emissions, they use the 2005 National Emission Inventory (NEI) (EPA, 2008). In our study, we focus on the damages from long-term exposure to $PM_{2.5}$ versus short-term exposure due to the availability of adjoint sensitivity results.

For the road sector, we convert the annual number of avoided deaths per annual avoided emissions (kg) in each region to annual number of avoided deaths per mile in each region, using the emission factors (g mi^{-1}) for different vehicle size classes of GV and BEV200, adapted from the Greenhouse gas, Regulated Emissions, and Energy use in Transportation (GREET) model (ANL, 2016), and vehicle size distribution in each region, adapted from the Environmental Protection Agency (EPA) U.S. 9-region (US9R) database (2016, V1.0) (Lenox et al., 2013). For the electric sector, we convert the annual number of deaths per annual emissions (kg) in each region to annual number of deaths per kWh in each region, using the environmental activity of different generation technologies (g kWh^{-1} of input fuel), regional generation mix, and the average efficiency of each

generation type, adapted from the EPA US9R database (Lenox et al., 2013). Section 4.6.4 provides more details on these calculations.

For the road sector, AEE_S for each region and species per vehicle ($/year/vehicle) is calculated by multiplying the annual number of avoided deaths per mile by the value of a statistical life (VSL), and annual vehicle mileage for that region (Table 4.8). For the electric sector, we multiply the annual deaths per kWh by the VSL and the average annual kWh per vehicle (BEV200) for each region. We use a VSL of 7.4 million (2006) USD, inflated to 8.9 million (2015) USD, from EPA's Mortality Risk Valuation (EPA, 2017c). Net AEE_S per BEV200 for each region is the difference of total environmental benefits from the road sector and total damages from the electric sector.

4.2.6.2 Annual Environmental Externalities from Ozone

Ozone is a secondary pollutant formed from NO_x and VOCs in the presence of sunlight. Short-term exposure to ozone is associated with increased daily mortality (EPA, 2017b). We focus on effects of short-term exposure as opposed to long-term exposure due to the availability of adjoint sensitivity results for the former (Pappin et al., 2015).

For estimating AEE_S from ozone, we follow a similar procedure as described for $PM_{2.5}$ and in Section 4.6.4. For ozone, we estimate regional marginal benefits (MBs) per unit of NO_x reduction by aggregating grid-cell level MBs from Pappin et al. (2015) (Table 4.26). Pappin et al. (2015) use CMAQ adjoint model to estimate the MBs of NO_x emissions abatement ($ per ton) in each grid cell and day of the 2007 ozone season. The MBs are partial derivatives of monetized premature deaths in the U.S. attributable to short-term ozone exposure with respect to NO_x emissions, with a model grid resolution of 36 km $\times$ 36 km. The monetized total premature deaths are estimated using all-age non-accidental mortality rate and population data obtained from the Centers for Disease Control (CDC) at the county level (CDC, 2016), change in daily maximum 8-hour average ozone concentration (DM8A) in each grid cell, a concentration response effect estimate of 4.27×10^{-4} deaths per ppb for DM8A ozone (Bell et al., 2004), and VSL (EPA, 2010). The VSL used in Pappin et al. (2015) is $7.9 million (2008 USD) or $9.0 million (2015 USD). For emissions, Pappin et al.

(2015) use the 2005 EPA NEI dataset (EPA, 2008) projected to 2007. Meteorological inputs are from the Weather Research and Forecasting (WRF) model (Skamarock et al., 2008). They present MBs for the baseline emission levels (2007 in their study) as well as for different emission abatement scenarios. We use MBs from the 40% abatement scenario in their study for the road sector (mobile sources), and the 0% abatement scenario for the electric sector (point sources), consistent with our prior work on changes in emissions for these sectors with EV penetration (Keshavarzmohammadian et al., 2017).

We opt to neglect the impact of VOCs on ozone mortality in our analysis. While this limitation penalizes BEV, as VOC emissions from EV charging are negligible compared to those from GV, we note that the sensitivity of ozone mortality to VOC emissions is, on average, considerably lower than for NO_x (Pappin and Hakami, 2013).

4.2.6.3 Annual Environmental Externalities from CO_2

For CO_2, we use the marginal damages of CO_2 emissions from EPA's estimate of the SCC (Marten and Newbold, 2012) with a 3% discount rate (section 4.6.4.3), applied uniformly to all sectors and regions. After adjusting estimates in the original from 2007 to 2015 USD, the value used for this study is \$40 metric ton^{-1}. SCC incorporates the impacts of climate change on different categories such as human health, coastal communities, energy production, water resources, and biodiversity (Marten and Newbold, 2012). CO_2 emission factors for different vehicle size classes (Table 4.27) are adapted from the EPA US9R database (2014, V1.1), as estimated in our previous study (Keshavarzmohammadian et al., 2017). CO_2 emissions factors for different electricity generation technologies are presented in Table 4.28 and are from the EPA US9R database (2016, V1.0).

4.2.7 Sensitivity Analysis

To understand the impact of uncertainties associated with our assumptions we examine the sensitivity of the reference WTP and related subsidies to the discount rate, years of vehicle owner-

ship, battery replacement, and peak charging, and the sensitivity of environmental externalities to the regional electricity mix. Table 4.1 lists the sensitivity cases and the assumptions that distinguish them from the reference WTP calculations. Section 4.6.5 details the basis for these assumptions.

Table 4.1. Description of sensitivity cases.

Sensitivity case	**Description**
Discount rates	Low (3%) and high (10%) discount rates vs. the base calculation assuming 5% discount rate.
Years of vehicle ownership	Short (5) and long (15) years of vehicle ownership vs. base calculation assuming 10 years of vehicle ownership.
Battery replacement	One-time battery replacement in the tenth year of ownership vs. base calculation assuming no replacement.
Peak charging	25% of charging happens during the peak hours vs. base calculation assuming all charging off peak.
Cleaner electricity generation mix	Less generation from coal (ranging from 2% less in R9 to 22% less in R7) and more generation from renewables and natural gas (from 7% in R2 to 24% in R7). See Section 4.6.5 for further explanation.

4.3 RESULTS

In this section, we compare BEV learning curves with U.S. regional market curves, and estimate the minimum cumulative subsidies required to stimulate the BEV200 market diffusion to the set target level of production. Subsidy totals and external costs across U.S. regions are compared based on two approaches – a cascading diffusion model based on WTP, and the augmented minimum social cost (MSC) model that also considers how environmental externalities vary across regions. Section 4.6.6.1 provides results for our international analysis, which shows the most favorable countries for initial subsidies based on WTP, with and without including current gasoline taxes in the calculation of GV operating costs.

4.3.1 U.S. Regional Market

Figure 4.2 shows reference and optimistic market curves for the nine U.S. regions for the base calculation, starting from current production levels and incremental vehicle costs, and for a

"pre-diffusion" case in which the incremental cost of BEV200 is reduced due to production for international markets before diffusion starts in the U.S. In each case, the market size in each U.S. region is taken as 25% of the region's new vehicle sales projections to 2020. In the pre-diffusion case the starting incremental cost of a BEV200 is reduced from the current value of $15062 to $9570 following the optimistic learning curve, or to $10732 following the pessimistic learning curve, due to an assumed 4.2 million units of production for international markets before the U.S. diffusion starts. This number of pre-diffusion units is taken from the reference WTP case with gasoline taxes included in GV operating costs, and corresponds to filling BEV sales targets in the six countries with the highest WTP: Korea, Norway, Ireland, the Netherlands, Great Britain, and France. Note that if gasoline taxes are excluded, China and the U.S. would have the highest WTP in the international market.

As shown in Figure 4.2, R7 (West South Central) shows the highest WTP in the reference and optimistic market curves for the U.S., followed by R8 (Mountain). The differences between the highest and lowest WTP across U.S. regions are 2667 \$ vehicle^{-1} and 3188 \$ vehicle^{-1} for the reference and optimistic market curves, respectively. Reference gasoline prices do not vary significantly across regions. Instead, the difference between regional WTP values is driven by electricity prices and annual miles per vehicle. R7 has the highest annual miles per vehicle (14832 miles) among the regions and the lowest reference electricity price (8.3 cents kWh^{-1}).

The minimum subsidies, calculated based on WTP, required to incentivize BEV200 purchases to a target stock level of 12 million vehicles are shown in Table 4.2 for the base calculations and for the case assuming 4.2 million pre-diffusion units are sold elsewhere. With zero pre-diffusion units and with reference WTP, subsidies cannot make BEV200 vehicles competitive with GVs in the remaining regions, even with the optimistic progress ratio. This also holds for the reference WTP with 4.2 million pre-diffusion units. That is, the optimistic WTP level, more pre-diffusion units, or larger market sizes than assumed in our calculation would be required to enable subsidies for 12 million vehicles to suffice to make BEV200s cost-competitive.

In the case of optimistic WTP with the optimistic learning curve and 4.2 million pre-diffusion

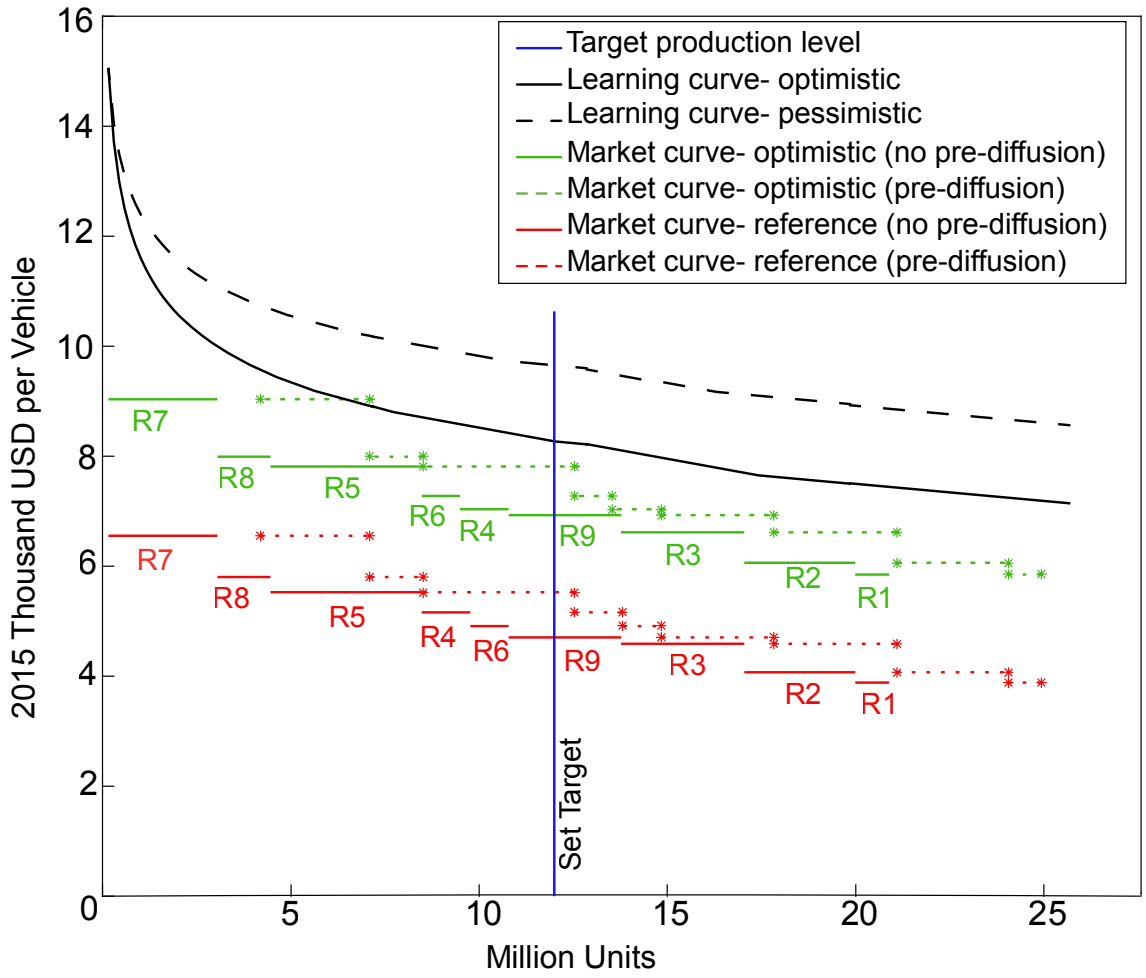

Figure 4.2. BEV learning curves (corresponding to 6% and 9% progress ratios), and optimistic and reference WTP market curves for both cases with zero and 4.2 million pre-diffucion units in the U.S. market.

units, which has the lowest amount of subsidies in Table 4.2, the average subsidy would be about 571 \$ vehicle^{-1}. In the case of reference WTP with the pessimistic learning curve and no pre-diffusion units, which has the highest total subsidy amount, the average subsidy would be about 5031 \$ vehicle^{-1}. Both values are lower than the 7500 \$ vehicle^{-1} Federal income tax credit currently offered in the U.S. for purchasing EVs.

The results of our sensitivity cases show that using a lower discount rate and assuming longer vehicle ownership increases WTP and decreases the required subsidy to meet the set target. One-time battery replacement at the tenth year of vehicle ownership generates negative WTP in all

Table 4.2. Minimum cumulative subsidies, calculated based on WTP, with a 12 million BEV target production level for the U.S., with and without 4.2 million units of advance production for international markets.

Market/Learning curves	**Subsidies (billion 2015 USD)**	
	With no pre-diffusion units (Base)[a]	With 4.2 million pre-diffusion units[b]
Reference/Optimistic	45.9	22.3
Reference/Pessimistic	59.6	32.3
Optimistic/Optimistic	18.9	4.08 (applied to 7.1 million units)
Optimistic/Pessimistic	32.6	14.0

[a] Subsidies are applied in R7, R8, R5, R6, R4, and R9.
[b] Subsidies are applied to R7, R8, and R5.

regions. In the reference case, WTP without the cost of battery replacement ranged from $3884 (R1, New England) to $6551 (R7); the cost of a replacement battery in year 10 reduced WTP to the range of -$3143 (R1) to -$260 (R5, South Atlantic). Assuming 25% peak charging at tripled electricity prices reduces WTP to the range of $2680 (R1) to $5643 (R7). These WTP reductions would correspondingly increase the required amount of subsidies. More details on the sensitivity analysis results are provided in section 4.6.6.2.

4.3.2 Environmental Externalities

Table 4.3 shows estimated $PM_{2.5}$, ozone, CO_2, and net environmental externalities (EE_S) associated with switching from GV to EV over 10 years of vehicle ownership, for each U.S. region. As noted above, environmental benefits for BEV would be somewhat higher if damages from GV emissions of VOC were included in the analysis. Table 4.3 also shows how precursor species and sectors contribute to the externalities for $PM_{2.5}$, ozone, and CO_2.

As shown in Table 4.3, switching to EVs is estimated to produce net environmental damage from $PM_{2.5}$ for all regions except R1 and R9 (Pacific). In all regions, contributions of reduced road sector NO_x and primary $PM_{2.5}$ emissions to lowering $PM_{2.5}$ concentrations contribute significantly to benefits of switching to EVs. On the other hand, the contribution of power plant SO_2 emissions

to damages from $PM_{2.5}$ exposure accounts for the largest share of damages from EVs in almost all regions, with NO_x emissions from power plants the second largest contributor (Table 4.3). Across the regions, R6 (East South Central) has the largest share of SO_2 damages from electric sector emissions, because R6 has a high fraction of generation from coal (46%), including a relatively high fraction from high sulfur coal.

Switching to EVs is estimated to provide net environmental benefits for ozone in six of the nine regions. R9 has the highest ozone benefits from switching to EVs, due to high population exposure and relatively clean electricity generation. In R3 (East North Central), R4 (West North Central), and R6, the effect of increased NO_x emissions from electricity generation outweighs the reductions in NO_x emissions from vehicles, to yield net ozone damages from switching to EVs (Table 4.3).

CO_2 externalities from switching to EVs are positive in all regions. R9 has the lowest CO_2 benefits from removing GV road emissions and R7 has the highest benefit. These results are mainly determined by annual vehicle mileage, as average fuel economies show small variations across regions (Table 4.8). Similarly, in switching to EVs, R9 has the lowest CO_2 damages from electric sector emissions and R7 has the highest damages. R7 has the highest share of generation from coal and natural gas (80%) and R9 has the lowest share (48%), almost all from natural gas (Table 4.23).

Figure 4.3 illustrates how the most favorable region to start the cascading diffusion and the minimum subsidy required to meet the target production level changes when the environmental externalities are incorporated into the U.S. regional market curves. While R7 is the most favorable region based on WTP (Figure 4.2), R9 is the most favorable region when environmental externalities are also considered. Table 4.4 compares the minimum subsidies needed to meet the 12 million vehicle target when sub-markets are ordered by minimum social cost and compares them with subsidies required when they are distributed based on WTP alone. As shown in Table 4.4, subsidies distributed based on the MSC model are higher than subsidies distributed based on WTP, however, the MSC-based subsidies sharply lower the social cost.

Table 4.4 shows that in the case with reference WTP and no pre-diffusion units, targeting the

Table 4.3. Total and net $PM_{2.5}$, ozone, and CO_2 for each precursor species, sector, and region and net environmental externalities (EE_S) for each region in \$ vehicle^{-1}. The negative sign indicates EVs would cause greater damage than GVs. The net value for each species is calculated from the total road sector benefits less total electric sector damages. Net EE_S is sum of net values for all species.

Species	**R1**	**R2**	**R3**	**R4**	**R5**	**R6**	**R7**	**R8**	**R9**
$PM_{2.5}$									
Environmental Benefits from the Road sector									
NO_x	1569	1726	1188	935	1205	771	789	345	1099
Primary $PM_{2.5}$[a]	930	1698	1003	465	805	563	587	470	1385
Total Road $PM_{2.5}$	2499	3424	2191	1400	2010	1334	1376	815	2484
Environmental Damages from the Electric sector									
NH_3	157	269	105	42	87	96	63	18	46
NO_x	144	621	1150	1312	805	824	567	329	62
Primary $PM_{2.5}$	71	417	729	333	500	516	279	157	46
SO_2	140	2209	2731	1472	1981	3945	1210	974	33
Total Electric $PM_{2.5}$	510	3516	4714	3158	3373	5382	2119	1478	187
Net $PM_{2.5}$ Externalities	1988	-93	-2523	-1758	-1363	-4048	-743	-663	2297
O_3									
Environmental Benefits from the Road sector									
NO_x	110	259	300	303	594	621	394	364	490
Environmental Damages from the Electric sector									
NO_x	13	198	454	456	543	653	253	317	20
Net O_3 Externalities	97	61	-154	-153	51	-32	141	47	470
CO_2									
Environmental Benefits from the Road sector									
CO_2	1204	1269	1274	1327	1479	1615	1646	1422	1186
Environmental Damages from the Electric sector									
CO_2	235	273	435	479	448	523	545	497	199
Net CO_2 Externalities	969	996	839	848	1031	1092	1102	925	987
Net Environmental Externalities (EE_S)									
Net EE_S	**3053**	**964**	**-1838**	**-1063**	**-281**	**-2988**	**499**	**309**	**3754**

[a] Primary $PM_{2.5}$ includes black carbon (BC) and organic carbon (OC).

regions based on the MSC model increases the subsidies by 4% and 3%, respectively, for optimistic and pessimistic learning curves. However, the corresponding social costs are decreased by 68% and 52%, respectively. With 4.2 million pre-diffusion units, the subsidies estimated with optimistic and pessimistic learning curves are increased by 18% and 12%, respectively, while the respective social costs are decreased by 137% and 93%. In the case with 4.2 million pre-diffusion units, reference WTP, and the optimistic learning curve, the external benefits exceed the subsidies.

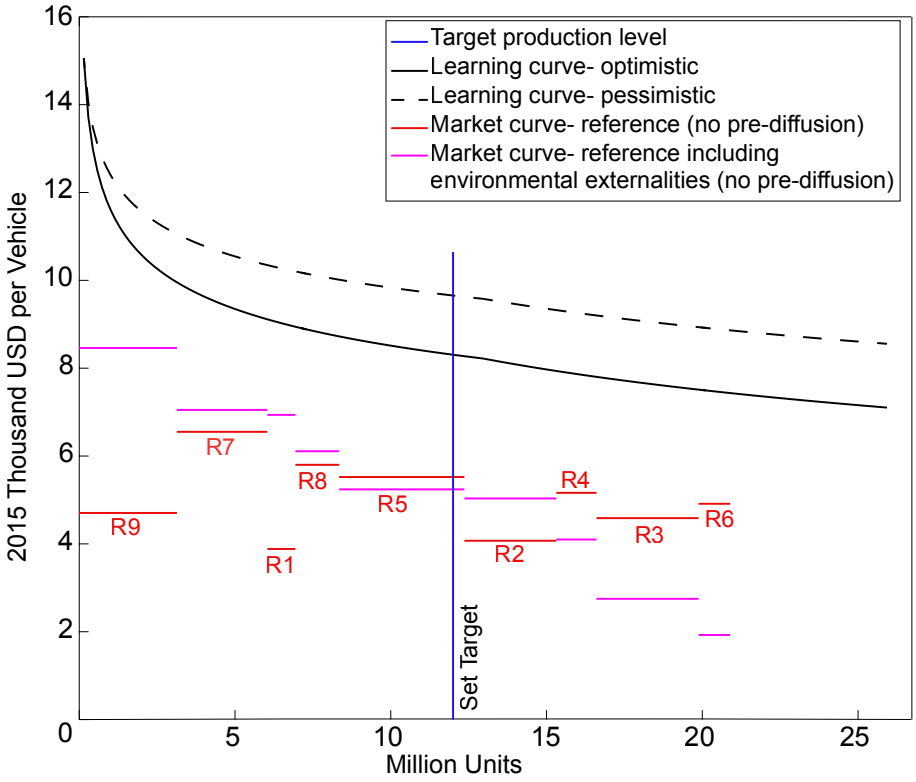

Figure 4.3. BEV learning curves (corresponding to 6% and 9% progress ratios), and reference WTP market curves with and without environmental externalities from driving EVs in the U.S. market. Sub-markets are ordered based on MSC.

The environmental externalities from deploying BEV200s in each region are sensitive to electricity mix and the type of fuel used for electricity generation. We considered a cleaner electricity mix adapted from MARKAL modeling for the year 2030 with implementation of the Clean Power Plan provisions in the EPA US9R database (Table 4.1 and Section 4.6.5). As shown in Table 4.5, with less generation from coal and more generation from renewables and natural gas, the environmental benefits of switching to EVs are increased in all regions compared to those estimated in our base calculations (Table 4.3). The improvement ranges from 184 \$ vehicle^{-1} in R9 to 2315 \$ vehicle^{-1} in R3. The increased benefits are mainly from removing exposure to $PM_{2.5}$ formed from SO_2 emissions. Regions R3 and R5 show positive environmental externalities from EVs with the new electricity mix as opposed to the base mix. With the cleaner electricity mix used to estimate externalities, the order in which subsidies would optimally be applied shifts to start with R7. As

Table 4.4. Effect of WTP versus minimum social cost ordering of regional markets on subsidies to achieve a 12 million BEV production level, air quality and climate externalities, and overall social costs. Results are shown for reference market curves and pessimistic or optimistic learning curves. All costs are in billion 2015 USD.

	With no pre-diffusion units		With 4.2 million pre-diffusion units	
Market curve/	Reference	Reference	Reference	Reference
Learning curve	Optimistic	Pessimistic	Optimistic	Pessimistic
Subsidies for vehicle purchase[a] (based on WTP ordering)	45.9	59.6	22.3	32.3
Environmental Externalities (based on WTP ordering)	0.94	0.94	0.90	0.90
Social Cost (based on WTP ordering)	45.0	58.7	21.4	31.4
Subsidies for vehicle purchase[b] (based on MSC ordering)	47.8	61.5	26.3	36.3
Environmental Externalities (based on MSC ordering)	33.3	33.3	34.2	34.2
Social Cost (based on MSC ordering)	14.5	28.2	-7.90	2.10

[a] Subsidies are applied in R7, R8, R5, R4, R6, and R9 for the case with no pre-diffusion units and in R7, R8, and R5 for the case with 4.2 million pre-diffusion units.
[b] Subsidies are applied in R9, R7, R1, R8, and R5 for the case with no pre-diffusion units and in R9, R7, R1, R8 for the case with 4.2 million pre-diffusion units.

shown in Table 4.6, this case presents lower subsidies for vehicle purchase and lower social costs compared to the cases with the current electricity mix. Except in the case with the pessimistic learning curve and reference market curve, the social cost is negative, meaning external benefits of EVs outweigh the subsidies.

Table 4.5. Net $PM_{2.5}$, ozone, CO_2, and environmental externalities (EE_S) in \$ vehicle^{-1} for the electricity mix sensitivity case in each region. Negative sign indicates damages.

Species	**R1**	**R2**	**R3**	**R4**	**R5**	**R6**	**R7**	**R8**	**R9**
$PM_{2.5}$	2286	534	-462	-1033	-4	-2404	642	-216	2395
O_3	105	90	1	-83	271	163	304	140	481
CO_2	1064	1049	939	933	1140	1192	1277	1045	1062
EE_S	3456	1673	478	-184	1407	-1049	2222	969	3938

Table 4.6. Effect of cleaner electricity production on subsidies, air and climate externalities, and overall social costs required for a 12 million BEV production level. All costs are in billion 2015 USD.

	With no pre-diffusion units		With 4.2 million pre-diffusion units	
Market curve/	Reference	Reference	Reference	Reference
Learning curve	Optimistic	Pessimistic	Optimistic	Pessimistic
Subsidies for vehicle purchase[a]	19.9	33.6	3.95	13.8
Environmental Externalities	28.0	28.0	21.3	21.3
Social Cost	-8.10	5.60	-17.35	-7.50

[a] Subsidies are applied in R7, R9, R1, R5, and R8 for the case with no pre-diffusion units and in R7, R9, R1, and R5 for the case with 4.2 million pre-diffusion units.

4.4 DISCUSSION

This study estimates how WTP and air quality and climate benefits of EVs differ across U.S. regions and how these differences could be exploited to make EV subsidies more efficient. In order to focus on these influences, the study makes the assumption that vehicle purchase choices are based on cost of vehicle ownership over the lifetime of the vehicle. Other factors that influence consumer purchases, including make and model preferences and infrastructure limitations, are neglected for simplicity.

The choice of external damage estimates for air pollution emissions is an important source of uncertainty in our study. As detailed in the methods section, we estimate the number of premature deaths or marginal damages of $PM_{2.5}$ and ozone precursors for each sector and region (Tables 4.18 and 4.26) using grid cell marginal damages from Dedoussi and Barrett (2014) and Pappin et al. (2015), respectively. These specific studies were selected over other studies in the literature (e.g., Fann et al. (2009); Heo et al. (2016); Muller and Mendelsohn (2007); NRC (2010)) because their results could be readily aggregated to match the U.S. regions and sectors required in our study.

While results cannot be directly compared at the regional level, it is instructive to compare our external damage estimates with nationally averaged values from other references. Our estimates of marginal damages due to exposure to $PM_{2.5}$ from electric sector SO_2 emissions range from $34491

to \$48830 (2015USD) per metric ton, corresponding to R8 and R3. These values are in the range of previously published SO_2 damage estimates summarized by Brown et al. (2013): from \$1856 ton^{-1} for an average of all resources (Muller and Mendelsohn, 2007) to \$98960 ton^{-1} for average power plants (Fann et al., 2009). Our estimates of marginal damages due to $PM_{2.5}$ from electric sector NO_x range from \$9142 to \$42268 (2015USD) per metric ton, for R8 and R2 (Middle Atlantic), respectively. In comparison, Brown et al. (2013) report prior estimates for NO_x damages ranging from \$458 ton^{-1} for an average of all resources (Muller and Mendelsohn, 2007) to \$18555 ton^{-1} for average power plants (Fann et al., 2009). Factors driving the differences in damage estimates include the value and treatment of VSL, the emission sources or sectors considered, baseline emissions (year and reference), urban or rural population exposure, and the concentration-response function used.

Uncertainties in the SCC estimates include those associated with quantifying the physical effects of GHG emissions and those associated with future changes in human behavior and well-being such as population, economic growth, and GHG emissions (IWG, 2016). Since 2009, the U.S. Government Interagency Working Group (IWG) has tried to harmonize key modeling assumptions (including socio-economic-emission scenarios, discount rate, and climate sensitivity probability distribution) used in the integrated assessment models (IAMs) by assuming five socio-economic-emission scenarios and three discount rates and using three well-known IAMs (IWG, 2016; Marten and Newbold, 2012). Accordingly, their estimates of SCC for 2015 are 11, 36, 56, and 105 2007USD metric ton^{-1} of CO_2, corresponding to 5%, 3%, 2.5% discount rates, and 95^{th} percentile with 3% discount rate, respectively (IWG, 2016). This study used the value corresponding to a 3% discount rate, inflated to 2015USD. While IWG was able to consider these sources of uncertainty quantitatively, uncertainties that have not been fully quantified in the SCC estimates include quantification of catastrophic damages, treatment of technology change and adoption, and modeling of inter-regional and inter-sectoral linkages (IWG, 2016). We found that replacing GVs with BEVs reduces CO_2 emissions in all U.S. regions, so using a higher value of SCC would favor BEVs in the externalities comparison.

A further limitation of our study is that it only covers a subset of health and welfare exter-

nalities associated with vehicles. While mortality effects dominate air pollution damage estimates, other endpoints could also present tradeoffs between GV and BEV. Effects neglected in our study include morbidity effects for $PM_{2.5}$ and ozone, and mortality from short-term exposure to $PM_{2.5}$ and from long-term exposure to ozone. The contribution of VOC emissions to ozone-related damages is also neglected. Based on current inventories, our analysis assumes that the contribution of NH_3 emissions from GVs to $PM_{2.5}$ formation is negligible. However, recent studies question the NH_3 emissions inventories for the road sector. Sun et al. (2017) measured NH_3:CO_2 emission ratios and concluded that the current emission inventories underestimate NH_3 emissions from the road sector; our estimated benefits of switching to EVs would be biased low if a significant amount of these under-reported emissions are associated with LDVs. Our study also overlooks environmental or welfare damages from $PM_{2.5}$ and ozone, including damage to crops, building materials, and climate, as well as water consumption and land use tradeoffs from electricity generation and oil and gas production. We also focus on direct emissions from GV or emissions from electricity generation for EV, neglecting other stages of the well-to-wheels and vehicle life cycles (Nealer et al., 2015; NRC, 2010; Tamayao et al., 2015; Yuksel et al., 2016). A more comprehensive suite of externalities could be considered in future work that builds on the framework presented here.

Despite differences in the models used to estimate them, the general trend of our estimates of emissions-related environmental externalities from replacing GVs with BEV200 is similar to that found by Holland et al. (2016), who estimated state-level external costs of driving GV versus BEV accounting for damages associated with CO_2, SO_2, NO_x, $PM_{2.5}$, and VOC emissions. They found net benefits from EV adoption in California and Washington (R9), Utah, Colorado, and Arizona (R8), and Texas (R7) and found net damages in Georgia, Florida, North Carolina, and Virginia (R5), and Illinois and Ohio (R3).

4.5 CONCLUSIONS AND POLICY IMPLICATIONS

In this study, we utilize the cascading diffusion model to investigate how regionally heterogeneous subsidies could efficiently promote the diffusion of BEV200s internationally and across the

U.S. For the U.S. analysis, we compare the minimum subsidies distributed based on WTP and BEV200 learning curves, with those accounting for air quality and climate externalities. Although the numerical results presented are specific to the assumed market sizes and target production level, the framework can be applied to any set of markets with different sizes and target levels of production.

Our analysis shows that WTP is mainly affected by gasoline prices, the annual miles driven per vehicle, and the vehicle size distribution in a particular sub-market. Our U.S. analysis excluded gasoline taxes from the price of gasoline, because tax policies may change in the future as more EVs enter the fleet. Road-use taxes or other taxes that cover all types of vehicle technologies may be required to avoid revenue losses (Aasness and Odeck, 2015; U.S. Congress, 2014). The international analysis shows that if current gasoline taxes are omitted, markets with higher base fuel prices, such as the U.S., are more favorable for advancing BEV diffusion.

Our results highlight the importance of the international market on the level of subsidies required within the U.S. to achieve a specified EV penetration level. For example, with the sequential market curve in the U.S., advance international sales of about 4 million vehicles cuts the subsidy required to reach a 12 million vehicle target in the U.S. by about half. The international analysis presented in Section 4.6.6 also demonstrates how influential larger markets are for bringing down the cost of BEV technology. Thus, in addition to the per vehicle subsidy amount, the overall budget for cumulative subsidies, which accordingly defines the target level of production, is also important.

Our estimates indicate that the air quality and climate externalities from deploying BEV200s vary significantly across U.S. regions, depending on the fuel source for electricity generation and the level of population exposure. Switching to BEV200s generates net benefits in regions with low reliance on coal for electricity generation and with high population exposure to GV emissions (R1, R2, R7, R8, and R9). However, BEVs create net damages in regions with high reliance on coal and relatively low population exposure to GV emissions (R3, R4, R5, and R6). Our results convey that incorporating environmental externalities into the subsidy design might change the choice of

the more favorable region for applying targeted subsidies and starting the BEV200 diffusion with respect to the ordering based only on WTP. In our analysis, for example, R7 shows more favorable conditions for consumer WTP, but R9 gains the highest environmental benefits from deploying EVs.

Our sensitivity analyses show that one-time battery replacement over the years of vehicle ownership generates negative WTP in all U.S. regions. Previous studies have discussed the effect of customers' concerns about the battery life and replacement cost on EV adoption (Egbue and Long, 2012; Eppstein et al., 2011; Krupa et al., 2014; Tran et al., 2012). Overall, they found that in addition to the perceived benefits of EVs, the battery cost is among the most important factors influencing EV purchases.

Our sensitivity analysis with respect to peak charging shows considerable reduction in WTP in all regions, assuming 25% peak-charging at tripled electricity prices compared to the off-peak. There is a large variation in electricity prices offered by the utilities across the country, which results in different levels of reduction in WTP by peak-charging. Policies informing customers to increase their benefits by avoiding unnecessary peak charging can help reduce the extra pressure on the grid. However, Tamayao et al. (2015) suggest that with the 2009 U.S. generation mix, delayed charging at midnight could lead to higher emissions than convenience charging, which starts upon arrival home after last trip of day and occurs mostly during the peak hours, mainly due to the increased electricity generation from coal at night. This issue warrants further investigation with updated information on the electricity generation mix.

Our sensitivity analysis with respect to the electricity mix shows that policies boosting the move toward more generation from renewables and natural gas switched the externalities associated with EVs from negative to positive in regions R3 and R5. Switching to the cleaner electricity mix might also change the order of regions in which the subsidies might be applied. In our case, with the cleaner electricity mix the most favorable region for subsidies switches from R9 to R7.

Our analysis finds that with a 12 million vehicle target, external benefits of EVs exceed subsidy costs in cases with an optimistic learning curve and pre-diffusion units sold elsewhere, or

with a cleaner electricity mix. The analysis also shows that while required subsidies distributed across U.S. regions based on the MSC approach would be modestly higher than those required if distributed based purely on WTP, the MSC approach would deliver substantially higher external benefits.

4.6 SUPPORTING INFORMATION

4.6.1 Willingness-to-pay Calculations

4.6.1.1 Annual Fuel Cost Calculation for Gasoline Vehicles

The annual fuel costs ($) for gasoline vehicles (GVs) in each sub-market "S" are calculated from annual miles per vehicle in sub-market "S" divided by the average mpg in that sub-market and multiplied by unit gasoline price ($ gallon^{-1}) in that sub-market.

For the international market, different countries serve as the sub-markets. The countries we have included in our analysis are Austria, Canada, China, Denmark, France, Germany, India, Ireland, Japan, Netherlands, Norway, Portugal, South Korea, Spain, United Kingdom, and the U.S. (We use ISO ALPHA-3 codes for naming the countries in our results). We have selected these countries because they either had considerable EV stocks by 2015 or they have set EV stock targets to 2020 (Cazzola et al., 2016). Table 4.7 shows the ISO ALPHA-3 codes (ISO, 2017), average annual miles per vehicle (adapted from various references), average fleet fuel economy (An et al., 2011), and reference, high, and low gasoline prices (World Bank, 2017) for each country. The average annual miles per vehicle range from 3208 miles for JPN to 12304 miles for the U.S. The first set of market curves considered in our analysis is based on prices that include gasoline taxes. Among the reference gasoline prices (including taxes), the highest price belongs to NOR (9.25 $ gallon^{-1}) and the lowest belongs to the U.S. (3.10 $ gallon^{-1}). The lowest of the low gasoline prices happens in CHN (1.53 $ gallon^{-1}) and the highest of high gasoline prices happens in NOR (10.38 $ gallon^{-1}). The low gasoline prices are 18%–68% lower (corresponding to JPN and CHN) than the reference prices and high gasoline prices are 3%–46% higher (corresponding to DNK and JPN).

Table 4.7. ALPHA-3 country code, average annual miles per vehicle, average fleet fuel economy, gasoline prices (reference, low, and high), and gasoline taxes for all countries.

Country	ISO ALPHA-3 code[a]	Average annual miles per vehicle[b]	Fuel economy[c,d] (mpg)	Gasoline prices[e] ($ gallon^{-1})			Gasoline taxes[g]
				Reference	Low[f]	High[f]	
Austria[I]	AUT	9658	43.1	6.52	4.27	7.43	2.62
Canada	CAN	7288	28.7	4.77	2.24	5.42	1.33
China	CHN	8777	34.0	4.77	1.53	5.62	0.62
Denmark[II]	DNK	8749	43.1	8.19	5.33	8.44	3.14
France	FRA	8480	43.1	7.29	5.22	8.35	3.26
Germany	DEU	7715	43.1	7.33	4.80	8.04	3.50
India[III]	IND	5479	43.1	4.48	2.75	5.13	0.72
Ireland	IRL	10497	43.1	7.82	3.80	8.29	3.14
Japan	JPN	3208	41.0	5.62	4.62	8.20	2.30
Netherlands	NLD	8078	43.1	8.76	5.44	9.56	4.03
Norway	NOR	7697	43.1	9.25	6.25	10.38	3.91
Portugal	PRT	3766	43.1	7.70	4.06	8.82	3.14
South Korea[I,IV]	KOR	12089	41.0	6.32	4.53	7.48	2.86
Spain[I]	ESP	5956	43.1	6.64	3.85	7.18	2.50
United Kingdom	GBR	9285	43.1	7.82	5.28	8.90	3.67
U.S.	USA	12304	28.7	3.10	1.75	3.98	0.56

[a] ISO (2017)

[b] Data for Canada, China, France, Germany, Japan, United Kingdom, and the U.S. are from FHWA (2008).
Data for Austria and Spain are estimated from UNECE (2015).
Data for Denmark are estimated from Nielsen et al. (2012).
Data for India are from Schievelbein et al. (2017).
Data for Ireland are from SEI (2005).
Data for Netherlands are from CBS (2015).
Data for Norway are from Statistics Norway (2017).
Data for Portugal are from Azevedo and Cardoso (2009).
Data for South Korea are estimated from Statista (2017c) and from Iaych et al. (2009).

[c] Data from An et al. (2011).

[d] All fuel economies are adjusted values.

[e] Data from World Bank (2017).

[f] Low and high gasoline prices for each country correspond to the lowest and highest gasoline prices, since 1995, deflated to 2015 USD.

[g] Data for OECD countries are from OECD (2014).
Data for India are from IEA (2013).
Data for China is from Lin and Zeng (2013).

[I] We estimated average annual miles per vehicle for these countries from total annual vehicle miles traveled and total annual registered vehicles for passenger cars.

[II] For Denmark, we estimated the average annual miles per vehicle by taking the average of miles traveled by different size classes, categorized by the engine capacity, in a year.

[III] We assumed the average fuel economy in India is similar to that of the European Union countries.

[IV] We assumed the average fuel economy in South Korea is similar to that of Japan.

For the second set of international market curves, we calculate the annual fuel costs for GVs excluding the gasoline taxes. For most of the countries in our study, the gasoline taxes, which are shown in Table 4.7, are adapted from OECD (2014). We have studied both cases due to the possibility that countries will change their fuel tax policies after deploying more EVs, in order to avoid partial deficits in their revenue for road infrastructure and maintenance (Aasness and Odeck, 2015; U.S. Congress, 2014). That is, more equitable tax policies covering all technologies may apply. However, due to the diversity and complexity of these policies, their purposes and their relations with road funding inside and across the countries, it is hard to predict what changes would be made and when they would happen. Therefore, we also include calculations for the international market assuming no change in the current status of policies that currently tax gasoline and hence favor EVs.

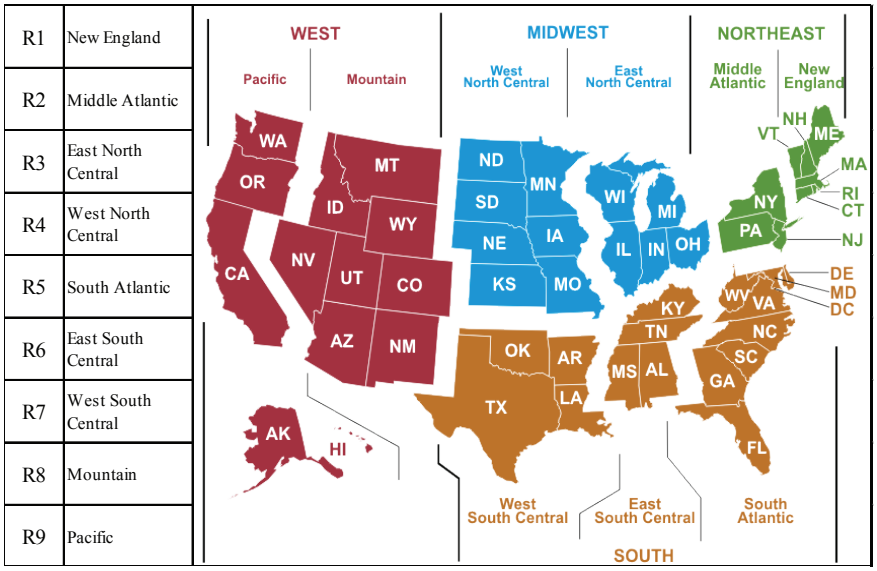

Figure 4.4. Map of U.S. Census Divisions (EIA, 2017b) and the U.S. EPA MARKAL region associated with each Division (Lenox et al., 2013).

For the U.S. market, we define the regions (as sub-markets) as defined in the Environmental Protection Agency (EPA) U.S. 9-region (US9R) database, which in turn are based on the U.S. Census Divisions (Lenox et al., 2013). Figure 4.4 depicts the nine regions and the states located in each region. To estimate the average annual gasoline expenses for each region, we first calculate the

average fleet fuel economy for each region (Table 4.8) from the fuel economies for each vehicle size class in 2015 (Table 4.9), adapted from NRC (2013). The NRC report presents the fuel economy projections in specific years for average cars and trucks without distinction among vehicle size classes. The results have been presented for two scenarios, including optimistic and midrange. Our previous work (Keshavarzmohammadian et al., 2017) explained how we have extrapolated the NRC efficiency projections for average cars and trucks in 2030, and 2050, to seven size classes and years in between these years, with five year increments. We have repeated similar calculations here with the only difference being in the NRC (2013) scenario used. Here, we apply our previous method on the NRC's midrange scenario with the low-volume production assumptions. In contrast, our previous calculation was based on their optimistic scenario with mass volume production. This is because our current study is focused on the transition period for deploying BEV200s. The average fuel economy in each region is the sum of point-wise multiplication of region-specific vehicle size distribution factors by the corresponding fuel economy for each size. The region-specific vehicle size shares (Table 4.10), counting for the vehicle size distribution in each region, are fractions less than one and are summed to one for each region. The regional vehicle size shares are from the EPA US9R database (2016, V1.0) (Lenox et al., 2013). EPA presents the shares for all regions in 2010 and 2020. We estimate the shares in 2015 using interpolation. In all regions, the full-size class has the biggest share, followed by the compact and small SUV classes. Table 4.8 also shows the annual miles per vehicle for each region, which are calculated by taking a weighted average of annual miles per vehicle for states located in a region, using the number of registered vehicles as the weight factor for each region. The values for annual miles per vehicle and numbers of registered vehicles in each state are taken from the Federal Highway Administration website (FHWA, 2017). The annual miles per vehicle range from 10893 miles for R1 (New England) to 14832 miles for R7 (West South Central). Gasoline prices in each region are estimated by taking the average over gasoline prices in the states located in that region. Reference, high, and low gasoline prices for each state (Table 4.8) are taken from the Energy Information Administration (EIA, 2016a) and are converted to the gasoline prices excluding taxes using federal and state gasoline tax data from

EIA (2016b). Among the reference gasoline prices, the highest price belongs to R9 (Pacific) (2.56 \$ gallon^{-1}) and the lowest belongs to R3 (East North Central) (2.05 \$ gallon^{-1}). In the bounding cases, the lowest gasoline price happens in R5 (South Atlantic) (0.73 \$ gallon^{-1}) and the highest price happens in R9 (3.02 \$ gallon^{-1}). The low gasoline prices are 18%–29% lower (corresponding to R9 and R6 (East South Central)) than the reference prices and high gasoline prices are 71%–82% higher (corresponding to R8 (Mountain) and R5).

Table 4.8. Average annual miles per vehicle, average fleet fuel economy, and gasoline prices (reference, low, and high) for all U.S. regions.

Region	**Average annual miles per vehicle**	**Fuel economy (mpg)**	**Gasoline prices[a,b] (\$ gallon^{-1})**		
			Reference	**Low[c]**	**High[c]**
R1	10893	30.4	2.18	0.52	2.75
R2	11545	30.5	2.09	0.44	2.67
R3	11496	30.3	2.05	0.45	2.62
R4	11908	30.2	2.13	0.51	2.64
R5	13548	30.7	2.12	0.38	2.66
R6	14724	30.5	2.13	0.55	2.74
R7	14832	30.3	2.12	0.52	2.72
R8	12755	30.2	2.20	0.64	2.76
R9	10981	30.9	2.56	0.73	3.02

[a] Data is from the EIA (2016a).
[b] The numbers show gasoline prices excluding taxes. EIA website presents state gasoline prices with taxes. We excluded Federal and states taxes, using the tax information from EIA (2016b).
[c] Low and high gasoline prices for each region correspond to the lowest and highest gasoline prices, since 1984, deflated to 2015 USD.

Table 4.9. Average fuel economy for different GV size classes in 2015, adapted from NRC (2013) midrange scenario with low-volume production assumption.

Vehicle size class	Compact	Full-size	Large SUV	Minivan	Mini-compact	Pickup	Small SUV
Fuel economy (mpg)[a]	40	32	22	27	27	21	32

[a] All Fuel economies are adjusted values.

Table 4.10. Regional vehicle size class shares in 2015, adapted from EPA US9R database (2016, V1.0).

Size class	R1	R2	R3	R4	R5	R6	R7	R8	R9
Compact	0.22	0.22	0.21	0.21	0.23	0.22	0.21	0.21	0.24
Full-size	0.27	0.27	0.26	0.26	0.28	0.28	0.26	0.25	0.29
Large SUV	0.13	0.13	0.13	0.13	0.12	0.12	0.13	0.13	0.12
Minivan	0.05	0.05	0.05	0.05	0.05	0.05	0.05	0.05	0.05
Mini-compact	0.01	0.01	0.01	0.01	0.01	0.01	0.01	0.01	0.01
Pickup	0.13	0.13	0.14	0.14	0.13	0.13	0.14	0.14	0.12
Small SUV	0.19	0.18	0.19	0.19	0.17	0.18	0.19	0.19	0.16

4.6.1.2 Annual Fuel Cost Calculation for BEV200s

Annual fuel costs ($) for electricity for BEV200s in each sub-market "S" are calculated from annual miles per vehicle in sub-market "S" multiplied by average efficiency of BEV200s in that sub-market (kWh mi^{-1}) multiplied by unit electricity price in that sub-market ($ kWh^{-1}).

To estimate annual electricity expenses for both international and the U.S. regional markets, we follow a similar approach as explained for calculating annual gasoline expenses for the U.S. regional markets. That is, we estimate the average BEV200 efficiencies for each country (Table 4.11) and region (Table 4.12), from the efficiencies for each BEV200 size class (Table 4.13), and the size distribution for each country (Table 4.14) or region (Table 4.10). We adapted the efficiencies for each size of BEV200 from the NRC (2013) midrange scenario with low-volume production assumptions in 2015, using the same approach introduced in our previous work (Keshavarzmohammadian et al., 2017). The same average annual miles per vehicle as those used in calculating annual gasoline expenses are used here for each country and region (Tables 4.7 and 4.8). The electricity prices (reference, high, and low) for each country and region are shown in Tables 4.11, and 4.12, respectively. Electricity prices in each country are from various references. Electricity prices in each U.S. region are estimated by taking the average over electricity prices in the states located in that region. Reference, high, and low electricity prices for each state are adapted from EIA (2016c).

In the international market, among the reference electricity prices, the highest price belongs

to DNK (33.7 ¢ kWh^{-1}) and the lowest belong to CHN and IND (8.8 ¢ kWh^{-1}). In the bounding cases, the lowest electricity price happens in KOR (8.7 ¢ kWh^{-1}) and the highest price happens in DEU (42.5 ¢ kWh^{-1}). In the U.S. regional market, among the reference electricity prices, the highest price belongs to R9 (16.4 ¢ kWh^{-1}) and the lowest belongs to R7 (8.3 ¢ kWh^{-1}). The lowest of the low electricity prices happens in R6 (7.3 ¢ kWh^{-1}) and the highest of high prices happens in R9 (17.9 ¢ kWh^{-1}). The low electricity prices are 8%–34% lower than the reference prices (corresponding to R6 and R7) and high electricity prices are 7%–34% higher (corresponding to R7 and R9).

Table 4.11. Average BEV200 efficiencies, and electricity prices (reference, low, and high) for all countries.

Country	**Average efficiency**[a] **(kWh/mi)**	**Electricity prices**[b] **¢ kWh^{-1}**		
		Reference	**Low**[c]	**High**[c]
Austria	0.17	22.2	22.2	30.1
Canada	0.19	10.7	9.4	11.6
China	0.17	9.0	8.8	9.7
Denmark	0.17	33.7	33.7	45.2
France	0.17	18.1	17.9	22.3
Germany	0.17	32.7	32.7	42.5
India	0.20	8.8	8.8	8.8
Ireland	0.17	25.2	25.2	32.9
Japan	0.18	22.5	21.6	31.5
Netherlands	0.17	20.7	20.7	33.2
Norway	0.17	9.5	9.5	19.6
Portugal	0.17	25.3	24.0	31.4
South Korea	0.19	10.3	8.7	11.9
Spain	0.17	32.5	21.8	32.5
United Kingdom	0.17	23.5	20.5	27.6
U.S.	0.19	12.7	12.4	13.5
World Average	0.18			

[a] All efficiencies are adjusted values.

[b] Data for OECD countries are adapted from IEA energy prices in the OECD (2017).
Data for China is adapted from Electricity Local (2017), OVO Energy (2017), and Climate Scope (2017).
Data for India is adapted from OVO Energy (2017).

[c] Low and high electricity prices for each country correspond to the lowest and highest electricity prices, since 2007, deflated to 2015 USD.

Table 4.12. Average BEV200 efficiencies, and electricity prices (reference, low, and high) for all U.S. regions.

Region	**Average efficiency**[a] **(kWh/mi)**	**Electricity prices**[b] **¢ kWh^{-1}**		
		Reference	**Low**[c]	**Hight**[c]
R1	105.9	15.0	17.9	13.0
R2	106.3	13.5	16.1	12.1
R3	105.7	10.0	11.3	8.2
R4	105.3	9.0	10.4	7.7
R5	106.8	10.2	12.1	8.4
R6	106.4	9.1	9.9	7.3
R7	105.6	8.3	11.1	7.7
R8	105.2	9.0	10.4	7.4
R9	107.6	16.4	17.9	10.8

[a] All efficiencies are adjusted values.
[b] Electricity prices are adapted from the EIA (2016c).
[c] Low and high electricity prices for each region correspond to the lowest and highest electricity prices, since 1990, deflated to 2015 USD.

Table 4.13. Average efficiencies for different BEV200 size classes in 2015, adapted from NRC (2013) midrange scenario with low-volume production assumption.

Vehicle size class	Compact	Full-size	Large SUV	Minivan	Mini-compact	Pickup	Small SUV
Efficiency (kWh/mi)[a]	0.14	0.17	0.26	0.20	0.22	0.25	0.18

[a] All efficiencies are adjusted values.

Table 4.14. Vehicle size class shares for each country, adapted from various references.

	Mini-compact	**Compact**	**Full-size**	**SUV (Small and Large)**	**Minivan**	**Pickup**
Austria[a]	9.9	51.2	12.8	20.7	3.9	1.5
Canada[b]	1.4	24.2	29.8	12.8	16.6	15.2
China[c]	5.9	46.3	13.8	9.9	22.7	1.5
Denmark[a]	9.9	51.2	12.8	20.7	3.9	1.5
France[a]	9.9	51.2	12.8	20.7	3.9	1.5
Germany[a]	9.9	51.2	12.8	20.7	3.9	1.5
India[d]	46.0	23.0	2.0	9.0	16.0	4.0
Ireland[a]	9.9	51.2	12.8	20.7	3.9	1.5
Japan[e]	29.7	33.7	28.7	6.9	1.0	0.0
Netherlands[a]	9.9	51.2	12.8	20.7	3.9	1.5
Norway[a]	9.9	51.2	12.8	20.7	3.9	1.5
Portugal[a]	9.9	51.2	12.8	20.7	3.9	1.5
South Korea[f]	17.3	22.3	34.2	21.8	2.6	1.8
Spain[a]	9.9	51.2	12.8	20.7	3.9	1.5
United Kingdom[a]	9.9	51.2	12.8	20.7	3.9	1.5
United States of America[g] (the)	1.3	21.9	27.0	31.1	5.2	13.2

[a] The vehicle size distribution for European Union countries is adapted from ICCT (2017).
[b] The vehicle size distribution for Canada is adapted from Natural Resources Canada (2009).
[c] The vehicle size distribution for China is adapted from ICCT (2012).
[d] The vehicle size distribution for India is adapted from Sehgal (2011).
[e] The Vehicle size distribution for Japan is adapted from Statista (2017b).
[f] The Vehicle size distribution for South Korea is adapted from Kama (2013).
[g] The vehicle size distribution for the U.S. is adapted from EPA US9R database (2016, V1.0).

4.6.2 Market Size

4.6.2.1 International Market Size

For the international analysis, we define the market size in each country based on their targets for EV stocks, presented in the Global EV Outlook (Cazzola et al., 2016) for most of the countries in our study. We assume the same targets as presented in the Global EV Outlook for 2015–2020 (Table 4.15). The smallest and largest market sizes belong to NOR with 29 thousand units and CHN with 4.3 million units, respectively.

Table 4.15. Target market size of each country (2015–2020), adapted from various references.

Country Name	Market Size[a] (Thousand units)
Austria	195
Canada[b]	582
China	4288
Denmark	192
France	1946
Germany	951
India	294
Ireland	98
Japan	874
Netherlands	213
Norway[c]	29
Portugal	198
South Korea	196
Spain	194
United Kingdom	1550
United States of America (the)	1099
Total	**12897**

[a] The market size for all countries expect Canada and Norway are adapted from Cazzola et al. (2016).
[b] The market size for Canada is adapted from WWF (2012).
[c] The market size for Norway is adapted from CNBC (2016).

4.6.2.2 U.S. Regional Market Size

Table 4.16. Market size in each U.S. region, which is assumed as 25% of the 5-year (2015–2020) new car sales projections, adapted from AEO, 2017 (EIA, 2017a).

Region	Market Size (Thousand units)
R1	900
R2	2951
R3	3276
R4	1290
R5	4021
R6	1014
R7	2902
R8	1404
R9	2990
Total	**20748**

4.6.3 Generating BEV200 Learning Curves from Battery Learning Curves

For this study, battery learning curves estimated by Nykvist and Nilsson (2015) are converted to learning curves for BEV200. To do this, we first convert the units in the battery curve from \$ kWh^{-1} versus cumulative kWh production to \$ $vehicle^{-1}$ versus cumulative vehicle production. We apply the world-average energy requirements for a BEV200 (35.7 kWh per vehicle) as the unit conversion factor. The average energy requirement for an average BEV200 is calculated from the world average efficiency of an average BEV200 (Table 4.11). In the next step, we add the average incremental costs (excluding the battery cost) of BEV200 over an equivalent GV to the battery learning curve. To this end, we calculate the world average incremental cost (excluding the battery

Table 4.17. Average BEV200 incremental cost (excluding the battery costs) over an average GV for each size class, adapted from NRC (2013) midrange scenario with low-volume production, following the approach from Keshavarzmohammadian et al. (2017).

Incremental cost excluding battery (\$)								
	Production level (Million Units)							
Size class	**0.15**	**13.0**	**26.0**	**39.0**	**51.7**	**64.5**	**77.5**	**90.3**
Compact	2707	1181	759	373	207	168	245	393
Full-size	4220	2418	1917	1506	1322	1300	1422	1636
Large SUV	7538	4657	3706	2909	2369	2074	1993	2032
Minivan	5027	2745	2033	1432	1067	899	907	1018
Mini-compact	7216	4742	3821	3009	2603	2377	2311	2340
Pickup	7443	4773	4026	3465	3117	3020	3146	3404
Small SUV	3599	1582	964	410	60	-118	-145	-85

cost) of BEV200 over an equivalent GV from the average incremental costs (excluding the battery cost) for each country, which in turn is calculated from the incremental cost of BEV200 over an equivalent GV for each vehicle size class and production level (Table 4.17), and vehicle size class shares in each country (Table 4.14). The incremental cost (excluding the battery cost) of each size class corresponding to each production level is adapted from NRC (2013) midrange scenario with low-volume production. We apply the same approach as our previous work (Keshavarzmohammadian et al., 2017) to estimate the incremental cost of each size class. We assume that the rest of the incremental costs other than the battery costs follow the learning process. That is, we fit the

power law to estimate the incremental costs for the production levels in between.

4.6.4 Annual Environmental Externalities (AEE_S)

4.6.4.1 Annual Environmental Externalities from $PM_{2.5}$

To estimate the annual environmental externalities from $PM_{2.5}$ for each region, we calculate the annual number of avoided or caused deaths per annual avoided or emitted emissions (kg) from the road and electric sectors, respectively, for each region by aggregating grid cell-level sensitivities, adapted from Dedoussi and Barrett (2014), in each region for each sector (Table 4.18).

Table 4.18. Annual premature deaths per annual emissions (kg), due to the exposure to $PM_{2.5}$ in each U.S. region per species and sector, adapted from Dedoussi and Barrett (2014).

Precursor	**R1**	**R2**	**R3**	**R4**	**R5**	**R6**	**R7**	**R8**	**R9**
NH_3 Electric	1.01×10^{-4}	2.08×10^{-4}	7.90×10^{-5}	3.31×10^{-5}	4.81×10^{-5}	4.94×10^{-5}	2.43×10^{-5}	1.04×10^{-5}	3.36×10^{-5}
NO_x Electric	4.54×10^{-6}	4.77×10^{-6}	3.49×10^{-6}	3.57×10^{-6}	3.10×10^{-6}	2.46×10^{-6}	2.49×10^{-6}	1.03×10^{-6}	2.75×10^{-6}
NO_x Road	9.19×10^{-6}	9.67×10^{-6}	6.55×10^{-6}	4.91×10^{-6}	5.85×10^{-6}	3.40×10^{-6}	3.35×10^{-6}	1.69×10^{-6}	6.76×10^{-6}
$PM_{2.5}$ Electric	7.93×10^{-5}	1.06×10^{-4}	7.54×10^{-5}	3.30×10^{-5}	6.72×10^{-5}	5.26×10^{-5}	3.68×10^{-5}	1.67×10^{-5}	5.17×10^{-5}
$PM_{2.5}$ Road	1.86×10^{-4}	3.23×10^{-4}	1.89×10^{-4}	8.41×10^{-5}	1.32×10^{-4}	8.41×10^{-5}	8.55×10^{-5}	7.91×10^{-5}	2.84×10^{-4}
SO_2 Electric	4.19×10^{-6}	5.26×10^{-6}	5.51×10^{-6}	4.90×10^{-6}	4.71×10^{-6}	5.06×10^{-6}	4.89×10^{-6}	3.89×10^{-6}	4.58×10^{-6}

For the road sector, we convert the annual number of avoided deaths per annual avoided emissions (kg) in each region to annual number of avoided deaths per mile, using the average regional emission factors per species (Table 4.19). The average regional emission factors per species are calculated from the sum of point-wise multiplication of emission factors (Table 4.20) for different vehicle sizes from the Greenhouse gas, Regulated Emissions, and Energy use in Transportation Model (GREET1), 2016 model (ANL, 2016) for the model year 2015, by the corresponding vehicle size distribution factors in each region (Table 4.10). We adjust the three vehicle size classes in GREET (car, LDT1, LDT2) to seven size classes in our study, which are similar to the size classes

in the EPA US9R database.

Table 4.19. Average regional emission factors for the road sectors (g mi^{-1}).

Emission species	**R1**	**R2**	**R3**	**R4**	**R5**	**R6**	**R7**	**R8**	**R9**
NO_x	0.229	0.226	0.231	0.233	0.222	0.225	0.232	0.234	0.216
$PM_{2.5}$	0.007	0.007	0.007	0.007	0.007	0.007	0.007	0.007	0.006

Table 4.20. Emission factors (g mi^{-1}) for different vehicle size classes of GV and BEV, from GREET model (ANL, 2016). Emission factors are from model year 2015 in GREET.

Technology	**GREET size class**	**EPA US9R (this study) size class**	**NO_x**	**$PM_{2.5}$[a] (Exhaust + TBW)**
GV	Car	Mini-compact	0.111	0.009
	Car	Compact	0.111	0.009
	Car	Full-size	0.111	0.009
	LDT2	Minivan	0.461	0.018
	LDT2	Pickup	0.461	0.018
	LDT1	Small SUV	0.157	0.014
	LDT2	Large SUV	0.461	0.018
BEV	Car	Mini-compact	0.000	0.005
	Car	Compact	0.000	0.005
	Car	Full-size	0.000	0.005
	LDT2	Minivan	0.000	0.007
	LDT2	Pickup	0.000	0.007
	LDT1	Small SUV	0.000	0.007
	LDT2	Large SUV	0.000	0.007

[a] We use the difference between $PM_{2.5}$ emissions of the GV and the BEV for each size class in our calculation.

For the electric sector, we convert the annual number of deaths per annual emissions (kg) in each region to annual number of deaths per kWh in each region, using the estimated average emission factors (g kWh^{-1} of output electricity) per each emission species in each region (Table 4.21). These regional average emission factors are estimated by sum of point-wise multiplication of average regional environmental activity (ENV-ACT) of each type of generation (g kWh^{-1} of output electricity) and each species (Table 4.22) by the fraction of generation from that type of generation in 2015 (Table 4.23), estimated from the EPA US9R database.

Table 4.21. Average regional emission factors (g kWh^{-1} of output electricity) for electric sector in 2015 per species.

Region	**NH_3**	**NO_x**	**$PM_{2.5}$**	**SO_2**
R1	0.011	0.222	0.006	0.235
R2	0.009	0.868	0.026	2.799
R3	0.009	2.189	0.064	3.296
R4	0.008	2.350	0.070	1.921
R5	0.010	1.484	0.042	2.402
R6	0.010	1.754	0.051	4.076
R7	0.013	1.171	0.039	1.272
R8	0.010	1.901	0.056	1.492
R9	0.010	0.160	0.006	0.052

Table 4.22. Average regional environmental activity (ENV-ACT) in g kWh^{-1} of output electricity for each type of generation in 2015 per species.

Region	**NH_3**	**NO_x**	**$PM_{2.5}$**	**SO_2**
Generation from Natural gas (NG)				
R1	0.020	0.116	0.003	0.001
R2	0.020	0.167	0.009	0.003
R3	0.020	0.260	0.019	0.005
R4	0.020	0.136	0.005	0.002
R5	0.020	0.114	0.002	0.001
R6	0.020	0.159	0.008	0.002
R7	0.020	0.177	0.009	0.002
R8	0.020	0.115	0.003	0.001
R9	0.020	0.154	0.008	0.003
Generation from coal				
R1	0.011	3.714	0.107	5.341
R2	0.011	3.714	0.107	12.730
R3	0.011	3.736	0.107	5.711
R4	0.011	3.598	0.107	2.949
R5	0.011	3.720	0.107	6.164
R6	0.011	3.728	0.107	8.686
R7	0.011	3.361	0.107	3.934
R8	0.011	3.644	0.107	2.901
R9	0.011	3.762	0.107	2.160

The average regional ENV-ACT of each generation type and species (Table 4.22) is the sum of point-wise multiplication of ENV-ACT for different technologies, utilized for each generation type (for example gas turbine, steam turbine, and combined cycle technologies for natural gas

Table 4.23. Regional generation mix (%) in 2015, estimated from EPA US9R database (2016, V1.0).

Region	Coal	Nuclear	Hydropower	Renewables[a]	Natural Gas[b]
R1	4	31	8	5	51
R2	22	38	7	2	31
R3	58	25	1	3	13
R4	65	14	0	15	5
R5	39	26	3	2	30
R6	46	22	7	0	26
R7	32	11	1	8	48
R8	51	9	10	7	24
R9	2	6	33	12	46

[a] Renewables include generation from wind, solar, fuel cell, and biomass.
[b] Natural gas includes other generations than those listed here as well.

generation type), by the share of generation from each technology in each region. We take ENV-ACT for different technologies from EPA US9R database (Table 4.24). We also estimate the regional share by technology from EPA US9R database (Table 4.25). EPA US9R presents the ENV-ACT based on the fuel input. We convert average emission factors for each region per species based on the fuel input to the electricity output using the average generation efficiency for each generation type (35% for generation from natural gas and 34% for coal) in 2015, estimated from the EPA US9R database.

For the road sector, the annual environmental benefits for each region and species per vehicle ($/year/vehicle) is calculated by multiplying annual number of avoided deaths per mile by the value of a statistical life (VSL), and annual mile per vehicle for that region (Table 4.8). For the electric sector, we multiply the annual environmental damages by the VSL, and average annual kWh per vehicle (BEV200) for each region, estimated before in our WTP calculations. Total annual externalities per vehicle for each region is the difference of total environmental externalities from the road sector and total damages from the electric sector.

Table 4.24. Environmental activity (ENV-ACT) of different generation technologies (g kWh^{-1} of input fuel) in 2015 per species from EPA US9R database (2016, V1.0).

Generation Type	Technology[a]	NH_3	NO_x	$PM_{2.5}$	SO_2
Natural gas	CC	0.007	0.032	0.000	0.000
	GT	0.007	0.112	0.011	0.004
	ST	0.007	0.241	0.011	0.000
Coal	BH	0.004	1.246	0.036	4.269
	BL	0.004	1.246	0.036	0.529
	BM	0.004	1.246	0.036	1.893
	LH	0.004	0.724	0.036	3.470
	LM	0.004	0.724	0.036	2.405
	SL	0.004	1.263	0.036	0.749
	SM	0.004	1.263	0.036	1.296

[a] CC: Combined Cycle; GT: Gas Turbine; ST: Steam Turbine; BH: Bituminous High sulfur; BL: Bituminous Low sulfur; BM: Bituminous Medium sulfur; LH: Lignite high sulfur; LM: Lignite medium sulfur; SL: Subbituminous Low sulfur; SM: Subbituminous Medium sulfur.

Table 4.25. Regional share (%) by technology per generation type, adapted from EPA US9R database (2016, V1.0).

Technology[a]	R1	R2	R3	R4	R5	R6	R7	R8	R9
Natural Gas									
CC	90	71	39	83	93	74	70	89	73
GT	9	26	52	16	5	23	24	11	26
ST	1	3	9	2	2	3	5	0	1
Coal									
BH	0	100	27	0	18	61	2	0	0
BL	7	0	12	1	9	4	1	16	11
BM	93	0	20	0	61	6	1	4	0
LH	0	0	0	0	0	0	7	0	0
LM	0	0	0	11	0	0	18	7	0
SL	0	0	40	76	12	28	71	55	89
SM	0	0	1	12	0	0	0	18	0

[a] CC: Combined Cycle; GT: Gas Turbine; ST: Steam Turbine; BH: Bituminous High sulfur; BL: Bituminous Low sulfur; BM: Bituminous Medium sulfur; LH: Lignite high sulfur; LM: Lignite medium sulfur; SL: Subbituminous Low sulfur; SM: Subbituminous Medium sulfur.

4.6.4.2 Annual Environmental Externalities from Ozone

To estimate the annual environmental externalities from ozone, we follow a similar procedure to that explained for $PM_{2.5}$. We adapt the regional marginal benefits (MBs) from NO_x emission

abatement from Pappin et al. (2015) (Table 4.26). We use MBs from the 40% abatement scenario in their study for the road sector (mobile sources) and we use results for the 0% abatement scenario for the electric sector (point sources).

Table 4.26. Regional marginal benefits ($ kg^{-1}) from summertime NO_x emission abatement, from mobile sources (40% abatement scenario), and point sources (0% abatement scenario), adapted from Pappin et al. (2015).

	R1	**R2**	**R3**	**R4**	**R5**	**R6**	**R7**	**R8**	**R9**
Mobile Source (40% abatement scenario)	5.71	12.87	14.68	14.14	25.59	24.30	14.68	15.78	26.72
Point Source (0% abatement scenario)	4.44	16.83	15.00	12.06	21.99	20.04	11.71	9.79	8.39

NO_x emission factors for different vehicle size classes are presented in Table 4.20. NO_x environmental activity (ENV-ACT) of different generation technologies (g kWh^{-1} of input fuel) in 2015 are presented in Table 4.24.

4.6.4.3 Annual Environmental Externalities from CO_2 Emissions

Following the same procedure as described for ozone, we take the marginal damages of CO_2 emissions from EPA's (Marten and Newbold, 2012) estimation of the social cost of carbon (SCC) with 3% discount rate (0.04 $ kg^{-1} in 2015). CO_2 emission factors for different vehicle size classes

Table 4.27. CO_2 emission factors (g mi^{-1}) for different vehicle size classes of GV and BEV200 in 2015, adapted from EPA US9R database (2014, V1.1). Estimated in Keshavarzmohammadian et al. (2017).

	Mini-compact	**Compact**	**Full-size**	**Minivan**	**Pickup**	**Small SUV**	**Large SUV**
CO_2	349.9	233.3	288.7	366.6	476.3	315.2	458.4

(Table 4.27) are adapted from the EPA US9R database (2014, V1.1), estimated in our previous study (Keshavarzmohammadian et al., 2017). CO_2 environmental activity (ENV-ACT) of different generation technologies (g kWh^{-1} of input fuel) in 2015 (Table 4.28) is from the EPA US9R database

(2016, V1.0).

Table 4.28. CO_2 environmental activity (ENV-ACT) of different generation technologies (g kWh^{-1} of input fuel) in 2015 from EPA US9R database (2016, V1.0).

Generation Type	Technology[a]	CO_2
Natural gas	CC	208.204
	GT	198.074
	ST	182.657
Coal	BH	300.061
	BL	300.061
	BM	300.061
	LH	315.209
	LM	315.209
	SL	308.819
	SM	308.819

[a] CC: Combined Cycle; GT: Gas Turbine; ST: Steam Turbine; BH: Bituminous High sulfur; BL: Bituminous Low sulfur; BM: Bituminous Medium sulfur; LH: Lignite high sulfur; LM: Lignite medium sulfur; SL: Subbituminous Low sulfur; SM: Subbituminous Medium sulfur.

4.6.5 Assumptions for Sensitivity Cases

To understand the impact of key uncertainties associated with our input assumptions on the results of the base calculations for the U.S. regions, we examine the sensitivity of the reference WTP and the related subsidies to the discount rate, years of vehicle ownership, need for battery replacement and peak charging; and the sensitivity of environmental externalities to the regional electricity mix assumptions (Table 4.1).

The U.S. government's cost-benefit assessments often use 5% and 3% discount rates, as applied in our base calculations and low discount rate sensitivity case, as the upper range and mean discount rate values. Our rough estimations of the cost of capital (COC) for Tesla Motors and average COC for some gasoline car manufactures such as Honda, Toyota, and General Motors are also close to 5%. Therefore, we chose 5% as the conservative discount rate for our base calculation and 3% as the low discount rate. We chose a 10% discount rate as the upper bound to consider

the uncertainties associated with the risk level in the car manufacturing market. Furthermore, according to Tran et al. (2012) customers heavily discount (18%–30%) the future cost savings from increased fuel economy.

A lower bound of five years of vehicle ownership (short) is chosen based on the average years of vehicle ownership in the U.S. (5.25 years for used cars and 6.5 years for new cars (Statista, 2017a)). An upper bound of 15 years vehicle ownership (long) is chosen based on the average scrappage patterns in the U.S. (12.2 to 15.6 years between 1970s and 2000s (Bento et al., 2016)).

To understand the effect of potential need for battery replacement on the WTP from operation of BEV200, we assume the battery replacement is required in the tenth year of vehicle ownership. We assume a price of \$300 kWh^{-1} for battery replacement, which is equal to the current price of a new battery in our learning curves. It should be noted that this a conservative assumption, as the cost of batteries might come down, ten years from now, following the battery learning curves.

The peak charging sensitivity case assumes 25% of charging happens in the peak hour period in all regions. We have estimated this number from the Idaho National Laboratory, Advanced Vehicles, ARRA-Chrysler RAM PHEV Fleet- Phase 2 project (INL, 2014). We assume peak hours extend from 2:00 pm to 9:00 pm. The estimate of 25% peak charging is close to the range assumed in the Union of Concerned Scientists report (76%–94% off-peak charging) (Anair and Mahmassani, 2012). We assume electricity prices are three times higher in the peak hours compared to the off-peak hours, based on the factor derived from time-of-use rates for EV charging by the Los Angeles Department of Water and Power (Anair and Mahmassani, 2012).

To examine the sensitivity of the environmental externalities from deploying EVs in each region to the way the electricity is generated, we consider a cleaner electricity mix for each region than assumed in our base calculations. The corresponding changes range 2% less generation from coal in R9 to 22% less generation from coal in R7; and from 7% higher generation from renewables and natural gas in R2 (Middle Atlantic) to 24% higher generation from renewables and natural gas in R7. This case also assumes more generation from combined cycle power plants versus gas turbines for natural gas generation technologies, resulting in higher average efficiency for natural gas

generation, and assumes less generation from high sulfur coal. This case is adapted from midterm MARKAL modeling for the year 2030 with implementation of Clean Power Plan provisions in EPA US9R database (2016, V1.0). Our cleaner electricity case assumes this electricity mix happens in 2015.

4.6.6 Additional Results

4.6.6.1 International Market

Figure 4.5 shows the estimated BEV learning curves and the reference and optimistic international WTP market curves based on the countries' targets for 2020. WTP for each country is shown with and without including gasoline taxes. When gasoline taxes are included, KOR shows the highest WTP, followed by NOR in both the reference and optimistic market curves. Both countries have relatively low electricity and high gasoline prices, which is favorable for promoting BEV200s (Tables 4.7 and 4.11). KOR also has relatively large annual miles per vehicle (second after the U.S.) resulting in the higher WTP (Table 4.7). JPN, at the other end of the range, has high electricity and moderate gasoline prices with relatively low annual miles per vehicle. In comparison, the U.S. has relatively moderate electricity and cheap gasoline prices, but high annual miles per vehicle. The highest difference in WTP between the optimistic and reference WTP market curves happens in the U.S. (2972 \$ vehicle^{-1}), shifting the U.S. to a more favorable condition within the international market in the optimistic case.

Figure 4.5 also shows the learning curves and the international market curves with gasoline taxes excluded from the WTP calculation. This lowers the highest reference and optimistic WTP values by about 40% compared to the corresponding values with gasoline taxes included. Countries with lower gasoline taxes and relatively higher annual miles per vehicle have more favorable market conditions in this case. In particular, the U.S. becomes the most favorable market for BEV200 diffusion in the case with optimistic market curves.

The minimum subsidies (see Equation 4.1) required for stimulation of BEV200s to a target

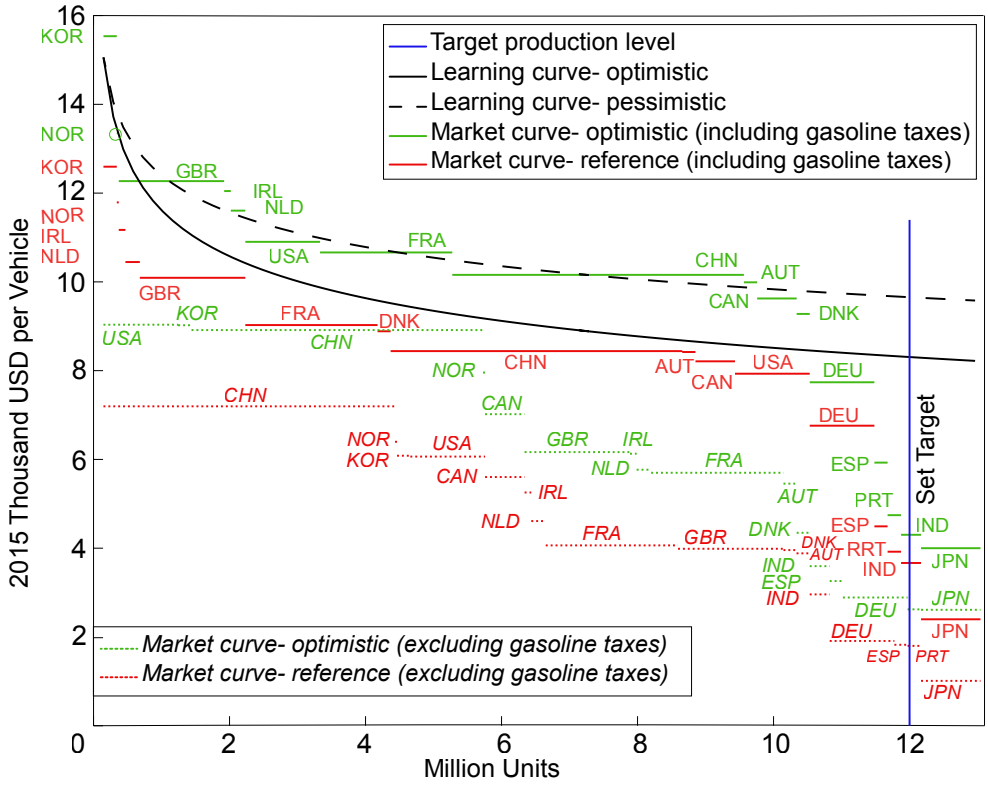

Figure 4.5. BEV learning curves (corresponding to 6% and 9% progress ratios), and optimistic and reference WTP market curves for both cases including and excluding gasoline taxes in the international market.

vehicle stock level of 12 million vehicles within the international market are shown in Table 4.29 for the base calculations, including gasoline taxes. With the reference WTP and the optimistic learning curve, a cumulative subsidy of about 11.8 billion dollars is required to stimulate purchase of 12 million vehicles, with the subsidy applied across all countries except Japan. With the reference WTP and the pessimistic learning curve, a cumulative subsidy of about 25.5 billion dollars is required in the same countries. With the optimistic WTP and optimistic learning curve a subsidy of about 2.4 billion dollars applied to 1.8 million units in NOR, GBR, DEU, ESP, PRT, and IND is required to meet the same target. In this case, after the implementation of subsidies in GBR, BEVs become competitive with GVs in IRL, NLD, USA, FRA, CHN, AUT, CAN, DNK and further subsidies are not required. Finally, with the optimistic WTP and pessimistic learning curve a subsidy of about 5.7 billion dollars, applied to 7.2 million units in NOR, GBR, USA, FRA,

Table 4.29. Minimum Subsidies, calculated based on WTP, required for 12 million target cumulative production level for international market curves including gasoline taxes.

Market-Learning Curves	**Subsidies and Production Units**
Reference - Optimistic	A subsidy of 0.30, 0.05, 0.19, 0.44, 1.61, 1.80, 0.13, 2.60, 0.05, 0.24, 0.64, 1.56, 0.75, 0.87, and 0.58 billion dollars applied to 196, 29, 98, 213, 1550, 1946, 192, 4288, 195, 582, 1099, 951, 194, 198, and 125 thousand units in KOR, NOR, IRL, NLD, GRB, FRA, DNK, CHN, AUT, CAN, USA, DEU, ESP, PRT, and IND, respectively, is required.
Reference - Pessimistic	A subsidy of 0.34, 0.06, 0.23, 0.57, 2.97, 3.93, 0.35, 7.93, 0.30, 1.00, 2.09, 2.83, 1.01, 1.14, and 0.75 billion dollars applied to 196, 29, 98, 213, 1550, 1946, 192, 4288, 195, 582, 1099, 951, 194, 198, and 125 thousand units in KOR, NOR, IRL, NLD, GRB, FRA, DNK, CHN, AUT, CAN, USA, DEU, ESP, PRT, and IND, respectively, is required.
Optimistic - Optimistic	BEV200s are competitive in KOR. A subsidy of 0.5 million dollars applied to 14 thousand units in NOR (up to 356 thousand cumulative units) push the market to 371 thousand cumulative units. A subsidy of 132.4 million dollars applied to 295 thousand units in GBR (up to 666 thousand cumulative units) push the market to 10.5 cumulative million units (end of DNK market). A subsidy of 633.5, 469.3, 709.6, and 501.2 million dollars applied to 951, 194, 198, 294, and 125 thousand units in DEU, ESP, PRT, and IND, respectively, is required.
Optimistic - Pessimistic	BEV200s are competitive in KOR. A subsidy of 12 and 427.9 million dollars applied to 29 and 742 thousand units in NOR and GBR push the market to 2.2 million units (end of NLD market). A subsidy of 322.3 and 175.4 million dollars applied to 1.0 and 1.1 million units in USA and FRA (up to 4.5 million cumulative units) push the market to 5.3 million cumulative units. A subsidy of 305.3 million dollars applied to 2.0 million units in CHN (up to 7.2 million cumulative units) push the market to 9.8 million cumulative units (end of AUT market). A subsidy of 117.9, 98.50, 1902, 729.6, 975.8, and 669.5 million dollars applied to 582, 192, 951, 194, 198, 294, and 125 thousand units in CAN, DNK, DEU, ESP, PRT, and IND, respectively, is required.

CHN, CAN, DNK, DEU, ESP, PRT, and IND is required for meeting the target. The market is competitive in IRL and NLD in this case. Note that the subsidies shown are in addition to the

favorable tax treatment of relatively high taxes on gasoline sales compared to those on electricity. Table 4.30 provides additional results for the case excluding the gasoline taxes.

With both reference and optimistic market curves, the level of WTP in ESP, PRT, IND, and JPN are so low that international subsidies for 12 million vehicles cannot make BEV200s competitive with GVs with either the pessimistic or optimistic learning curves. Further cost reductions would be required. This is also true for DEU with the reference WTP and pessimistic or optimistic learning curves, or the optimistic WTP in combination with the pessimistic learning curve. These results convey that both market size and WTP are important for pushing the new technology into the market. While KOR and NOR have favorable WTP conditions compared to the other countries, their 2020 target market sizes are too small to provide a significant push. CHN, on the other hand, has a relatively big market size, but moderate to low WTP.

Table 4.30. Minimum Subsidies, calculated based on WTP, required for 12 million target cumulative production level for international market curves excluding gasoline taxes.

Market-Learning Curves	**Subsidies and Production Units**
Reference - Optimistic	A subsidy of 15.3, 0.09, 0.66, 3.56, 2.04, 0.37, 0.94, 9.28, 7.14, 0.87, 0.89, 1.61, 6.15, 1.26, and 0.19 billion dollars (50.3 billion dollars total) in CHN, NOR, KOR, USA, CAN, IRL, NLD, FRA, GRB, DNK, AUT, IND, DEU, ESP, and PRT respectively, is required.
Reference - Pessimistic	A subsidy of 19.3, 0.13, 0.89, 4.88, 2.76, 0.49, 1.20, 11.8, 9.17, 1.12, 1.15, 2.00, 7.42, 1.52, and 0.23 billion dollars (64.0 billion dollars total) in CHN, NOR, KOR, USA, CAN, IRL, NLD, FRA, GRB, DNK, AUT, IND, DEU, ESP, and PRT respectively, is required.
Optimistic - Optimistic	A subsidy of 3.76, 0.42, 4.14, 0.04, 1.22, 4.27, 0.26, 0.64, 5.67, 0.59, 0.79, 1.42, 1.00, 5.20, and 0.16 billion dollars (29.6 billion dollars total) in USA , KOR, CHN, NOR, CAN, GRB, IRL, NLD, FRA, AUT, DNK, IND, ESP, DEU, and PRT respectively, is required.
Optimistic - Pessimistic	A subsidy of 4.42, 0.59, 8.89, 0.07, 1.93, 6.22, 0.39, 0.91, 8.21, 0.85, 1.04, 1.82, 1.26, 6.47, and 0.20 billion dollars (43.3 billion dollars total) in USA, KOR, CHN, NOR, CAN, GRB, IRL, NLD, FRA, AUT, DNK, IND, ESP, DEU, and PRT respectively, is required.

4.6.6.2 Sensitivities

We examine the sensitivity to selected input assumptions of the reference WTP and the corresponding subsidies required for a 12 million BEV target production level. Sensitivity analysis is conducted by reference to the case for the U.S. with zero pre-diffusion units. Using 3% and 10% discount rates results in a 10% increase and 20% decrease in the WTP in all regions, respectively. Assuming a 3% discount rate reduces the amount of required subsidies (Table 4.31). However, with a 3% discount rate, subsidies are unable to make BEV200 competitive with GVs in all regions with either optimistic or pessimistic learning curves.

Table 4.31. Cumulative subsidies (billion dollars), calculated based on WTP, required for 12 million target cumulative production level for the reference WTP and sensitivity cases. Subsidies assume zero pre-diffusion units.

Market-Learning Curves	**Subsidies (billion dollars)[a]**			
	Base (with 5% discount rate, 10-year vehicle ownership, and no peak charging)	With 3% discount rate	With 15-year vehicle owner-ship	With 25% peak charging
Reference - Optimistic	45.9	38.9	23.0	57.0
Reference - Pessimistic	59.6	52.7	36.7	70.7

[a] The subsidies are applied in R7, R8, R5, R4, R6, and R9 for all sensitivity cases.

Assuming 5 years or 15 years of vehicle ownership, instead of 10 years, the reference WTP is decreased by 44% or increased by 34%, respectively. Assuming 15 years of vehicle ownership reduces the amount of required subsidies (Table 4.31). However, subsidies applied to 12 million vehicles are still unable to make BEV200 competitive with GVs in all regions with either optimistic or pessimistic learning curves.

It should be noted that although longer years of vehicle ownership increases WTP and reduces the amount of required subsidies, there is an increased risk of the need for a battery replacement in the later years of the vehicle's life, which in turn can offset those benefits. The battery cost ranges

from about 8600–15700 \$ vehicle^{-1} corresponding to the compact and pickup size classes, respectively. The average battery cost across the regions, considering regional vehicle size distributions, ranges from about 5800–7100 \$ vehicle^{-1} corresponding to R8 and R5, respectively. Considering one-time battery replacement in the tenth year of vehicle ownership results in negative WTP in all regions, with values ranging from about –260 to –3143 \$ vehicle^{-1}, corresponding to R5 and R1.

Assuming that 25% of BEV charging occurs during peak electricity pricing periods with tripled electricity prices reduces WTP by 14 to 31% (corresponding to R5 and R7). Accordingly, the WTP in this case ranges from 2677 \$ vehicle^{-1} in R1 to 5643 \$ vehicle^{-1} in R7. This sensitivity case, shows the importance of off-peak charging to the level of financial benefits gained by BEV owners. R9 shows the biggest difference between reference WTP and WTP assuming the peak charging (1300 \$ vehicle^{-1}), mainly due to the higher electricity prices in that region. Table 4.31 highlights how much subsidies would need to increase in this case compared to the base calculation.

Chapter 5

Conclusion

In this section, we summarize and discuss the main findings of all three parts of our research. We analyze the impacts of introducing inexpensive and efficient electric vehicles (EVs) on energy use and emissions from the U.S. transportation sector using an integrated energy model, conduct life cycle assessment (LCA) for a pyrite battery suitable for EV applications, and design efficient regionally targeted subsidies using a modified cascading diffusion model which minimizes the social costs of driving EVs in place of gasoline vehicles (GVs).

In the first part of this thesis, we analyze how application of improved electric vehicles, including plug-in hybrid (PHEVs) and battery EVs (BEVs), in the U.S. light-duty vehicle (LDV) sector affects emissions not only from the LDV and its upstream sectors (including the electric sector) but also from entire sectors of the economy. We utilize ANSWER-MARKAL (MARKet ALocation) model in connection with the modified version of U.S. Environmental Protection Agency's (EPA) nine-region (US9R) database. This part of the analysis assumes EVs are improving following optimistic assumptions about efficiencies and costs, they are produced in mass scale, and they will become competitive with GVs in the midterm. However, EVs are not the only technologies that are being improved and knowledge spill-over occurs across different technologies. Therefore, we consider the technology improvement assumptions to apply consistently across major vehicle alternatives including GVs and hybrid EVs (HEVs). The objective is to understand whether the technology advances in the LDV sector, affecting fuel economies and technology mixes in different sectors of the economy, could reduce emissions. For EVs in particular, these advances include

the application of breakthrough battery technologies with new chemistries having higher energy capacities and longer cycle life.

Our results show that compared to the base case (BAU scenario) in which GVs are the dominant technology for the entire time horizon, the LDV technology mix changes under optimistic assumptions about LDV technologies' cost and efficiency projections (OPT scenario). The share of BEV penetrations out of total demand increases in the midterm and long-term. HEVs gain the same share as BEVs in the midterm but they vanish in the long-term. The regional results more or less follow the same pattern as the national results, except that the ethanol vehicle share varies significantly across regions, depending on the availability of corn and the relative price of ethanol. The changes in the U.S. LDV technology mix in the OPT scenario result in an insignificant increase in electricity demand. Changes in LDV demand (high and low) also have a negligible impact on the electricity demand in both scenarios. In both BAU and OPT scenarios, the electricity generation mix moves toward more generation from natural gas and less generation from coal. The changes in the U.S. LDV technology mix in the OPT scenario result in a reduction in gasoline consumption which provides more capacities in refineries for the production of other products such as jet fuel. Therefore, the total change in oil consumption from BAU to OPT is not as large as the reduction in gasoline use. The changes in the U.S. LDV technology mix in the OPT scenario result in significant reduction in GHG emissions from the LDV sector but a smaller reduction in total GHG emissions than that from the LDV sector. This is because LDV emissions represent a declining share of total emissions, mainly due to the existing CAFE regulations, and because of intersectoral shifts in emissions. The reduction in the GHG emissions in the OPT scenario compared to the BAU scenario varies significantly across the regions with the most reductions in the Pacific region and the least reductions in the West South Central region. The same pattern as the GHG emissions is seen for other emissions including NO_x and SO_2, again due to the existing control technologies and regulations and because of intersectoral shifts. We estimate higher well-to-wheel (WTW) GHG emissions for GVs compared to BEVs. Following OPT assumptions, WTW GHG emissions for both technologies are reduced by a similar factor throughout the time horizon. Regional WTW emissions

vary significantly across the regions with the most reductions in the Pacific region (which has the lowest share of electricity from coal) and the least reductions in the West North Central (which has the highest share of generations from coal). We estimate higher WTW NO_x and SO_2 emissions for BEVs than GVs throughout the entire time horizon. The influence of economy-wide GHG fees on the LDV technology and fuel mix is limited, due to their modest impacts on the cost of vehicle ownership. For all technologies, the impact of emissions fees in future decades would be lower than it would be in the near term due to improved efficiencies. The GHG fees have little influence on the total electricity demand; however, the generation mix moves toward more generations from natural gas. The GHG fees have little impact on reduction in GHG emissions from the LDV sector but have a modest impact on reduction in total emissions and significant impact on reduction in GHG emissions from the electric sector. Application of GHG fees has little impact on NO_x emissions from the LDV sector and total NO_x emissions but reduces the SO_2 emissions from the electric sector and total SO_2 emissions. In the OPT scenario, the SO_2 emissions from the industrial sector are also reduced.

The results of MARKAL analysis should be interpreted with caution. It is notable that the goal of the study is not to predict any outcome in the future. Instead, it sets a framework that shows the extent to which the LDV technology improvements would be effective for emission reductions from each sector and from the whole sectors of the economy. MARKAL is considered a bottom-up model and is rich in the number of technologies it considers, in particularly for the LDV and electric sectors, but there are still uncertainties in the input parameters such as costs and efficiencies. This is partly due to uncertainties in projecting different parameters to the future (including population growth, and demand), and partly due to use of an average value for each parameter (such as emission factors and costs) instead of a distribution. End-use demands are also assumed inelastic in the standard version of MARKAL used here. While this is not an improper assumption for the LDV sector (as the LDV demand does not show strong elasticity to oil prices), this can affect the results of other end-use sectors. Moreover, in the current version of the EPA US9R database, the technology learning curves are treated exogenously. That is, the cost of a new technology comes

down only over time. However, technology learning curves could be treated endogenously as well. Therefore, the cost of a new technology comes down over time in addition to the level of investment. Further, MARKAL is not a suitable tool for detailed impact analyses of different factors influencing customer behaviors (such as make, and model) on the market penetration of a new technology like EVs.

Our results show that having 50% of the fleet demands fulfilled by BEVs as a result of technology advances including battery advances can reduce the emissions from the LDV sector significantly, but the reductions in economy-wide emissions are smaller. It is important to note that these reductions from the LDV sector are still important from the perspective of health impacts and environmental externalities. The mobile emissions are harder to control and lead to a higher chance of people being exposed to air pollution resulting from LDV emissions. In contrast, stationary power plants with tall stacks can be controlled more easily and are mainly located in less populated areas. It is expected that shifting the emissions from the LDV sector to remote areas generates health benefits, particularly in more populated areas and regions relying on clean electricity generation. However, our environmental externalities calculations across the U.S. regions (conducted in the third part of our research for the purpose of the subsidy calculation) show that this conclusion is subjective. That is, the environmental benefits are highly location-dependent and BEVs may even result in environmental damages in less-populated areas with high reliance on generation from coal.

One of the reasons that market penetration of BEVs are more effective to reduce emissions from the LDV sector and less effective to reduce total emissions is that LDV emissions represent a declining share of total emissions. Due to the regulations such as CAFE and existing control technologies, emissions from the LDV sector are declining even in the BAU scenario. Similarly, due to existing control technologies and regulations such as renewable portfolio standard (RPS), shifting emissions to the electric sector does not significantly change total emissions. This suggests that in order to have more reductions in total emissions, additional policies targeting other sectors such as the heavy-duty vehicle (HDV) and industrial sectors could be more effective. Moderate economy-wide GHG fees are mainly effective at reducing emissions from the electric sector rather than other

sectors. Another reason that total emissions do not change drastically is the intersectoral shifts in emissions. It should be noted that we are not attempting to predict precise shifts in emissions rather, our study suggests that having a significant technology change in one sector can affect the energy carrier mix not only in the upstream sectors but also throughout the entire energy system. This can change the technology mix and emissions in the sectors beyond the upstream sectors, resulting in less or more reductions in total emissions compared to the case in which the intersectoral shifts in emissions are ignored.

Using an integrated assessment model helps us to understand how the energy carrier mix would change throughout the entire system when a transformative technology, like BEVs, is introduced in one sector. The results of our study show that when BEV market penetration achieves 50% of the fleet, significant reduction in gasoline demand follows. This generates more capacity in refineries for other refined products. This leads to no significant change in modeled oil consumption. However, in reality, this outcome can result in critical policy decisions about changes in capacity of oil production and imports, refined product imports and exports, and refineries.

We complement the first part of the research by conducting an LCA on a newly developed solid-state pyrite lithium battery. This battery has higher energy density and potentially longer cycle life compared to current Li-ion batteries (LIB) and holds high promise for EV applications. The reason to focus on an LCA of the battery instead of the whole vehicle is because the battery manufacturing for EVs has resulted in a majority of the cumulative energy demand (CED) and global warming impacts compared to their GV counterparts (Dunn et al., 2012; Elgowainy et al., 2016; Hawkins et al., 2013; Kim et al., 2016; Majeau-Bettez et al., 2011; Nealer et al., 2015; Notter et al., 2010).

To conduct the LCA analysis, we utilize US-EI as one of the LCA databases in the Ecoinvent center. It should be noted that although LCA databases provide useful inventories and characterizations for production of different materials and processes, there are uncertainties associated with them. First, they represent an average value for each material and process. Also, they consider fixed fractions for input and output materials, emissions, wastes, and energy flows. Second, al-

though they include some geographical variations in data, those assumptions may not be valid for a certain study. Third, some portion of uncertainties come from characterization methods and how the values are estimated. Finally, there are processes that are estimated based on other available entries. This is mainly because the information for those processes is weak or limited. In the case of our study, for example, due to the lack of information about pyrite mining, US-EI estimates the impacts of pyrite production from iron mining. Moreover, despite a large number of entries included in these type of databases, there is a high possibility that some processes and materials cannot be found, in particular, if the LCA is prospective. Other available entries for similar materials and processes should be used as a proxy for missing ones. Otherwise, those materials and processes need to be estimated using other sources. These estimations always face uncertainties. In our study, for example, aluminum sheet rolling from US-EI is used as the proxy for Li sheet rolling; cathode conductive material (TiS_2) and electrolyte materials (Li_2S and P_2S_5) are not available in the database. Therefore, the energy requirements for their production are estimated based on three U.S. patents (Jacob and Brown, 1978; Taylor, 1965; Wainer, 1958). The energy requirements for processes related to the battery production are also estimated based on laboratory data.

In our study, we conduct a prospective LCA, as the pyrite battery is only available in the lab-scale. This can impose different kinds of uncertainty in our results. Mass inventory for a battery with suitable size for EV applications is estimated based on the lab compositions; the location of the factory is not defined, therefore, energy requirements for dry-room application and the assumed transportation distances are uncertain. It is also hard to track which exact pathways the materials go through for a certain product in a certain location. The energy requirements for processes related to the battery production are also estimated based on the lab data. It should be noted that the manufacturing process gets more efficient in large-scale production, compared to the small scale. Evaluating these assumptions based on primary data in the future, after moving to pilot and mass scale productions, would help to better understand the source of these uncertainties. Another limitation of our study is that we do not address the impacts of capital equipment; we also assume no credit from battery recycling in our analysis, partly because no established recycling

technology is yet available on a large industrial scale for recycling new battery chemistries including solid-state pyrite batteries. Our study assumes 100% yield factor for different processes of battery manufacturing, whereas in reality, it is not feasible to get 100% yield and turn all input materials to the final products in the large-scale production compared to the lab scale.

Our results show that direct energy requirements for cell production and battery production are almost the same. This conveys that cell production is the major contributor to direct energy requirements of total pack production. The energy requirements for clean dry-room applications comprise a significant portion of direct energy requirements for cell manufacturing, even with dry climate conditions assumed for the location of the factory, such as Reno, Nevada. Our estimate of CED for battery production falls on the upper side of the range for LIBs, summarized by Peters et al. (2017). The dry-room and cathode paste (mainly from the production of TiS_2) are the biggest contributors to the battery CED. Mining of pyrite plays a negligible role in the CED impacts of cathode paste. The energy requirements for dry-room and production of TiS_2 are uncertain and there is room for more optimized designs. Moreover, TiS_2 can be possibly eliminated based on the results of the further research on Pyrite battery. Our estimate of GWP_{100} impacts of pyrite battery production falls in the range of average LIBs, but is higher than the average value estimated by Peters et al. (2017). Our estimates of global warming potential based on 100-year (GWP_{100}) impacts of pyrite battery production are lower than that of Li-S battery. Owing to the fact that the pyrite battery needs a bigger dry-room, this result can be related to the elimination of some elements such as copper current collector, separator, and cooling system compared to LIBs and Li-S battery. We estimate slightly higher CED and GWP_{100} from battery production than CED and GWP_{100} impacts from the production of other vehicle components. However, the CED impacts associated with battery production are significantly lower than energy consumption in the use phase. The GWP_{100} impacts of battery production are lower than WTW GHG emissions for BEV200 and GVs in 2010, estimated in the first part of the thesis. However, moving toward more efficient vehicles in the future may change this result. The acidification impacts (ACD) from the battery production are slightly higher than WTW SO_2 emissions in the use-phase for both technologies.

To be able to fairly compare the impacts of the pyrite battery with the LIBs, other impact categories should be also compared. That is because, for example, negative current collector (Cu), which is not required for the pyrite battery, does not contribute significantly to GWP_{100} but is the main contributor to EUT (fresh water and terrestrial), toxicity (freshwater, marine, and human), and metal depletion in LIB production (Ellingsen et al., 2014). Its contributions to the impacts of photo-oxidation formation, particulate matter formation, and ACD are also considerable (Ellingsen et al., 2014). However, the cross-comparison across studies is not feasible when they differ in the impact assessment system. For example, we cannot closely compare our results with most of the studies listed in the review by Peters et al. (2017), as these studies use other impact assessment systems (such as ReCiPe Midpoint) rather than TRACI, which is used in this study. Moreover, not all studies have reported all the impact categories. Stage-by-stage comparison across the studies is also hard as different studies utilize different inventories and process break down in their analysis. These limitations prevent us from being able to fully understand the impacts of detailed differences between the chemistry, structure, and production processes of solid-state lithium battery with the counterpart LIBs.

Our results show that the energy requirements of clean dry-rooms are significant but uncertain. This conveys that significant attention should be paid to the location of the factory, with preference given to locations with dry weather conditions, and to the dehumidification system design. In our study, for example, shifting the location of the facility from Reno, Nevada to Sugar Land, Texas increased the impacts of the dry-room by 34%. Maximized level of production per certain dry-room area, also reduces the impacts of dry-room per each battery pack. This highlights the importance of mass scale production on impacts of each pack. The pyrite battery does not need any formation cycling and first charging for charge retention testing compared to the LIBs. These benefits offset, along with negligible impacts from pyrite mining, the impacts of bigger dry-room resulting in the impacts with almost the same order of magnitude as the LIBs.

This study focuses on the impacts of battery production only. Whereas, one advantage of solid-state batteries over LIBs would be their potentially longer cycle life (Takada, 2013); another

potential advantage of solid-state batteries would be their lower use-phase impacts than LIBs. Lastoskie and Dai (2015), show that use-phase impacts of BEVs with solid-state electrolyte are 5–6% lower than their counterpart LIBs, utilizing the same cathode chemistry and cycle life. They related this conclusion to the higher cell energy density of solid-state structure which results in lower battery mass and higher vehicle efficiency. The cycle life of pyrite battery is not defined yet, also there are uncertainties in the mass inventory of a pyrite battery pack for EV applications. Addressing these questions enables us to understand the use-phase benefits of solid-state lithium pyrite battery over the LIB chemistries.

In the last Chapter of this thesis, a cascading diffusion model is used to analyze how regional differences in driving patterns, fuel prices, and external costs could be applied to design more efficient subsidies for the purchase of EVs. Currently, we are in the transition phase in which EVs are produced in low-volume and the upfront cost of EVs is one of their major barriers to adoption (Krupa et al., 2014). The objective is to investigate how the willingness-to-pay (WTP) and air quality and climate benefits of EVs differ across U.S. regions and how these differences could be exploited to make EV subsidies more efficient. To this end, we develop a model which designs the subsidies based on the minimum social cost (MSC) compared to the original cascading diffusion model, developed by Herron and Williams (2013), which designs the minimum subsidies based on the customers' WTP, driven by economic performance.

Our results demonstrate that the West South Central region shows the highest WTP in both reference and optimistic market curves (optimistic market curves are generated based on high gasoline prices and low electricity prices), as it has the highest annual miles per vehicle among the regions and the lowest electricity prices. WTP varies across the U.S. regions moderately. Reference gasoline prices do not vary significantly across the regions. Thus, this result is mainly driven based on differences in electricity prices and annual miles per vehicle. The environmental externalities from driving EVs in place of GVs vary significantly across the regions. The Pacific region gains the highest benefits from switching to EVs due to the high population density and low reliance on coal generation. The East North Central region, on the other side of the spectrum, suffers the highest

damages. This result is mainly driven by the environmental externalities from exposure to $PM_{2.5}$, which in turn is mainly driven by SO_2 emissions from power plants. When the environmental externalities are incorporated into the U.S. regional market curves, the most favorable region to start the cascading diffusion changes. While the West South Central is the most favorable region based on WTP, the Pacific region is the most favorable region when environmental externalities are also considered. Accordingly, the minimum subsidy required to meet the target production level changes. Subsidies designed based on the minimum social cost model are slightly higher than those from the original model, but their social cost is significantly lower. Advance sales in the international market decrease the required subsidies and social cost in the U.S. Our results highlight the importance of the international market on the level of subsidies required within the U.S. to achieve a specified EV penetration level. The international analysis also demonstrates how influential larger markets are to lower the cost of BEV technology. Thus, in addition to per vehicle subsidy amount, the overall budget for cumulative subsidies, which accordingly defines the target level of production, is also important. Cleaner electricity production increases environmental benefits and reduces the social cost. The most favorable region to start the cascading diffusion may change when the electricity mix moves toward the cleaner production. Regions with less current clean generation would benefit more by switching to cleaner electricity production.

Our analysis shows that WTP is mainly affected by gasoline prices, annual miles driven per vehicle, and vehicle size distribution in a particular sub-market. Our U.S. analysis excluded gasoline taxes from the price of gasoline because tax policies may change in the future as more EVs enter the fleet. Road-use taxes or other taxes that cover all types of vehicle technologies may be required to avoid revenue losses (Aasness and Odeck, 2015; U.S. Congress, 2014). The international analysis shows that if current gasoline taxes are omitted, markets with higher base fuel prices, such as the U.S., are more favorable for advancing BEV diffusion.

We have developed our MSC model based on the cascading diffusion model, developed by Herron and Williams (2013). The minimum subsidy designed based on the cascading diffusion model actually estimates the lower bound for the amount of cumulative subsidies required to fill

the gap between the cost of BEVs and WTP, due to two main reasons. First, the subsidies calculated based on the technology learning curve assume continuous tapering while in the real world, subsidies need to be tapered in discrete steps to make their implementation feasible from an administrative standpoint. This increases the amount of required cumulative subsidies compared to continuous tapering (Matteson and Williams, 2015). Second, the cascading diffusion model assumes sequential adoption across sub-markets, which is not likely to happen in the real world. Parallel adoption in different sub-markets potentially increases the amount of required cumulative subsidies. Our study uses this lower bound formulation as the basis for examining how consideration of externalities might impact regionally differentiated subsidies.

When interpreting these results, it should be noted that the main goal of this study is to demonstrate the difference between minimum differentiated subsidies which are driven from economic performance and the subsidies designed based on the minimum social cost, rather than calculating the exact subsidy amounts for each region. Otherwise, higher resolution sub-markets and more precise treatment of environmental externalities and WTP calculations are required. We also make the assumption that vehicle purchase choices are based on cost of vehicle ownership over the lifetime of the vehicle. Other factors that influence consumer purchases, including make and model preferences and infrastructure limitations, are neglected for simplicity.

The choice of external damage estimates for air pollution emissions is an important source of uncertainty in our cascading diffusion study. We estimate the number of premature deaths or marginal damages of $PM_{2.5}$ and ozone precursors for each sector and region using grid cell marginal damages from Dedoussi and Barrett (2014) and Pappin et al. (2015), respectively. These specific studies were selected over other studies in the literature (e.g., Fann et al. (2009); Heo et al. (2016); Muller and Mendelsohn (2007); NRC (2010)) because their results could be readily aggregated to match the U.S. regions and sectors required in our study. In our study, we estimate the regional environmental externalities; consequently, these results cannot be directly compared with nationally averaged values from other references (although we provide such a comparison to draw a general picture for their order of magnitude). Moreover, the nationally averaged estimates for different

species and sectors vary significantly in the previous studies. Factors driving the differences in damage estimates include the value and treatment of value of a statistical life (VSL), the emission sources or sectors considered, baseline emissions (year and reference), urban or rural population exposure, and the concentration-response function used. Harmonizing key factors across different studies, similar to the work conducted by U.S. Government Interagency Working Group (IWG) for estimating social cost of carbon (SCC), can help to reduce the sources of uncertainties across the studies and make the comparison more informative. However, it should be noted that despite IWG efforts, the SCC estimates still face uncertainties. These uncertainties include those associated with quantifying the physical effects of GHG emissions and those associated with future changes in human behavior and well-being such as population, economic growth, and GHG emissions (IWG, 2016). Since 2009, IWG has been able to harmonize key modeling assumptions including socio-economic-emission scenarios, discount rate, and climate sensitivity probability distribution and has been able to consider the sources of uncertainties quantitatively. Uncertainties that have not been fully quantified in the SCC estimates include quantification of catastrophic damages, treatment of technology change and adoption, and modeling of inter-regional and inter-sectoral linkages (IWG, 2016). In our study, we use the average estimates of SCC, so using a higher value of SCC would favor BEVs in the externalities comparison, since we found that replacing GVs with BEVs reduces CO_2 emissions in all U.S. regions.

A further limitation of our study is that it only covers a subset of health and welfare externalities associated with vehicles. While mortality effects dominate air pollution damage estimates, other endpoints could also present tradeoffs between GV and BEV. Effects neglected in our study include morbidity effects for $PM_{2.5}$ and ozone and mortality from short-term exposure to $PM_{2.5}$ and from long-term exposure to ozone. The contribution of VOC emissions to ozone-related damages is also neglected. Based on current inventories, our analysis assumes that the contribution of NH_3 emissions from GVs to $PM_{2.5}$ formation is negligible. However, recent studies question the NH_3 emissions inventories for the road sector. Sun et al. (2017) measured NH_3:CO_2 emission ratios and concluded that the current emission inventories underestimate NH_3 emissions from the road sector;

our estimated benefits of switching to EVs would be biased low if a significant amount of these under-reported emissions are associated with LDVs. Our study also overlooks environmental or welfare damages from $PM_{2.5}$ and ozone, including damage to crops, building materials, and climate, as well as water consumption and land use tradeoffs from electricity generation and oil and gas production. We also focus on direct emissions from GV or emissions from electricity generation for EV, neglecting other stages of the WTW and vehicle life cycles (Nealer et al., 2015; NRC, 2010; Tamayao et al., 2015; Yuksel et al., 2016). A more comprehensive suite of externalities could be considered in future work that builds on the framework presented here.

In addition to the specific research results described above, work from this thesis lead to several methodological developments that refine existing tools or provide new frameworks for future studies. These include:

- The ANSWER-MARKAL energy model has been updated for a modified EPA database including more optimistic treatment of EV technologies, which can be used for other sensitivity and policy analyses.

- A framework has been developed for a process-based attributional life cycle assessment of solid-state lithium batteries. The framework is being demonstrated for the battery developed at University of Colorado Boulder and Solid Power but can be adapted for application to other solid-state lithium batteries.

- A framework has been developed for combining ownership costs, environmental externalities and production-based learning curves to estimate required subsidies and associated social costs of achieving specified target levels of EV penetration. The proposed model designs the efficient subsidies based on the minimum social costs in differentiated sub-markets and could be applied to other regions/sub-markets and/or other technologies.

This thesis presents the impacts of battery technology advances, via electrification, on U.S. emissions and fuel consumptions. The study aims to cover a reasonable suite of policies targeting WTW and vehicle cycles, a multidecadal timeframe, and a transition phase toward mass production.

However, there are still questions about implementation of such policies that remain to be further explored. Until now, most EV-related policies have been inclined to promote more adoption and the term "transition phase" refers to EVs. Provided that those transition policies work efficiently and EVs become more and more competitive with GVs and abundant, transition policies related to phasing out current technologies become important. That is, both technologies face a transition phase. Those policies will likely depend on the fleet turn-over rate and geographical location. They also can target many sectors such as refineries and the industrial sector. The results of our study suggest that policies targeting other sectors such as heavy-duty and industrial sectors, coupled with increased EV adoption, could be effective for emission reduction from all sectors of the economy. Different scenarios that can be analyzed include impact the of shifting from diesel to gasoline in other sectors (where feasible from a technical perspective) and desulfurization of fuel in other sectors.

So far, the results of battery and EV LCAs are presented based on midpoint indicators (mainly global warming potential). Further research on estimating endpoint indicators (such as health effects and mortalities) from these midpoint indicators, beyond GHG and air quality emissions, can improve subsidy design based on environmental externalities. The externalities can include other impact categories than GWP from battery and vehicle manufacturing sectors. In this study, we showed how moving toward more efficient vehicles can reduce the future WTW emissions for both EV and GV technologies. This study sets a framework for designing efficient subsidies toward EV adoption that are differentiated by sub-market and are designed based on minimum social cost. However, the implementation methods would also be influential for effectiveness of these policies and need to be investigated for each sub-market. The implementation decision in each sub-market would include different layers of government that grant the subsidy, the agents that receive the subsidy, overall budget, and the subsidy format (uniform or differentiated). Similar to the design of subsidies, the implementation methods should be differentiated by sub-market, since economic condition, level of income, and consumer behaviors are different.

Bibliography

Aasness, M. A. and Odeck, J. (2015). The increase of electric vehicle usage in Norway- incentives and adverse effects. European Transport Research Review, 7(4):34.

Amarakoon, S., Smith, J., and Segal, B. (2013). Application of life-cycle assessment to nanoscale technology: Lithium-ion batteries for electric vehicles. Technical report, Environmental Protection Agency (EPA); EPA 744-R-12-00.

An, F., Earley, R., and Green-Weiskel, L. (2011). Global overview on fuel efficiency and motor vehicle emission standards: policy options and perspectives for international cooperation. United Nations, Department of Economic and Social Affairs, Commission on Sustainable Development, The Innovation Center for Energy and Transportation (iCET).

Anair, D. and Mahmassani, A. (2012). State of charge: Electric vehicles' global warming emissions and fuel-cost savings across the United States. Union of Concerned Scientists.

ANL (2016). The Greenhouse gases, Regulated Emissions, and Energy use in Transportation (GREET) model. Argonne National Laboratory (ANL). `https://greet.es.anl.gov/`.

ANL (2017). A lithium-ion battery performance and cost (BatPac) model for electric-drive vehicles. Argonne National Laboratory (ANL). `http://www.cse.anl.gov/batpac/index.html`.

ASHRAE (2013). ASHRAE Handbook: Fundamentals. American Society of Heating, Refrigerating and Air-conditioning Engineers (ASHRAE): Atlanta, GA.

ASHRAE (2015). ASHRAE Handbook: Applications. American Society of Heating, Refrigerating and Air-conditioning Engineers (ASHRAE): Atlanta, GA.

ASHRAE (2016). ASHRAE Handbook: Systems and Equipment. American Society of Heating, Refrigerating and Air-conditioning Engineers (ASHRAE): Atlanta, GA.

Azevedo, C. L. and Cardoso, J. L. (2009). Estimation of annual traffic volumes- A model for Portugal. ECTRI – FEHRL – FERSI, Young Researchers Seminar, 3–5 June 2009.

Babaee, S., Nagpure, A. S., and DeCarolis, J. F. (2014). How much do electric drive vehicles matter to future US emissions? Environmental science & technology, 48(3):1382–1390.

Baker, R. (2011). Personal communication with Environmental Protection Agency (EPA) staff. Eastern Research Group Inc. (ERG); Austin Texas.

Balk, D. L., Deichmann, U., Yetman, G., Pozzi, F., Hay, S. I., and Nelson, A. (2006). Determining global population distribution: methods, applications and data. Advances in parasitology, 62:119–156.

Bandivadekar, A., Bodek, K., Cheah, L., Evans, C., Groode, T., Heywood, J., Kasseris, E., Kromer, M., and Weiss, M. (2008). On the road in 2035: Reducing transportation's petroleum consumption and GHG emissions, Laboratory for Energy and the Environment, Report No. LFEE 2008-05 RP, Massachusetts Institute of Technology, July 2008. Development of System Analysis Methodologies and Tools for Modeling and Optimizing Vehicle System Efficiency; ISBN: 978-0-615-23649-0.

Bell, M. L., McDermott, A., Zeger, S. L., Samet, J. M., and Dominici, F. (2004). Ozone and short-term mortality in 95 US urban communities, 1987-2000. JAMA, 292(19):2372–2378.

Bento, A., Roth, K., and Zuo, Y. (2016). Vehicle lifetime trends and scrappage behavior in the US used car market. Sol Price School of Public Policy and Department of Economics, University of Southern California, Los Angeles. http://faculty.sites.uci.edu/kevinroth/files/2011/03/Scrappage_18Jan2016.pdf.

Bradley, T. H. and Quinn, C. W. (2010). Analysis of plug-in hybrid electric vehicle utility factors. Journal of Power Sources, 195(16):5399–5408.

Brown, K. E. (2014). Internalizing air quality and greenhouse gas externalities in the US energy system and the effect on future air quality. Comprehensive exam report. PhD thesis, Department of Mechanical Engineering, University of Colorado Boulder.

Brown, K. E., Henze, D. K., and Milford, J. B. (2013). Accounting for climate and air quality damages in future US electricity generation scenarios. Environmental science & technology, 47(7):3065–3072.

Brown, K. E., Henze, D. K., and Milford, J. B. (2014a). The effect of criteria pollutant and greenhouse gas damage based fees on emissions from the US energy system. In CMAS Conference. www.cmascenter.org/conference/2014/agenda.cfm.

Brown, K. E., Henze, D. K., and Milford, J. B. (2014b). Internalizing life cycle externalities in the US energy system. Proceedings from the LCA XIV International Conference, San Francisco, CA, United States, 149–160. http://www.lcacenter.org/lca-xiv.aspx.

Bureau of Labor (2013). Hazmat shipment by mode of transportation. transtats.bls.gov.

CARB (2017). California Air Resources Board Clean Vehicle Rebate Project, Rebate statistics; Data last updated August 01, 2017. Center for Sustainable Energy. https://cleanvehiclerebate.org/rebate-statistics.

Cazzola, P., Gorner, M., Teter, J., and Yi, W. (2016). Global EV outlook 2016. International Energy Agency, France.

CBS (2015). Transport and mobility 2015. Statistics Netherlands. http://download.cbs.nl/pdf/2015-transport-and-mobility.pdf.

CCA (2017). Cleanroom Construction Associate (CCA) website. http://cleanroom-construction.net/who-we-are/.

CDC (2016). Underlying cause of death 1999–2015 on CDC Wonder Online Database, released December, 2016. Data are from the Multiple Cause of Death Files, 1999-2015, as compiled from data provided by the 57 vital statistics jurisdictions through the Vital Statistics Cooperative Program. Centers for Disease Control and Prevention, National Center for Health Statistics. http://wonder.cdc.gov/ucd-icd10.html.

Çengel, Y. A. and Boles, M. A. (2011). Thermodynamics: An Engineering Approach; Seventh Edition. McGraw-Hill: New York, USA.

Choi, D. G., Kreikebaum, F., Thomas, V. M., and Divan, D. (2013). Coordinated EV adoption: double-digit reductions in emissions and fuel use for $40/vehicle-year. Environmental science & technology, 47(18):10703–10707.

Cleanroom Technology (2017). Cleanroom Technology website:. https://www.cleanroomtechnology.com/news/article_page/Building_the_worlds_biggest_lithium_ion_battery_plant/119947.

Climate Scope (2017). Climate Scope 2016, China. http://download.cbs.nl/pdf/2015-transport-and-mobility.pdf.

CNBC (2016). Sustainable Energy, a CNBC special report 24 May 2016. http://www.cnbc.com/2016/05/24/this-country-has-hit-a-major-milestone-for-electric-cars-heres-how.html.

Cooper, C. D. and Alley, F. C. (2002). Air pollution control: A design approach; Fourth Edition. Waveland Press, Inc.: IL, USA.

Copper Development Association Inc. (2017). Annual data 2017, copper supply & consumption 1996-2016. Copper Alliance. https://www.copper.org/resources/market_data/pdfs/annual_data.pdf.

Crutzen, P. J., Mosier, A. R., Smith, K. A., and Winiwarter, W. (2008). N_2O release from agro-biofuel production negates global warming reduction by replacing fossil fuels. Atmospheric Chemistry and Physics, 8(2):389–395.

Dedoussi, I. C. and Barrett, S. R. H. (2014). Air pollution and early deaths in the United States. Part II: Attribution of $PM_{2.5}$ exposure to emissions species, time, location and sector. Atmospheric environment, 99:610–617.

Deloitte Consulting LLC (2010). Gaining traction: A customer view of electric vehicle mass adoption in the U.S. automotive market. New York: Deloitte Global Services.

Deng, Y., Li, J., Li, T., Gao, X., and Yuan, C. (2017). Life cycle assessment of lithium sulfur battery for electric vehicles. Journal of Power Sources, 343:284–295.

DOE (2017a). Qualified Plug-in Electric Drive Motor Vehicle Tax Credit, U.S. Department of Energy, Office of Energy Efficiency and Renewable Energy, Alternative Fuels Data Center. https://afdc.energy.gov.

DOE (2017b). Reducing pollution with electric vehicles. Department of Energy, Office of Energy Efficiency and Renewable Energy. https://energy.gov/eere/electricvehicles/reducing-pollution-electric-vehicles.

DOT (2010). Transportation's role in reducing U.S. greenhouse gas emissions volume 1: synthesis report. Report to Congress, US Department of Transportation. http://ntl.bts.gov/lib/32000/32700/32779/DOT_Climate_Change_Report_-_April_2010_-_Volume_1_and_2.pdf.

Dunn, J. B., Gaines, L., Kelly, J. C., James, C., and Gallagher, K. G. (2015a). The significance of Li-ion batteries in electric vehicle life-cycle energy and emissions and recycling's role in its reduction. Energy & Environmental Science, 8(1):158–168.

Dunn, J. B., Gaines, L., Sullivan, J., and Wang, M. Q. (2012). Impact of recycling on cradle-to-gate energy consumption and greenhouse gas emissions of automotive lithium-ion batteries. Environmental science & technology, 46(22):12704–12710.

Dunn, J. B., James, C., Gaines, L., Gallagher, K., Dai, Q., and Kelly, J. C. (2015b). Material and energy flows in the production of cathode and anode materials for lithium ion batteries. Technical report, Argonne National Lab.(ANL), Energy System Division; ANL/ESD-14/10 Rev.

Egbue, O. and Long, S. (2012). Barriers to widespread adoption of electric vehicles: an analysis of consumer attitudes and perceptions. Energy policy, 48:717–729.

EIA (2012). Primary energy consumption by source and sector, 2012 (quadrillion Btu). https://www.eia.gov/totalenergy/data/monthly/pdf/flow/primary_energy.pdf.

EIA (2014a). Annual Energy Outlook (AEO) 2014 with projections to 2040. US Energy Information Administration, US Department of Energy; Washington, DC.

EIA (2014b). What drives U.S. gasoline prices? Independent Statistics and Analysis; US Energy Information Administration (EIA). http://www.eia.gov/analysis/studies/gasoline/pdf/gasolinepricestudy.pdf.

EIA (2015). Annual Energy Outlook (AEO) 2015 with projections to 2040. US Energy Information Administration, US Department of Energy; Washington, DC.

EIA (2016a). Gasoline prices by formulation, grade, sales type. Energy Information Administration (AEO). http://www.eia.gov/dnav/pet/pet_pri_allmg_a_EPM0_PTC_Dpgal_m.htm.

EIA (2016b). State-by-state fuel taxes. Energy Information Administration (AEO). https://www.eia.gov/tools/faqs/faq.cfm?id=10&t=10.

EIA (2016c). State electricity profiles. Energy Information Administration (AEO). http://www.eia.gov/electricity/state/.

EIA (2016d). Use of energy in the United States, energy use for transportation. Energy Information Administration (EIA). https://www.eia.gov/energyexplained/?page=us_energy_transportation.

EIA (2017a). Annual energy outlook (AEO) 2017 with projections to 2040. US Energy Information Administration, US Department of Energy; Washington, DC.

EIA (2017b). U.S. census regions and divisions map. https://www.eia.gov/consumption/commercial/maps.php.

Electricity Local (2017). Residential electricity rates in China. http://www.electricitylocal.com/states/texas/china/.

Elgowainy, A., Burnham, A., Wang, M., Molburg, J., and Rousseau, A. (2009). Well-to-wheels energy use and greenhouse gas emissions analysis of plug-in hybrid electric vehicles. Argonne National Laboratory (ANL); Center for Transportation Research; Energy Systems Division; ANL/ESD/09-2.

Elgowainy, A., Han, J., Ward, J., Joseck, F., Gohlke, D., Lindauer, A., Ramsden, T., Biddy, M., Alexander, M., Barnhart, S., Sutherland, I., Verduzco, L., and Wallington, T. (2016). Cradle-to-grave lifecycle analysis of U.S. light-duty vehicle-fuel pathways: A greenhouse gas emissions and economic assessment of current (2015) and future (2025–2030) technologies. Technical report, Argonne National Lab.(ANL). ANL/ESD-16/7.

Elgowainy, A., Rousseau, A., Wang, M., Ruth, M., Andress, M. D., Ward, J., Joseck, F., Nguyen, T., and Das, S. (2013). Cost of ownership and well-to-wheels carbon emissions/oil use of alternative fuels and advanced light-duty vehicle technologies. Energy for Sustainable Development, 17(6):626–641.

Ellingsen, L. A., Majeau-Bettez, G., Singh, B., Srivastava, A. K., Valøen, L. O., and Strømman, A. H. (2014). Life cycle assessment of a lithium-ion battery vehicle pack. Journal of Industrial Ecology, 18(1):113–124.

EPA (2008). Documentation for the 2005 point source. National Emission Inventory (NEI). Environmental Protection Agency (EPA). https://www.epa.gov/sites/production/files/2015-11/documents/nei_point_2005_9-10.pdf.

EPA (2010). Guidelines for preparing economic analyses. EPA Publication 240-R-10-001, U.S. Environmental Protection Agency (EPA), National Center for Environmental Economics, Office of Policy.

EPA (2011). The benefits and costs of the Clean Air Act from 1990 to 2020. Technical Report March. Final report of U.S. Environmental Protection Agency (EPA); Office of Air and Radiation. http://www.epa.gov/cleanairactbenefits/prospective2.html.

EPA (2012a). Light-duty automotive technology, carbon dioxide emissions, and fuel economy trends: 1975 through 2011; Executive Summary. Environmental Protection Agency (EPA); Transportation and Climate Division; QTAC. EPA-420-S-12-001. http://nepis.epa.gov/Exe/ZyPDF.cgi/P100DYX6.PDF?Dockey=P100DYX6.PDF.

EPA (2012b). Tool for the Reduction and Assessment of Chemical and other environmental Impacts (TRACI), TRACI version 2.1 User's Guide. Technical report, EPA/600/R-12/554. http://nepis.epa.gov/Adobe/PDF/P100HN53.pdf.

EPA (2015). Clean Power Plan Final Rule; Federal Registrar, 40 CFR part 60. Environmental Protection Agency (EPA); RIN 2060-AR33, Vol. 80, No.205; EPA-HQ-OAR-2013-0602; FRL-9930-65-OAR. http://www.epa.gov/cleanpowerplan/clean-power-plan-existing-power-plants.

EPA (2017a). Fast facts; U.S. transportation sector greenhouse gas emissions 1990-2015. Environmental Protection Agency (EPA). https://nepis.epa.gov/Exe/ZyPDF.cgi?Dockey=P100S7NK.pdf.

EPA (2017b). Health effect of ozone in the general population. Environmental Protection Agency (EPA). https://www.epa.gov/ozone-pollution-and-your-patients-health/health-effects-ozone-general-population#observedeffects.

EPA (2017c). Mortality risk valuation. Environmental Protection Agency (EPA). https://www.epa.gov/environmental-economics/mortality-risk-valuation#means.

EPA (2017d). Smog, soot, and other air pollution from transportation. Environmental Protection Agency (EPA). https://www.epa.gov/air-pollution-transportation/smog-soot-and-local-air-pollution.

Eppstein, M. J., Grover, D. K., Marshall, J. S., and Rizzo, D. M. (2011). An agent-based model to study market penetration of plug-in hybrid electric vehicles. Energy Policy, 39(6):3789–3802.

Eppstein, M. J., Rizzo, D. M., Lee, B. H. Y., Krupa, J. S., and Manukyan, N. (2015). Using national survey respondents as consumers in an agent-based model of plug-in hybrid vehicle adoption. IEEE Access, 3:457–468.

Fann, N., Fulcher, C. M., and Hubbell, B. J. (2009). The influence of location, source, and emission type in estimates of the human health benefits of reducing a ton of air pollution. Air Quality, Atmosphere & Health, 2(3):169–176.

Federal Registrar (2010). Light-duty vehicle greenhouse gas emission standards and corporate average fuel economy standards. Final Rule.

FHWA (2008). Federal Highway Administration Website. https://www.fhwa.dot.gov/policyinformation/statistics/2008/pdf/in5.pdf.

FHWA (2017). Population, drivers, vehicles, fuel and travel by state, Federal Highway Administration. https://www.fhwa.dot.gov/ohim/onh00/onh2p11.htm.

Goldman Sachs Group Inc. (2017). Electric vehicle boom: ICE-ing the combustion engine; What if EV adoption shifts to hyper mode? https://www.iape-mobility.nl/wp-content/uploads/2017/09/GS-EV-boom-6-Sep-2017.pdf.

Gonder, J. and Simpson, A. (2007). Measuring and reporting fuel economy of plug-in hybrid electric vehicles. NREL/JA-540-41341, WEVA-2007-025. http://www.nrel.gov/docs/gen/fy07/41341.pdf.

Greene, D. L., Baker, H. H. Jr., and Plotkin, S. E. (2011). Solutions: Reducing greenhouse gas emissions from U.S. transportation. Prepared for PEW Center on Global Climate Change and Argonne National Laboratory (ANL). http://www.c2es.org/publications/reducing-ghg-emissions-from-transportation.

Hawkins, T. R., Singh, B., Majeau-Bettez, G., and Strømman, A. H. (2013). Comparative environmental life cycle assessment of conventional and electric vehicles. Journal of Industrial Ecology, 17(1):53–64.

Heo, J., Adams, P. J., and Gao, H. O. (2016). Public health costs of primary $PM_{2.5}$ and inorganic $PM_{2.5}$ precursor emissions in the United States. Environmental science & technology, 50(11):6061–6070.

Herron, S. and Williams, E. (2013). Modeling cascading diffusion of new energy technologies: case study of residential solid oxide fuel cells in the U.S. and internationally. Environmental science & technology, 47(15):8097–8104.

Heywood, J. B., Baptista, P., Berry, I., Bhatt, K., Cheah, L., Sisternes, F., Karplus, V., Keith, D., Khusid, M., MacKenzie, D., and McAulay, J. (2009). An action plan for cars, the policies needed to reduce US petroleum consumption and greenhouse gas emissions. An MIT Energy Initiative Report; Massachusetts Institute of Technology; ISBN 978-0-615-34325-9.

Hill, J., Nelson, E., Tilman, D., Polasky, S., and Tiffany, D. (2006). Environmental, economic, and energetic costs and benefits of biodiesel and ethanol biofuels. Proceedings of the National Academy of sciences, 103(30):11206–11210.

HIS Markit (2016). Vehicles getting older: average age of light cars and trucks in U.S. rises again in 2016 to 11.6 years; HIS Markit says. http://news.ihsmarkit.com/press-release/automotive/vehicles-getting-older-average-age-light-cars-and-trucks-us-rises-again-201.

Hischier, R., Weidema, B., Althaus, H., Bauer, C., Doka, G., Dones, R., Frischknecht, R., Hellweg, S., Humbert, S., Jungbluth, N., Köllner, T., Loerincik, Y., Margni, M., and Nemecek, T. (2010). Implementation of life cycle impact assessment methods. Ecoinvent report No.3, Ecoinvent Center, Swiss Centre for Life Cycle Inventories: St. Gallen.

Holland, S. P., Mansur, E. T., Muller, N. Z., and Yates, A. J. (2016). Are there environmental benefits from driving electric vehicles? the importance of local factors. American Economic Review, 106(12):3700–3729.

Huijbregts, M., Hauschild, M., Jolliet, O., Margni, M., McKone, T., Rosenbaum, R. K., and Meent, D. (2010). USEtox^{TM} User manual. USEtox^{TM} Team.

Iaych, K., Alexeev, V., and Latipov, O. (2009). IRF world road statistics 2009, data 2002-2007 booklet. International Road Federation (IRF). http://www.irfnet.org/files-upload/stats/2009/wrs2009_web.pdf.

ICCT (2012). The new passenger car fleet in China, 2010, technology assessment and international comparison. International Council on Clean Transportation (ICCT). http://www.theicct.org/sites/default/files/publications/ICCT_New_Passenger_Car_Fleet_China_2010.pdf.

ICCT (2017). European vehicle market statistics, pocketbook 2016/2017. International Council on Clean Transportation (ICCT). http://www.theicct.org/sites/default/files/publications/ICCT_Pocketbook_2016.pdf.

IEA (2013). Energy prices and taxes, documentation for beyond 2020 files, data for non-OECD countries, country notes, 1^{st} Quarter 2012. International Energy Agency (IEA). http://wds.iea.org/wds/pdf/EPT_Documentation-NMC.pdf.

INL (2014). ARRA – Chrysler RAM, Chrysler RAM PHEV Fleet- Phase 2, Advanced Vehicle Testing Activity. Idaho National Laboratory (INL). https://avt.inl.gov/project-type/chrysler-ram-phev.

INL (2017). How do gasoline & electric vehicle compare? Advanced Vehicle Testing Activity. Idaho National Laboratory (INL). https://avt.inl.gov/sites/default/files/pdf/fsev/compare.pdf.

ISO (2017). ALPHA-3 country codes. International Standard Organization (ISO). https://www.iso.org/obp/ui/#search.

IWG (2013). Technical support document: technical update of the social cost of carbon for regulatory impact analysis, under Executive Order 12866; US Government, Interagancy Working Group on Social Cost of Carbon, Washington, DC. https://www.whitehouse.gov/sites/default/files/omb/inforeg/social_cost_of_carbon_for_ria_2013_update.pdf.

IWG (2016). Technical support document: technical update of the social cost of carbon for regulatory impact analysis, under Executive Order 12866; US Government, Interagancy Working Group on Social Cost of Carbon, Washington, DC. https://www.epa.gov/sites/production/files/2016-12/documents/sc_co2_tsd_august_2016.pdf.

Jacob, S. R. and Brown, P. M. (1978). Process for producing high purity lithium sulfide. US Patent 4,126,666.

Jorgenson, J., Detlor, J., Brinkman, G., and Milford, J. (2012). Emissions changes from electric vehicle use in Colorado. Technical report, Department of Mechanical Engineering, University of Colorado Boulder.

Kama (2013). Korean Automotive Industry, annual report 2013. Korea Automobile Manufacturers Association. http://kama.or.kr/eng/PS/pdf/Total2014.pdf.

KBB (2012). Average age of U.S. car and truck fleet hit record high levels. Kelly Blue Book. https://www.kbb.com/car-news/all-the-latest/average-age-of-us-car-and-truck-fleets-hit-record-high-levels/?contentid=2000007742.

Keshavarzmohammadian, A., Henze, D. K., and Milford, J. B. (2017). Emission impacts of electric vehicles in the U.S. transportation sector following optimistic cost and efficiency projections. Environmental Science & Technology, 51(12):6665–6673.

Kim, H. C., Wallington, T. J., Arsenault, R., Bae, C., Ahn, S., and Lee, J. (2016). Cradle-to-gate emissions from a commercial electric vehicle li-ion battery: a comparative analysis. Environmental science & technology, 50(14):7715–7722.

Kim, T. B., Choi, J. W., Ryu, H. S., Cho, G. B., Kim, K. W., Ahn, J. H., Cho, K. K., and Ahn, H. J. (2007). Electrochemical properties of sodium/pyrite battery at room temperature. Journal of Power Sources, 174(2):1275–1278.

Klein, C., Hurlbut, C. S. Jr. , and Dana, J. D. (1993). Manual of mineralogy; 21^{st} Edition. Wiley: New York, USA.

Kromer, M. A., Bandivadekar, A., and Evans, C. (2010). Long-term greenhouse gas emission and petroleum reduction goals: evolutionary pathways for the light-duty vehicle sector. Energy (Oxford, U.K.), 35(1):387–397.

Krupa, J. S., Rizzo, D. M., Eppstein, M. J., Lanute, D. B., Gaalema, D. E., Lakkaraju, K., and Warrender, C. E. (2014). Analysis of a consumer survey on plug-in hybrid electric vehicles. Transportation Research Part A: Policy and Practice, 64:14–31.

Lastoskie, C. M. and Dai, Q. (2015). Comparative life cycle assessment of laminated and vacuum vapor-deposited thin film solid-state batteries. Journal of Cleaner Production, 91:158–169.

Lenox, C., Dodder, R., Gage, C., Kaplan, O., Loughlin, D., and Yelverton, W. (2013). EPA U.S. nine-region MARKAL database: Database documentation. US Environmental Protection Agency (EPA); EPA 600/B-13/203. http://www.epa.gov/cleanpowerplan/clean-power-plan-existing-power-plants.

Li, B., Gao, X., Li, J., and Yuan, C. (2014). Life cycle environmental impact of high-capacity lithium ion battery with silicon nanowires anode for electric vehicles. Environ. Sci. Technol, 48(5):3047–3055.

Lin, C. C. and Zeng, J. J. (2013). The elasticity of demand for gasoline in China. Energy Policy, 59:189–197.

Loughlin, D. H., Kaufman, K. R., Lenox, C. S., and Hubbell, B. J. (2015). Analysis of alternative pathways for reducing nitrogen oxide emissions. Journal of the Air & Waste Management Association, 65(9):1083–1093.

Loulou, R., Goldstein, G., and Noble, K. (2004). Documentation for the MARKAL family of models. Energy Technology Systems Analysis Programme (ETSAP). http://www.etsap.org/web/mrkldoc-i_stdmarkal.pdf.

Majeau-Bettez, G., Hawkins, T. R., and Strømman, A. H. (2011). Life cycle environmental assessment of lithium-ion and nickel metal hydride batteries for plug-in hybrid and battery electric vehicles. Environmental science & technology, 45(10):4548–4554.

Marten, A. L. and Newbold, S. C. (2012). Estimating the social cost of non-CO_2 GHG emissions: methane and nitrous oxide. Energy Policy, 51:957–972.

Mathers, C. (2008). Global Burden of Disease, 2004 update. World Health Organization (WHO). http://www.who.int/healthinfo/global_burden_disease/2004_report_update/en/.

Matheys, J. and Autenboer, V. W. (2005). SUBAT: sustainable batteries. Work package 5: overall assessment; Final public report. Vrije Universiteit Brussel–ETEC, Brussels, Belgium.

Matteson, S. and Williams, E. (2015). Learning dependent subsidies for lithium-ion electric vehicle batteries. Technological Forecasting and Social Change, 92:322–331.

McLeod, J. D. (2014). Characterizing the emissions implications of future natural gas production and use in the U.S. and Rocky Mountain region: a scenario-based energy system modeling approach. Master's thesis, Mechanical Engineering Department, University of Colorado Boulder.

McLeod, J. D., Brinkman, G. L., and Milford, J. B. (2014). Emissions implications of future natural gas production and use in the US and in the Rocky Mountain region. Environmental science & technology, 48(22):13036–13044.

Meier, P. J., Cronin, K. R., Frost, E. A., Runge, T. M., Dale, B. E., Reinemann, D. J., and Detlor, J. (2015). Potential for electrified vehicles to contribute to U.S. petroleum and climate goals and implications for advanced biofuels. Environmental science & technology, 49(14):8277–8286.

Muller, N. Z. and Mendelsohn, R. (2007). Measuring the damages of air pollution in the United States. Journal of Environmental Economics and Management, 54(1):1–14.

Muller, N. Z. and Mendelsohn, R. (2009). Efficient pollution regulation: getting the prices right. The American Economic Review, 99(5):1714–1739.

Myhre, G. and Shindell, D. (2013). Climate Change 2013: the physical science basis, Intergovernmental Panel on Climate Change (IPCC), chap. 8. www.ipcc.ch/report/ar5/wg1/.

Natural Resources Canada (2009). Canadian vehicle survey, summary report, 2009. http://oee.nrcan.gc.ca/publications/statistics/cvs09/pdf/cvs09.pdf.

Nealer, R., Reichmuth, D., and Anair, D. (2015). Cleaner cars from cradle to grave: how electric cars beat gasoline cars on lifetime global warming emissions. Union of Concerned Scientists (UCS).

Nelson, P. A., Gallagher, K. G., Bloom, I. D., and Dees, D. W. (2012). Modeling the performance and cost of lithium-ion batteries for electric-drive vehicles; Second Edition. Technical report, Argonne National Laboratory (ANL), Chemical Sciences and Engineering Division; ANL-12/55.

Nielsen, O., Winther, M., Mikkelsen, M. H., Hoffmann, L., Nielsen, M., Gyldenkaerne, S., Fauser, P., Plejdrup, M. S., Albrektsen, R., Hjelgaard, K., and Bruun, H. G. (2012). Annual Danish informative inventory report to UNECE, emission inventories from the base year of protocols to year 2010. Scientific report from DCE - Danish Centre for Environment and Energy. AARHUS University. http://oee.nrcan.gc.ca/publications/statistics/cvs09/pdf/cvs09.pdf.

Notter, D. A., Gauch, M., Widmer, R., Wager, P., Stamp, A., Zah, R., and Althaus, H. (2010). Contribution of Li-ion batteries to the environmental impact of electric vehicles. Environmental science & technology, 44(17):6650–6656.

NRC (2010). Hidden costs of energy: unpriced consequences of energy production and use. National Research Committee on Health, Environmental, and Other External Costs and Benefits of Energy Production and Consumption. National Research Council (NRC). National Academies Press: Washington, DC.

NRC (2013). Transition to alternative vehicles and fuels, National Research Council report. Committee on Transitions to Alternative Vehicles and Fuels, Board on Energy and Environmental Systems, Division on Engineering and Physical Sciences. National Academies Press: Washington, DC.

Nykvist, B. and Nilsson, M. (2015). Rapidly falling costs of battery packs for electric vehicles. Nature Climate Change, 5(4):329–332.

Ober, J. A. (2001). Sulfur. U.S. geological survey. Minerals, Reston, VA.

OECD (2014). Consumption tax trends 2014, VAT/GST and excise rates, trends and policy issues. OECD publishing, Paris. http://dx.doi.org/10.1787/ctt-2014-en.

OECD (2017). IEA energy prices and taxes statistics. Organization for Economic Co-operation and Development (OECD). http://www.oecd-ilibrary.org/energy/data/iea-energy-prices-and-taxes-statistics_eneprice-data-en.

Oliveira, C. M., Machado, C. M., Duarte, G. W., and Peterson, M. (2016). Beneficiation of pyrite from coal mining. Journal of Cleaner Production, 139:821–827.

OVO Energy (2017). Average electricity prices around the world: $/kWh. https://www.ovoenergy.com/guides/energy-guides/average-electricity-prices-kwh.html.

Pappin, A. J. and Hakami, A. (2013). Source attribution of health benefits from air pollution abatement in Canada and the United States: an adjoint sensitivity analysis. Environmental health perspectives, 121(5):572–579.

Pappin, A. J., Mesbah, S. M., Hakami, A., and Schott, S. (2015). Diminishing returns or compounding benefits of air pollution control? the case of NO_x and ozone. Environmental science & technology, 49(16):9548–9556.

Pearre, N. S., Kempton, W., Guensler, R. L., and Elango, V. V. (2011). Electric vehicles: how much range is required for a day's driving? Transportation Research Part C: Emerging Technologies, 19(6):1171–1184.

Pedersen, N. J., Rosenbloom, S., and Skinner, R. E. (2011). Policy options for reducing energy use and greenhouse gas emissions from US transportation, special report 307. Committee for a Study of Potential Energy Savings and Greenhouse Gas Reductions from Transportation; Transportation Research Board of the National Academies, ; ISBN 978-0-309-16742-0.

Peters, J. F., Baumann, M., Zimmermann, B., Braun, J., and Weil, M. (2017). The environmental impact of Li-ion batteries and the role of key parameters–a review. Renewable and Sustainable Energy Reviews, 67:491–506.

Peters, M. S., Timmerhaus, K. D., and West, R. E. (1968). Plant design and economics for chemical engineers; Eighth Edition. McGraw-Hill Inc.: New York.

Peterson, S. B., Whitacre, J. F., and Apt, J. (2011). Net air emissions from electric vehicles: the effect of carbon price and charging strategies. Environmental science & technology, 45(5):1792–1797.

Plotkin, S. E. and Singh, M. K. (2009). Multi-path transportation futures study: vehicle characterization and scenario analyses. Technical report, Argonne National Laboratory (ANL), Energy System Division; ANL/ESD/09-5.

Pode, J. (2004). Thermal jacket for battery. US Patent 20040194489 A1.

PRé (2015). SimaPro database manual; Methods library. Ecoinvent Center.

Rhodes, J. D., King, C., Gulen, G., Olmstead, S. M., Dyer, J. S., Hebner, R. E., Beach, F. C., Edgar, T. F., and Webber, M. E. (2017). A geographically resolved method to estimate levelized power plant costs with environmental externalities. Energy Policy, 102:491–499.

Rhodes, J. S. and Keith, D. W. (2005). Engineering economic analysis of biomass IGCC with carbon capture and storage. Biomass and Bioenergy, 29(6):440–450.

Rudokas, J., Miller, P. J., Trail, M. A., and Russell, A. G. (2015). Regional air quality management aspects of climate change: impact of climate mitigation options on regional air emissions. Environmental science & technology, 49(8):5170–5177.

Schievelbein, W., Kockelman, K. M., Bansal, P., and Schauer-West, S. (2017). Indian vehicle ownership and travel behaviors: a case study of Bangalore, Delhi and Kolkata. Transportation Research Board 96^{th} annual meeting, 01.08.2017 to 01.12.2017.

Scoffield, D., Salisbury, S., and Smart, J. (2014). Driving and charging behavior of Nissan Leaf drivers in the EV project with access to workplace charging. Technical report, Idaho National Lab.(INL); INL/EXT-14-33700.

Sehgal, V. (2011). India automotive market 2020. Booz & Co. https://www.strategyand.pwc.com/media/file/Strategyand-India-Automotive-Market-2020.pdf.

SEI (2005). Sustainable energy Ireland, media information. http://www.sei.ie/News_Events/Press_Releases/2006/Transport9thAug06.pdf.

Sierzchula, W., Bakker, S., Maat, K., and Wee, B. (2014). The influence of financial incentives and other socio-economic factors on electric vehicle adoption. Energy Policy, 68:183–194.

Simpson, A. (2006). Plug-in hybrid modeling and application: cost/benefit analysis. National Renewable Energy Laboratory (NREL), presented at the 3^{rd} AVL Summer Conference on Automotive Simulation Technology: Modeling of Advanced Powertrain Systems; NREL/PR-540-40504.

Skamarock, W. C., Klemp, J. B., Dudhia, J., Gill, D. O., Barker, D. M., Duda, M. G., Haung, X.-Y., Wang, W., and Powers, J. G. (2008). A description of the advanced research WRF; Version 3. Technical report, NCAR/TN-475+STR, National Center for Atmospheric Research (NCAR).

Skerlos, S. J. and Winebrake, J. J. (2010). Targeting plug-in hybrid electric vehicle policies to increase social benefits. Energy Policy, 38(2):705–708.

Smart, J., Powell, W., and Schey, S. (2013). Extended range electric vehicle driving and charging behavior observed early in the EV project. SAE Int. Technical Paper; 2013-01-1441.

Statista (2017a). Average length of vehicle ownership in the United States in 2015, by vehicle type (in years). https://www.statista.com/statistics/581017/average-length-of-vehicle-ownership-in-the-united-states-by-vehicle-type/.

Statista (2017b). Distribution of passenger car ownership in Japan as of December 2014, by size. https://www.statista.com/statistics/645336/japan-share-passenger-car-ownership-by-size/.

Statista (2017c). Number of passenger cars in use in South Korea from 2006 to 2014 (in 1,000 units). https://www.statista.com/statistics/596586/passenger-cars-in-use-south-korea/.

Statistics Norway (2017). Road traffic volumes, 2015. https://www.ssb.no/en/transport-og-reiseliv/statistikker/klreg/aar/2016-04-22?fane=tabell&sort=nummer&tabell=263674.

Sullivan, J. L. and Gaines, L. (2010). A review of battery life-cycle analysis: state of knowledge and critical needs. Technical report, Argonne National Laboratory (ANL), Center for Transportation Research. Energy System Division; ANL/ESD/10-7.

Sullivan, J. L. and Gaines, L. (2012). Status of life cycle inventories for batteries. Energy conversion and Management, 58:134–148.

Sun, K., Tao, L., Miller, D. J., Pan, D., Golston, L. M., Zondlo, M. A., Griffin, R. J., Wallace, H. W., Leong, Y. J., Yang, M. M., Zhang, Y., Mauzerall, D. L., and Zhu, T. (2017). Vehicle emissions as an important urban ammonia source in the United States and China. Environ. Sci. Technol, 51(4):2472–2481.

Takada, K. (2013). Progress and prospective of solid-state lithium batteries. Acta Materialia, 61(3):759–770.

Tamayao, M. M., Michalek, J. J., Hendrickson, C., and Azevedo, I. M. L. (2015). Regional variability and uncertainty of electric vehicle life cycle CO_2 emissions across the United States. Environmental Science & Technology, 49(14):8844–8855.

Tamor, M. A., Gearhart, C., and Soto, C. (2013). A statistical approach to estimating acceptance of electric vehicles and electrification of personal transportation. Transportation Research Part C: Emerging Technologies, 26:125–134.

Tamor, M. A. and Milačić, M. (2015). Electric vehicles in multi-vehicle households. Transportation Research Part C: Emerging Technologies, 56:52–60.

Taylor, J. A. (1965). Method of producing phosphorus pentasulfide. US Patent 3,183,062.

Tran, M., Banister, D., Bishop, J. D. K., and McCulloch, M. D. (2012). Realizing the electric-vehicle revolution. Nature climate change, 2(5):328–333.

Troy, S., Schreiber, A., Reppert, T., Gehrke, H., Finsterbusch, M., Uhlenbruck, S., and Stenzel, P. (2016). Life cycle assessment and resource analysis of all-solid-state batteries. Applied energy, 169:757–767.

UNECE (2015). 2015 inland transport statistics, the UNECE transport statistics for Europe and North America; Volume LVII. United Nations Economic Commission for Europe. https://www.unece.org/fileadmin/DAM/trans/main/wp6/publications/ABTS-2015.pdf.

Uni Of Minnesota (2017). Pyrite. https://www.esci.umn.edu/courses/1001/minerals/pyrite.shtml.

U.S. Census (2014). U.S. census population. http://www.census.gov/population/projections/.

U.S. Congress (2014). National funding of road infrastructure: Australia, Brazil, Canada, China, England and Wales, France, Germany, Israel, Italy, Japan, Mexico, Netherlands, South Africa, Sweden. The Law Library of Congress, Global Legal Research Center, March 2014. https://loc.gov/law/help/infrastructure-funding/index.php.

USGS (2017). U.S. geological survey website (tin statistics and information). https://minerals.usgs.gov/minerals/pubs/commodity/tin/.

Vaishnav, P., Horner, N., and Azevedo, I. L. (2017). Was it worthwhile? where have the benefits of rooftop solar photovoltaic generation exceeded the cost? Environmental Research Letters, 12(9):094015.

Väyrynen, A. and Salminen, J. (2012). Lithium ion battery production. The Journal of Chemical Thermodynamics, 46:80–85.

Venkatesh, A., Jaramillo, P., Griffin, W. M., and Matthews, H. S. (2011). Uncertainty in life cycle greenhouse gas emissions from United States natural gas end-uses and its effects on policy. Environmental science & technology, 45(19):8182–8189.

Wainer, E. (1958). Production of titanium. US Patent 2,833,704.

Weatherbase (2017). Average climate condition. http://www.weatherbase.com/weather/weather.php3?s=88427&cityname=Reno-Nevada-United-States-of-America&units=metric.

WHO (2006). Health risks of particulate matter from long-range transboundary air pollution. WHO/ convention task force on the health aspects of air pollution. E88 189. World Health Organization. Europe.

World Bank (2017). Pump price for gasoline. http://data.worldbank.org/indicator/EP.PMP.SGAS.CD.

WWF (2012). World Wildlife Fund, Canada. http://www.wwf.ca/?11421/WWF-aims-for-600000-electric-vehicles-in-Canada-by-2020.

Yeh, S., Farrell, A., Plevin, R., Sanstad, A., and Weyant, J. (2008). Optimizing U.S. mitigation strategies for the light-duty transportation sector: what we learn from a bottom-up model. Environmental science & technology, 42(22):8202–8210.

Yersak, T. A., Macpherson, H. A., Kim, S. C., Le, V., Kang, C. S., Son, S., Kim, Y., Trevey, J. E., Oh, K. H., Stoldt, C., and Lee, S. (2013). Solid state enabled reversible four electron storage. Advanced Energy Materials, 3(1):120–127.

Yuksel, T., Tamayao, M. M., Hendrickson, C., Azevedo, I. M. L., and Michalek, J. J. (2016). Effect of regional grid mix, driving patterns and climate on the comparative carbon footprint of gasoline and plug-in electric vehicles in the United States. Environmental Research Letters, 11(4):044007.

Zackrisson, M. (2017). Life cycle assessment of long life lithium electrode for electric vehicle batteries – cells for Leaf, Tesla and Volvo bus. Swerea IVF, Mölndal, Sweden, Project Report 24603.

Zackrisson, M., Avellán, L., and Orlenius, J. (2010). Life cycle assessment of lithium-ion batteries for plug-in hybrid electric vehicles– critical issues. Journal of Cleaner Production, 18(15):1519–1529.